AN INTEGRATED USED FUEL DISPOSITION AND GENERIC REPOSITORY MODEL (v2.13.1)

by

Kathryn D. Huff

A dissertation submitted in partial fulfillment of
the requirements for the degree of

Doctor of Philosophy

(Nuclear Engineering and Engineering Physics)

at the

UNIVERSITY OF WISCONSIN–MADISON

2013

ACKNOWLEDGMENTS

CONTENTS

LIST OF TABLES

LIST OF FIGURES

ACRONYMS

ANDRA Agence Nationale pour la gestion des Déchets RAdioactifs, the French National Agency for Radioactive Waste Management. 13, 35

DOE Department of Energy. iv, v, 4, 11, 12

EBS Engineered Barrier System. 33, 35, 46

EDZ Excavation Disturbed Zone. 33

EPA Environmental Protection Agency. 8, 9

FCO Fuel Cycle Options. iv, v, 10

FEPs Features, Events, and Processes. 29

GDSM Generic Disposal System Model. 12, 13, 29–31, 33

HLW high level waste. 65

IAEA International Atomic Energy Agency. 65

MTHM Metric Ton of Heavy Metal. 45, 46

PEI Peak Environmental Impact. 10

RD&D Research Development and Design. 10

SNF spent nuclear fuel. 7, 46, 47

SWF Separations and Waste Forms. 10

UFD Used Fuel Disposition. iv, v, 10–13, 28, 29, 33, 65

US United States. 3, 11

UW University of Wisconsin. 16, 21

YMR Yucca Mountain Repository Site. 4, 5, 9

AN INTEGRATED USED FUEL DISPOSITION AND GENERIC REPOSITORY MODEL (v2.13.1)

Kathryn D. Huff

Under the supervision of Professor Paul P.H. Wilson
At the University of Wisconsin-Madison

As the United States Department of Energy (DOE) simultaneously considers alternative fuel cycles and waste disposal options, an integrated fuel cycle and generic disposal system analysis tool is increasingly necessary for informing domestic nuclear spent fuel policy. The Cyder generic repository model, capable of illuminating the distinct dominant physics of candidate repository geologies, designs, and engineering components, provides an interface between the Used Fuel Disposition (UFD) and Fuel Cycle Options (FCO) Campaign goals. Repository metrics such as necessary repository footprint and peak annual dose are affected by heat and radionuclide release characteristics specific to variable spent fuel compositions associated with alternative fuel cycles. Computational tools capable of simulating the dynamic, heterogeneous spent fuel isotopics resulting from transition scenarios and alternative fuel cycles are, however, lacking in repository modeling options. This work has resulted in such a generic repository model appropriate for systems analysis. By emphasizing modularity and speed, the work at hand provides a tool which captures the dominant physics of detailed repository analysis within the UFD Campaign and can be robustly and flexibly integrated within the Cyclus fuel cycle simulation tool.

Paul P.H. Wilson

ABSTRACT

As the United States Department of Energy (DOE) simultaneously considers alternative fuel cycles and waste disposal options, an integrated fuel cycle and generic disposal system analysis tool is increasingly necessary for informing domestic nuclear spent fuel policy. The Cyder generic repository model, capabable of illuminating the distinct dominant physics of candidate repository geologies, designs, and engineering components, provides an interface between the Used Fuel Disposition (UFD) and Fuel Cycle Options (FCO) Campaign goals. Repository metrics such as necessary repository footprint and peak annual dose are affected by heat and radionuclide release characteristics specific to variable spent fuel compositions associated with alternative fuel cycles. Computational tools capable of simulating the dynamic, heterogeneous spent fuel isotopics resulting from transition scenarios and alternative fuel cycles are, however, lacking in repository modeling options. This work has resulted in such a generic repository model appropriate for systems analysis. By emphasizing modularity and speed, the work at hand provides a tool which captures the dominant physics of detailed repository analysis within the UFD Campaign and can be robustly and flexibly integrated within the Cyclus fuel cycle simulation tool.

1 INTRODUCTION

The scope of this work includes implementation of Cyder, a software library of medium fidelity models to comprehensively represent various long-term disposal system concepts for nuclear material. This software library is integrated with the CYCLUS computational fuel cycle systems analysis platform in order to inform repository performance metrics with respect to candidate fuel cycle options. By abstraction of more detailed models, this work captures the dominant physics of radionuclide and heat transport phenomena affecting repository performance in various geologic media and as a function of arbitrary spent fuel composition.

1.1 Motivation

The development of sustainable nuclear fuel cycles is a key challenge as the use of nuclear power expands domestically and internationally. Accordingly, the United States is simultaneously considering a number of domestic nuclear fuel cycle and geologic disposal options [25]. These decisions are technologically coupled by repository capacity. That is, thermal and radionuclide containment behavior of a geologic repository is a function of spent fuel and high level waste composition, which varies among alternative fuel cycles. For this reason, a generic disposal model capable of integration with a systems analysis framework is necessary to illuminate performance distinctions of candidate repository geologies, designs, and engineering components in the context of fuel cycle options. In answer to this need, the algorithm in this work has been implemented in the Cyder software library which integrates with the Cyclus computational fuel cycle systems analysis platform [40, 84].

To support analysis of numerous combinatoric fuel cycle possibilities, a top-level simulation tool capable of modular substitution of various fuel cycle facility, repository, and engineered barrier components is needed. The modular waste package and repository models resulting from this work will assist in informing current technology choices, identifying important parameters contributing to key waste disposal metrics, and highlighting the most promising waste disposal combinations with respect to metrics chosen by the user.

A generic repository model appropriate for systems analysis must emphasize speed while providing modeling options at various levels of detail. Therefore, parameterized simulations and abstraction efforts conducted to develop the method described in this work sought to capture the dominant physics of thermal repository capacity assessment so that the Cyder disposal environment library could meet the simulation speed requirements of the Cyclus fuel cycle simulator.

System level fuel cycle simulation tools must facilitate efficient sensitivity and uncertainty analyses as well as simulation of a wide range of fuel cycle alternatives. Efficiency

is achieved with models at a level of detail that successfully captures significant aspects of the underlying physics while achieving a calculation speed in accordance with use cases requiring repeated simulations. Often termed abstraction, the process of simplifying while maintaining the salient features of the underlying physics is the method by which used fuel disposal system models were developed in this work.

Independent fuel cycle parameters of particular interest in fuel cycle systems analysis have historically been those related to the front end of the fuel cycle. However, independent variables representing decisions concerning the back end of the fuel cycle are of increasing interest as the United States further investigates repository alternatives to Yucca Mountain. Parameters such as repository geology, engineered barriers, appropriate loading strategies and schedules are all independent variables up for debate. Due to the feedback implication of repository capacity and performance, these parameters are coupled with decisions about the fuel cycle.

Thus, while independent parameters can be chosen and varied within a fuel cycle simulation, coupled parameters require full synthesis with a systems analysis code that appropriately determines the isotopic mass flows into the repository, their appropriate conditioning, densities, and other physical properties.

Future Fuel Cycle Options

Domestically, nuclear power expansion is motivated by the research, development, and demonstration roadmap being pursued by the United States Department of Energy Office of Nuclear Energy (DOE-NE), which seeks to ensure that nuclear energy remain a viable domestic energy option [24].

As the DOE-NE seeks to develop technologies and strategies to support a sustainable future for nuclear energy, various fuel cycle strategies and corresponding disposal system options are being considered. Specifically, the domestic fuel cycle option space under current consideration is described in terms of three distinct fuel cycle categories with the monikers Once Through, Full Recycle, and Modified Open. Each category presents unique disposal system siting and design challenges. Systems analyses for evaluating these options must be undertaken in order to inform a national decision to deploy a comprehensive fuel cycle system by 2050 [24].

The Once-Through Cycle category includes fuel cycles similar to the continuation of the business as usual case in the United States. Such fuel cycles neglect reprocessing and present challenges associated with high volumes of minimally treated spent fuel streams. In a business as usual scenario, conventional power reactors comprise the majority of nuclear energy production. Calculations from the Electric Power Research Institute corroborated by the United States (US) Department of Energy (DOE) in 2008 indicate that without an increase in the statutory capacity limit of the Yucca Mountain Repository Site (YMR), continuation of the current Once Through fuel cycle will generate a volume of spent fuel that will necessitate the siting of an additional federal geological repository to accommodate spent fuel [47, 23].

A Full Recycle option, on the other hand, requires the research, development, and deployment of partitioning, transmutation, and advanced reactor technology for the reprocessing of used nuclear fuel. In this scheme, conventional once-through reactors will be phased out in favor of advanced transmutation technologies. All fuel in the Full Recycle strategy will be reprocessed using an accelerator driven system or by cycling through an advanced fast reactor. Such fuel may undergo partitioning, the losses from which will require waste treatment and ultimate disposal in a repository. Thus, a repository under the Full Recycle scenario must support a waste stream composition that is highly variable during transition periods as well as myriad waste forms and packaging associated with isolation of differing waste streams.

Finally, the Modified Open Cycle category of options includes a variety of fuel cycle options that fall between once through and fully closed. Advanced fuel cycles such as deep burn and small modular reactors will be considered as will partial recycle options. Partitioning and reprocessing strategies, however, will be limited to simplified chemical separations and volatilization. This scheme presents a dual challenge in which spent fuel volumes and composition will both vary dramatically among various possibilities within this scheme [24] .

Clearly, the waste streams resulting from potential fuel cycles present an array of corresponding waste disposition, packaging, and engineered barrier system options. Differing spent fuel composition, partitioning, transmutation, and chemical processing decisions upstream in the fuel cycle demand differing performance and loading requirements of waste forms and packaging. The capability to model thermal and radionuclide transport phenomena through vitrified glass as well as ceramic waste forms with with various loadings of arbitrary isotopic compositions is therefore required. This work has produced a repository model that meets this need.

Future Waste Disposal System Options

In addition to reconsideration of the domestic fuel cycle policy, the uncertain future of the YMR has driven the expansion of the option space of potential repository host geologies to include, at the very least, granite, clay/shale, salt, and deep borehole concepts [61].

In accordance with various fuel cycle options, corresponding waste form, waste package, and other engineered barrier systems are being considered. Specifically, current considerations include ceramic (e.g. Uranium Oxide), glass (e.g. borosilicate glasses), and metallic (e.g. hydride fuels) waste forms. Waste packages may be copper, steel, or other alloys. Similarly, buffer and backfill materials vary from the crushed salt recommended for a salt repository to bentonite or concrete in other geologies. Therefore, this repository model was designed to be capable of modular substitution of waste form models and data in order to analyze the full option space.

The physical, hydrologic, and geochemical mechanisms that dictate radionuclide and heat transport vary between the geological and engineered containment systems in the domestic disposal system option space. Therefore, in support of the system

level simulation effort, models must be developed that capture the salient physics of these geological options and quantify associated disposal metrics. Furthermore, in the same way that system level modularity facilitates analysis, so too does modular linkage between subcomponent process modules. These subcomponent models and the repository environmental model must achieve a cohesively integrated disposal system model such as is proposed by this work.

Thermal Modeling Needs

The decay heat from nuclear material generates a significant heat source within a repository. In order to arrive at loading strategies that comply with thermal limits in the engineered barrier system and the geological medium, a thermal modeling capability must be included in the repository model. Such a model is also necessary to inform material and hydrologic phenomena that affect radionuclide transport and are thermally coupled.

Partitioning and transmutation of heat generating radionuclides within some fuel cycles will alter the heat evolution of the repository [77]. Thus, to distinguish between the repository heat evolution associated with various fuel cycles involving partitioning and transmutation, a repository analysis model, must at the very least, capture the decay heat behavior of dominant heat contributors. Plutonium, Americium, and their decay daughters dominate decay heat contribution within used nuclear fuels. Other contributing radionuclides include Cesium, Strontium, and Curium [65].

Thermal limits within a used nuclear fuel disposal system are waste form, package, and geology dependent. The heat evolution of the repository constrains waste form loadings and package loadings as heat generated in the waste form is transported through the package. It also places requirements on the size, design, and loading strategy in a potential geological repository as that heat is deposited in the engineered barrier system and host geology.

Thermal limits of various waste forms have their technical basis in the temperature dependence of isolation integrity of the waste form. Waste form alteration, degradation, and dissolution behavior is a function of heat in addition to redox conditions and constrains loading density within the waste form.

Thermal limits of various engineered barrier systems similarly have a technical basis in the temperature dependent alteration, corrosion, degradation, and dissolution rates of the materials from whence they are constructed.

Thermal limits of the geologic environment can be based on the mechanical integrity of the rock as well as mineralogical, hydrologic and geochemical phenomena. The isolating characteristics of a geological environment are most sensitive to hydrologic and geochemical effects of thermal loading. Thus, heat load constraints are typically chosen to control hydrologic and geochemical response to thermal loading. In the United States, current regulations necessitate thermal limits in order to passively steward the

repository's hydrologic and geochemical integrity against radionuclide release for the first 10,000 years of the repository.

Constraints for a broad set of possible geological environments depend on heat transport properties and geochemical behaviors of the rock matrix as well as its hydrologic state. Such constraints affect the repository waste package spacing and repository footprint among other parameters.

In addition to development of a concept of heat transport within the repository in order to meet heat load limitations, it is also necessary to model temperature gradients in the repository in order to support modeling of thermally dependent hydrologic and material phenomena. As mentioned above, waste form corrosion processes, waste form dissolution rates, diffusion coefficients, and the mechanical integrity of engineered barriers and geologic environment are coupled with temperature behavior. Only a coarse time resolution is necessary to capture that coupling however, since time evolution of repository heat is such that thermal coupling can typically be treated as quasi static for long time scales. [8].

Source Term Modeling Needs

Domestically, the Environmental Protection Agency (EPA) has defined a limit on human exposure due to the repository. This regulation places important limitations on capacity, design, and loading techniques for repository concepts under consideration. Repository concepts developed in this work must therefore quantify radionuclide transport through the geological environment in order to calculate repository capacity and other metrics.

The exposure limit set by the EPA is based on a 'reasonably maximally exposed individual.' For the YMR, the limiting case is a person who lives, grows food, drinks water and breathes air 18 km downstream from the repository. The Yucca Mountain Repository EPA regulations limit total dose from the repository to 15 mrem/yr, and limit dose from drinking water to 4 mrem/yr for the first 10,000 years. Predictions of that dose rate depend on an enormous variety of factors, most important of which is the primary pathway for release. In the YMR primary pathway of radionuclides from an accidental release will be from cracking aged canisters. Subsequently, transport of the radionuclides to the water table requires that the radionuclides come in contact with water and travel through the rock to the water table. This results in contamination of drinking water downstream.

Source term is a measure of the quantity of a radionuclide released into the environment whereas radiotoxicity is a measure of the hazardous effect of that particular radionuclide upon human ingestion or inhalation. In particular, radiotoxicity is measured in terms of the volume of water dilution required to make it safe to ingest. Studies of source term and radiotoxicity therefore make probabilistic assessments of radionuclide release, transport, and human exposure.

Importantly, due to the long time scale and intrinsic uncertainties required in such probabilistic assessments it is in general not advisable to base any maximum repository

capacity estimates on source term. This is due to the fact that in order to give informative values for the risk associated with transport of particular radionuclides, for example, it is necessary to make highly uncertain predictions concerning waste form degradation, water flow, and other parameters during the long repository evolution time scale. However, source term remains a pertinent metric for the comparison of alternative separations and fuel cycle scenarios as it is a fundamental factor in the calculation of risk.

Arriving at a generalized metric of probabilistic risk is fairly difficult. For example, the Peak Environmental Impact (PEI) metric from Berkeley (ref. [15]) is a multifaceted function of spent fuel composition, waste conditioning, vitrification method, and radionuclide transport through the repository walls and rock. Also, it makes the assumption that the waste canisters have been breached at $t = 0$. Furthermore, reported in m^3, PEI is a measure of radiotoxicity in the environment in the event of total breach. While informative, this model on its own does not completely determine a source-term limited maximum repository capacity. Additional waste package failure and a dose pathway model must be incorporated into it.

Domestic Research and Development Program

The DOE-NE Fuel Cycle Technology (FCT) program has three groups of relevance to this effort: these are the Used Fuel Disposition (UFD), the Separations and Waste Forms (SWF), and Fuel Cycle Options (FCO) (previously Systems Analysis) campaigns. The UFD campaign is conducting the Research Development and Design (RD&D) related to the storage, transportation, and disposal of radioactive wastes generated under both the current and potential advanced fuel cycles. The SWF campaign is conducting RD&D on potential waste forms that could be used to effectively isolate the wastes that would be generated in advanced fuel cycles. The SWF and UFD campaigns are developing the fundamental tools and information base regarding the performance of waste forms and geologic disposal systems. The FCO campaign is developing the overall fuel cycle simulation tools and interfaces with the other FCT campaigns, including UFD.

This effort has interfaced with those campaigns to develop the higher level dominant physics representations for use in fuel cycle system analysis tools. Specifically, this work has leveraged conceptual framework development and primary data collection underway within the Used Fuel Disposition Campaign as well as work by Radel, Wilson, Bauer et. al. to model repository behavior as a function of the contents of the waste [70]. It then incorporated dominant physics process models into the CYCLUS computational fuel cycle analysis tool [84] based on sensitivity analysis utilizing those detailed tools.

1.2 Methodology

In this work, concise dominant physics models suitable for system level fuel cycle codes were developed by comparison of analytical models with more detailed repository

modeling efforts. The ultimate result of this work is a software library capable of assessing a wide range of combinations of fuel cycle alternatives, potential waste forms, repository design concepts, and geological media.

Current candidate repository concepts have been investigated and reviewed here in order to arrive at a fundamental set of components to model. A preliminary set of combinations of fuel cycles, repository concepts, and geological environments has been chosen that fundamentally captures the domestic option space. Specifically, three candidate geologies and four corresponding repository concepts under consideration by the DOE UFD campaign have been chosen for modeling in this work. These have been implemented to interface with Cyclus simulations of a canonical set of potential fuel cycles within three broad candidate scenarios put forth by the US DOE.

A review and characterization of the physical mechanisms by which radionuclide and thermal transport take place within the materials and media under consideration was first undertaken. Potential analytical models to represent these phenomena were investigated and categorized within the literature review.

A review and characterization of current detailed computational tools for repository focused analysis was next conducted. Both international and domestic repository modeling efforts were summarized within the literature review. Of these, candidate computational tools with which to perform abstraction and regression analyses were identified. Specifically, a suite of Generic Disposal System Model (GDSM) tools under development by the DOE UFD campaign has informed radionuclide transport models and a pair of corresponding thermal analysis codes has informed the thermal models.

This suite of subcomponent modules, appropriate for use within the Cyclus fuel cycle simulator, has included the development of a robust architecture within the repository module that allows for interchangeable loading of system components. Within the system components, dominant physics is modeled based on domain appropriate approximation of analytical models and supported by abstraction with the chosen GDSM tools and thermal tools.

These concise models are a combination of two components: semi-analytic mathematical models that represent a simplified description of the most important physical phenomena, and semi-empirical models that reproduce the results of detailed models. By combining the complexity of the analytic models and regression against numerical experiments, variations were limited between two models for the same system. Different approaches have been been compared in this work, with final modeling choices balancing the accuracy and efficiency of the possible implementations.

Specifically, these models focus on the hydrology and thermal physics that dominate radionuclide transport and heat response in candidate geologies as a function of radionuclide release and heat generation over long time scales. Dominant transport mechanism (advection or diffusion) and disposal site water chemistry (redox state) provide primary differentiation between the different geologic media under consideration. In addition, the concise models are capable of roughly adjusting release pathways according to the characteristics of the natural system (both the host geologic setting and the site in

general) and the engineered system (such as package loading arrangements, tunnel spacing, and engineered barriers).

The abstraction process in the development of a geological environment model employs the comparison of semi-analytic thermal and hydrologic models and analytic regression of rich code results from more detailed models as well as existing empirical geologic data. Such results and data will be derived primarily from the UFD campaign GDSMs and data, as well as European efforts such as the RED-IMPACT assessment and Agence Nationale pour la gestion des Déchets RAdioactifs, the French National Agency for Radioactive Waste Management (ANDRA) Dossier efforts [51, 8, 21] .

Thereafter, a regression analysis concerning those parameters has been undertaken with available detailed models (e.g. 2D and 3D finite element thermal performance assessment codes) to further characterize the parametric dependence of thermal loading in a specific geologic environment.

Finally, the thermal behavior of a repository model so developed depends on empirical data (e.g. heat transfer coefficients, hydraulic conductivity). Representative values have been made available within the dominant physics models and rely on existing empirical data concerning the specific geologic environment being modeled (i.e. salt, clay/shale, and granite).

A similar process was followed for radionuclide transport models. The abstraction process in the development of waste form, package, and engineered barrier system models will be analogous to the abstraction process of repository environment models. Concise models have resulted from employing the comparison of semi-analytic models of those systems with regression analysis of rich code in combination with existing empirical material data.

Coupling effects between components were considered carefully. In particular, given the important role of temperature in the system, thermal coupling between the models for the engineered system and the geologic system were considered. Thermal dependence of radionuclide release and transport as well as package degradation were analyzed to determine the magnitude of coupling effects in the system.

The full abstraction process was be iterated to achieve a balance between calculation speed and simulation detail. Model improvements during this stage sought a level of detail appropriate for informative comparison of subcomponents, but with sufficient speed to enable systems analysis.

By varying input parameters and comparing with corresponding results from detailed tools, each model's behavior on its full parameter domain was validated.

1.3 Outline

A literature review, Chapter **??**, presents background material that organizes and reports upon previous relevant work. First it summarizes the state of the art of repository modeling integration within current systems analysis tools. It then describes current

domestic and international disposal system option space. Next, the literature review focuses upon current analytical and computational modeling of radionuclide and heat transport through various waste forms, engineered barrier systems, and geologies of interest. It also addresses previous efforts in generic geologic environment repository modeling in order to categorize and characterize detailed computational models of radionuclide and heat transport available for regression analysis.

Chapter 3 details the computational paradigm of the Cyclus systems analysis platform and Cyder repository model which constitute this work. It describes the Cyclus fuel cycle simulation context which drives fundamental Cyder design descisions.

Chapter 4 describes the radionuclide and heat transport models that were implemented. Models representing waste form, waste package, buffer, backfill, and engineered barrier componeents are defined by their interfaces and their relationships as interconnected modules, distinctly defined, but coupled. This modular paradigm allows exchange of technological options (i.e. borosilicate glass and concrete waste forms) for comparison but also exchange of models for the same technological option with varying levels of detail.

Chapter 5 describes simulation cases conducted to demonstrate radionuclide transport and thermal capacity analysis capabilities in Cyder. It also describes verification and validation procedures which benchmarked Cyder behavior against analytic solutions and more detailed models.

Finally, in Chapter **??**, contributions to the field and suggested future work are summarized.

2 LITERATURE REVIEW

This is a placeholder. The literature review is too verbose at the moment. Also, I'm not sure what to include (or what to neglect).

3   MODELING PARADIGM

The modeling paradigm with which this repository model and simulation platform are implemented are described here. Implications of the simulation platform architecture on the design of the repository model are discussed and the interfaces defining components of the repository model follow.

3.1   Cyclus Simulator Paradigm

The Cyclus project at the University of Wisconsin (UW) at Madison is the simulation framework in which this repository model is designed to operate. Modular features within this software architecture provide a great deal of flexibility, both in terms of modifying the underlying modeling algorithms and exchanging components of a fuel cycle system.

The Cyclus fuel cycle simulator is the result of lessons learned from experience with previous nuclear fuel cycle simulation platforms. The modeling paradigm follows the transaction of discrete quanta of material among discrete facilities, arranged in a geographic and institutional framework, and trading in flexible markets. Key concepts in the design of Cyclus include open access to the simulation engine, modularity with regard to functionality, and relevance to both scientific and policy analyses. The combination of modular encapsulation within the software architecture and dynamic module loading allows for robust but flexible reconfiguration of the basic building blocks of a simulation without alteration of the simulation framework.

The modeling paradigm adopted by Cyclus includes a number of fundamental concepts that comprise the foundation on which other, more flexible, design choices have been made.

Dynamic Module Loading

The ability to dynamically load independently constructed modules is a heavy focus of Cyclus development. Dynamically-loadable modules are the primary mechanism for extending Cyclus' capability. The primary benefit of this approach is encapsulation: the trunk of the code is completely independent of the individual models. Thus, any customization or extension is implemented only in the loadable module. A secondary benefit of this encapsulation is the ability for contributors to choose different distribution and licensing strategies for their contributions. By allowing models to have varied availability, the security concerns of developers can be assuaged (See Figure 3.1).

Finally, this strategy allows individual developers to explore different levels of complexity within their modules, including wrapping other simulation tools as loadable modules within the Cyclus framework. This last benefit of dynamically-loadable mod-
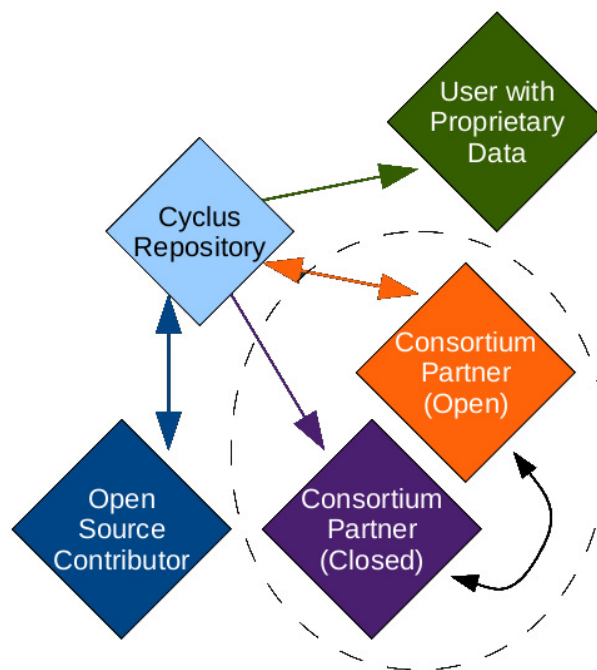
Figure 3.1: The CYCLUS code repository allows for varied accessibility.

ules addresses another goal of CYCLUS : ubiquity amongst its potential user base. By engineering CYCLUS to easily handle varying levels of complexity, a single simulation engine can be used by both users interested in big-picture policy questions as well as users focused on more detailed, technical analyses.

Encapsulation

CYCLUS implements an encapsulated structure that takes advantage of object-oriented software design techniques in order to create an extensible and modular user and developer interface. A primary workhorse for this implementation is the notion of dynamic module loading in combination with well defined module interfaces within a region, institution, and facility hierarchy. In this paradigm, the shared interface of polymorphic objects is abstracted from the logic of their instantiation by the model definition they inherit.

In this way, CYCLUS allows a level of abstraction to exist between the simulation and model instantiation as well as between model instantiation and behavior. An interface defines the set of shared functions of a set of subclasses in an abstract superclass. In CYCLUS main superclasses are Regions, Institutions, and Facilities while their subclasses are the concrete available model types (e.g. a RecipeReactorFacility). See Figure 3.2.

The interface for the FacilityModel class is the set of virtual functions declared in

the Facility class such as getName, getID, executeOrder(), sendMaterial(), receiveMaterial() etc. Through such an interface, the members of a subclass can be treated as interchangeable (polymorphic) instantiations of their shared superclass.
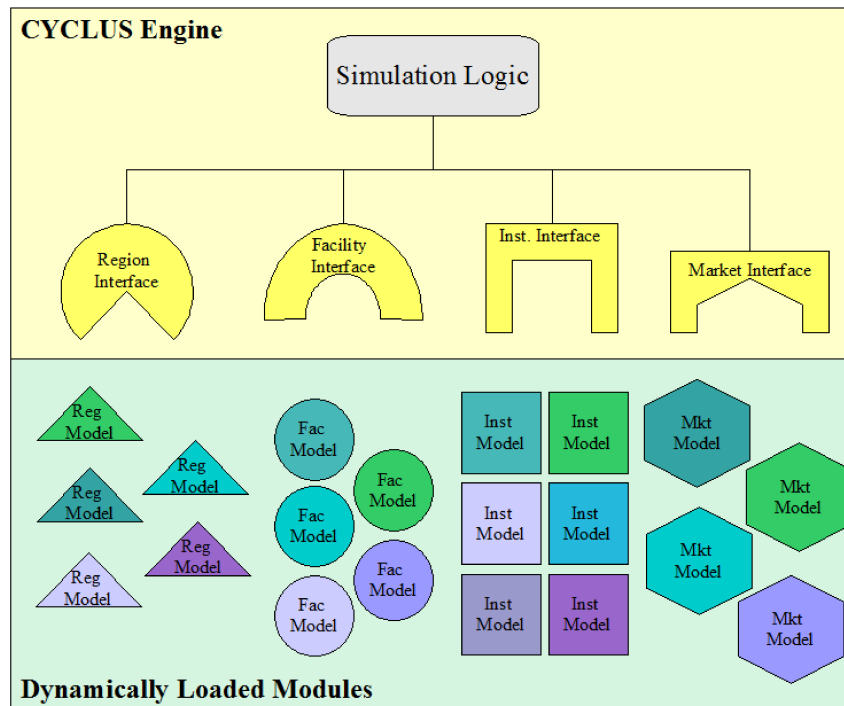
Figure 3.2: Modules are defined solely by their interfaces in a modular paradigm and can be arbitrarily interchanged with modules posessing equivalent interfaces.

Modularity and Extensibility

A modular code must have the traits of encapsulation and abstraction appropriate for a user or developer to flexibly make alterations to the simulation performance with minimal modification to the code. An extensible code should be both robustly suited to the addition of classes and subclasses as well as suited to communication with other codes. In Cyclus , addition of new models by dynamic loading is possible without any alteration of the software trunk. The modular design of Cyclus stresses avoidance of rigidity, in which changes to the code are potentially difficult, and fragility, in which changes to the code are potentially damaging.

Market-based Material Transactions

The foundation of a simulation is a commodity market that collects offers and requests and matches them according to some algorithm. The user is able to select which type of algorithm is used for each market by selecting a MarketModel and configure it with a particular set of parameters defined by that MarketModel. Changing the parameters of a market changes its performance and selecting a different MarketModel completely changes its behavior.

The transaction of nuclear materials takes place in markets that act as brokers matching a set of requests for material with a set of offers for that material. A variety of market models will be available to perform this brokerage role. It is important to note that each market is defined for a single commodity and acts independently of other markets. Once the requests and offers have been matched by each market in a simulation, the facilities exchange material objects.

Facilities are deployed to issue offers and requests in these markets. Like markets, the user may select which type of algorithm is used for each facility by selecting a Facility-Model and configure it with a particular set of parameters defined by that FacilityModel. Changing the parameters of a facility changes its performance and selecting a different FacilityModel completely changes its behavior. Unlike markets, multiple independent instances of each facility configuration can be deployed to represent individual facilities.

Discrete Materials and Facilities

The Cyclus modeling infrastructure is designed such that every facility in a global nuclear fuel cycle is treated and acts individually. Each facility has two fundamental tasks: the transaction of goods or products with other facilities and the transformation of those goods or products from an input form to an output form. For example, a reactor will receive fresh fuel assemblies from a fuel fabrication facility, transform them to used fuel assemblies using some approximation of the reactor physics, and supply those used fuel assemblies to a storage facility. In this manner, facilities can be thought of as black boxes in the simulation which request and produce resources as in Figure 3.3

A facility configuration is created by selecting a FacilityModel and defining the parameters for that facility configuration. Each FacilityModel will define its own set of parameters that govern its performance. The same FacilityModel may be used for multiple facility configurations in the same region, each with parameter values appropriate for that facility configuration.

The repository model that is the subject of this work is a facility model within the Cyclus simulation paradigm.

Material movement is the primary unit of information in Cyclus . Discrete materials passed, traded, and modified between and within facilities in the simulation are recorded at every timestep. This material history is stored in the output dataset of Cyclus . In
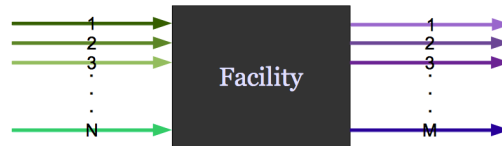
Figure 3.3: Facilities in Cyclus can be thought of as black boxes which make offers and requests for resources.

addition to holding the map of isotopes and their masses, a material object holds a comprehensive history of its own path as it moves through models within the simulation.

Implications for Cyder

The above sections outline the fuel cycle simulation platform currently under development at UW in which the Cyder repository model at hand is to be implemented. Implemented as a facility within this framework, the repository model interface is defined by the Facility Model interface defined within the Cyclus paradigm. Though some Facility models make both requests and offers to the system, the Cyder model is a type of sink, making only requests as in Figure 3.4.
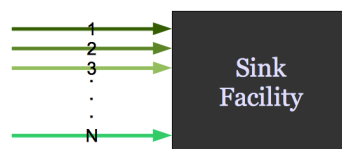
Figure 3.4: The Cyder model is a type of sink facility, making only resource requests.

That interface requires that a capacity be defined by the repository at every Cyclus timestep so that the repository may make appropriate requests of disposable material.

Furthermore, the capability for dynamic module loading possible within the Cyclus paradigm allows the repository system subcomponents to be interchangeably loaded at runtime, enabling comparison of various repository subcomponents, physical models of varying levels of detail.

The repository is both a subclass and a superclass. It is a subclass of the FacilityModel class, and a superclass of its own subcomponents. That is, dynamically loaded subcomponents of the repository inherit data, parameters and behaviors from the repository itself.

3.2 Cyder Repository Modeling Paradigm

The Cyder repository model architecture is intended to modularly permit exchange of disposal system Component models (e.g., detailed nuclide transport model vs. less detailed) and data (e.g., exchange clay for granite geologic data) and accept arbitrary waste stream isotopic compositions. Finally, in order to participate in the simulation as a facility model, must make requests for spent material up to its capacity. Determination of the repository capacity for various types of spent fuel commodities comprises the interfacing functionality of the repository model.

Waste Stream Acceptance

The repository model must accept arbitrary spent fuel and high level waste streams. A waste stream is a material data object resulting from the Cyclus simulated fuel cycle. As radionuclides are gained, lost, and transmuted within the spent fuel object, a history of its isotopic composition is recorded. It arrives at the repository and is emplaced if it obeys all repository capacity limits.

For waste streams that vary from each other in composition, the thermal capacity of the repository to receive that waste stream must therefore be recalculated. Since disposable material in most simulations of interest will be of variable composition and therefore heterogeneous in heat production capability, the repository model will repeatedly need to recalculate its own capacity as new materials are offered. That capacity calculation will be discussed in Section 4.2.

Waste Stream Conditioning

Waste conditioning is the process of packing a waste stream into an appropriate waste form. As Cyclus lacks a conditioning facility, the Cyder repository fulfills this need as a part of the repository behavior. As a waste stream is accepted into the repository, it is associated with a waste form according to its commodity name. This pairing is input by the user during simulation setup when a number of waste form Component configurations are specified and associated with allowed waste stream commodities. It is according to these pairings that Cyder model loads discrete waste forms with discrete waste stream contaminant vectors as depicted in Figure 3.5.

$$\vec{m}_{CsSr} = \begin{bmatrix} {}^{134}Cs \\ {}^{135}Cs \\ \cdot \\ \cdot \\ \cdot \\ {}^{90}Sr \end{bmatrix}$$

WF + WS =
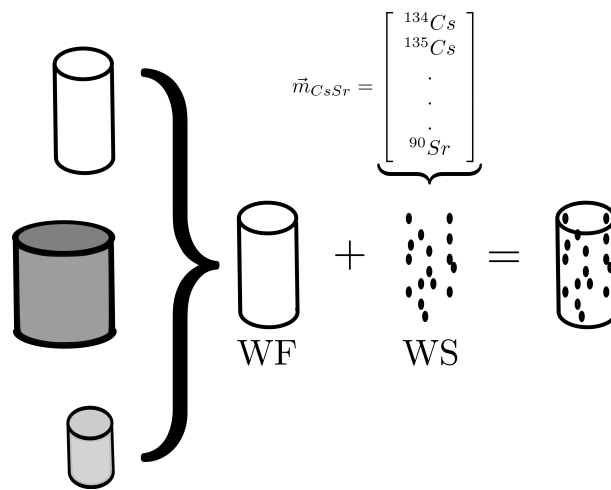
Figure 3.5: Waste streams are conditioned into the appropriate waste form according to user-specified pairings.

Waste Form Packaging

Waste packaging is the process of placing one or many waste forms into a (typically metallic) containment package. Once the waste stream has been conditioned into a waste form, that waste form Component is loaded into a waste package Component, also according to allowed pairs dictated by the user, as depicted in Figure 3.6.

WP + WF =
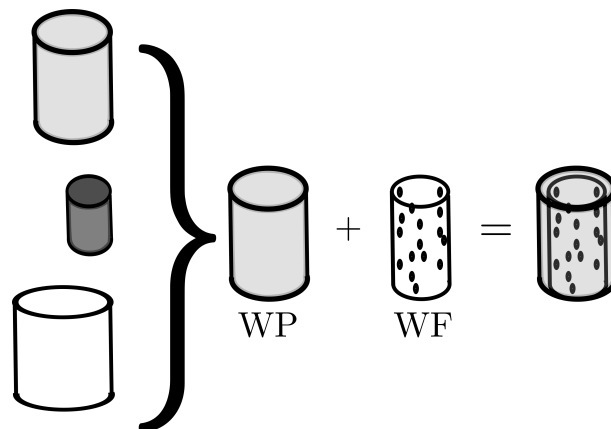
Figure 3.6: Waste forms are loaded into the appropriate waste package according to user-specified pairings.

Package Emplacement

Finally, the waste package is emplaced in a buffer component, which contains many other waste packages, spaced evenly in a grid. The grid is defined by the user input and depends on repository depth, Δz, waste package spacing, Δx, and tunnel spacing, Δy as in Figure 3.7.
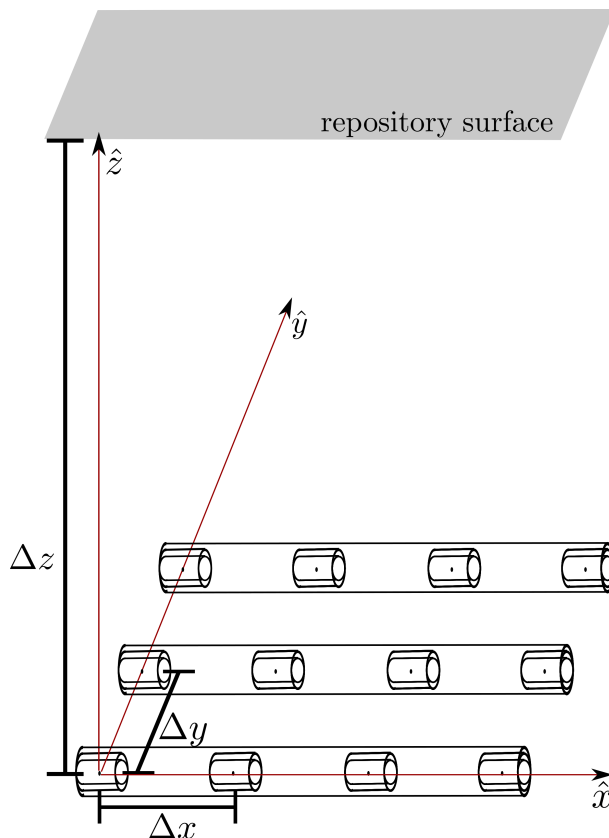
Figure 3.7: The repository layout has a depth and a uniform package spacing.

Nested Components

The fundamental unit of information in the repository model is radionuclide contaminant presence at each stage of containment. The repository model, in this way, is fundamentally a tool to determine thermal and contaminant transport evolution as a result of an arbitrary waste stream. The repository model in this work conducts this calculation by treating each containment Component as nested volumes in a release chain.

Each Component is defined by a Geometry, some Material Data, a ThermalModel, and a NuclideModel. It is also defined by the Parent Component which contains it and the Daughter Components which it contains. An emplaced waste package Component, for example, possesses a pointer to the buffer that surrounds it, its Parent Component. It also possesses a list of pointers to the waste form or waste forms within it, its Daughter Components.

Component Geometry

Each Component of the repository system (i.e. waste form, waste package, buffer, and geologic medium) is modeled as a discrete control volume. Each control volume performs its own mass balance at each time step and assesses its own internal heat transfer and degradation phenomena separately from the other nested Components. This control volume is defined by the Component Geomtry, a class which keeps track of the inner and outer radii, length, and centroid coordinates of the (assumed cylindrical) volume.

Component Material Data

Each Component of the repository system possesses a notion of the material that it is made of. Supporting thermal and hydrologic data for canonical engineered barrier and geologic media is provided with the code in the mat_data.sqlite SQLite database.

Each table in the database holds data related to one of a canonical set of engineered barrier and geological medium materials (e.g. clay, glass, etc.). The columns of that table hold data such as thermal diffusivity, thermal conductivity, porosity, effective porosity, and solubility and sorption coefficients for each element.

Component ThermalModel

Each Component possesses a thermal transport model that determines the temperature inside the Component over time. This calculation is distinct from the model used to estimate capacity, though that model is available for modeling at the component level. The thermal modeling options are discussed further in Section 4.2.

Component NuclideModel

Each Component possesses a radionuclide contaminant transport model that determines the contaminant transport inside the Component over time. The choices available for this NuclideModel are discussed further in Section 4.1.

Implicit Timestepping

Each Component passes some information radially outward to the nested Component immediately containing it and some information radially inward to the nested Component it contains.

In the case of radionuclide transport, for example, each Component model requires information about the radionuclides released from the Component it immediately contains. Thus, nuclide release information is passed radially outward from the waste stream sequentially through each containment layer to the geosphere. However, the solutions within each Component often rely on the external boundary conditions of that Component. Thus, the Cyder model uses an implicit timestepping method to arrive at the future state of each Component, radially outward, as a function of both the past state and the current state.

That is, in Component 0, the innermost Component in a nested series, the mass or concentration distribution in the Component at time t_n is found from the inner boundary condition at time t_n and the outer boundary condition at t_{n-1}. Then, from the resulting mass or concentration distribution, I can solve, numerically, for the outer boundary condition at t_n which can, in turn, be used by the parent component 1 as the t_n inner boundary condition of its own solution. For each timestep :

$$BC(i, r_o, c_1, t_n) = f(BC(i, r_i, c_0, t_n), BC(i, r_o, c_1, t_{n-1})) \tag{3.1}$$

where

$$
\begin{aligned}
BC &= \text{boundary condition} \\
i &= \text{the isotope} \\
r_i &= \text{the inner boundary radius } [m] \\
r_o &= \text{the outer boundary radius } [m] \\
c_0 &= \text{the innermost Component} \\
c_1 &= \text{the Component that contains } c_0 \\
f &= \text{functional form of the contaminant transport algorithm} \\
t_n &= \text{timestep n.}
\end{aligned}
$$

Output Tables

Cyder output tables utilize the Cyclus Table class and rely on the Cyclus simulation logic to record table entries in the cyclus.sqlite output database. Current Cyder output tables include a number of tables. First, a repository parameters table, **gen_repo_params**, keeps data from the user input that parameterized the generic repository, for reproducibility. Similarly, a Componet parameters table, **gen_repo_components**, keeps data

that parameterized each component, both from the user input and from the Cyder procedures that position and arrange these components. An example is shown in Figure 3.8. Finally, a contaminants table, **gen_repo_contaminants**, keeps track of the isotopic composition of the contaminants in each component as they move radially outward. An example of the contaminants table is show in Figure 3.9.

	compID	parentID	compType	name	material_data	nuclidemodel	thermalmodel	innerradius	outerradius	x	y	z
1	4	0	2	FF	clay	DEGRATE_NUCLIDE	STUB_THERMAL	3	100	0	0	0
2	5	0	0	BUFFER	clay	DEGRATE_NUCLIDE	STUB_THERMAL	2	3	50	0	100
3	6	0	4	WF	clay	DEGRATE_NUCLIDE	STUB_THERMAL	0	1	50	50	100
4	7	0	5	WP	clay	DEGRATE_NUCLIDE	STUB_THERMAL	1	2	50	50	100
5	8	0	4	WF	clay	DEGRATE_NUCLIDE	STUB_THERMAL	0	1	50	150	100
6	9	0	5	WP	clay	DEGRATE_NUCLIDE	STUB_THERMAL	1	2	50	150	100
7	10	0	4	WF	clay	DEGRATE_NUCLIDE	STUB_THERMAL	0	1	50	250	100
8	11	0	5	WP	clay	DEGRATE_NUCLIDE	STUB_THERMAL	1	2	50	250	100
9	12	0	4	WF	clay	DEGRATE_NUCLIDE	STUB_THERMAL	0	1	50	350	100
10	13	0	5	WP	clay	DEGRATE_NUCLIDE	STUB_THERMAL	1	2	50	350	100
11	14	0	4	WF	clay	DEGRATE_NUCLIDE	STUB_THERMAL	0	1	50	450	100
12	15	0	5	WP	clay	DEGRATE_NUCLIDE	STUB_THERMAL	1	2	50	450	100

Figure 3.8: An example of the Cyder component parameters table recorded for provenance in the cyclus.sqlite database.

	CompID	Time	IsoID	MassKG	AvailConc
1	6	0	8016	0.115044	0
2	6	0	92235	0.0442478	0
3	6	0	92238	0.840708	0
4	7	0	92235	0	0
5	5	0	92235	0	0
6	4	0	92235	0	0
7	6	1	8016	0.115044	0
8	6	1	92235	0.0442478	0
9	6	1	92238	0.840708	0
10	8	1	8016	0.115044	0
11	8	1	92235	0.0442478	0
12	8	1	92238	0.840708	0
13	7	1	92235	0	0

Figure 3.9: An example of the Cyder contaminants table in the cyclus.sqlite database.

4 METHODOLOGY

4.1 Radionuclide Transport In Cyder

Each engineered barrier component within the Generic Repository calculates nuclide transport using a model selected from the four presented in this chapter. In order to be interchangeable within the simulation, these components have identical nuclide transport interfaces.

Radionuclide transport models may rely on a number of boundary condition forms. Each nuclide model interface therefore provides sufficient boundary condition information to support the calculation methods of all other nuclide models. That is, each must provide a superset of the boundary condition forms required by all four models. These include Dirichlet, specified species concentration along the boundary, Neumann, concentration gradients along the boundary, and Cauchy, a combination of the two that provides a concentration flux along the boundary.

Interfaces

The interfaces between the models are essential to the understanding of the models themselves. The interfaces define boundary conditions in a number of forms based on information available internally to the component implementation.

In a saturated, reducing environment, contaminants are transported by dispersion and advection. It is customary to define the combination of molecular diffusion and mechanical mixing as the dispersion tensor, D, such that the mass conservation equation becomes [74**?** , 30]:

$$
\begin{aligned}
J &= J_{dis} + J_{adv} \\
&= -\theta(D_{mdis} + \tau D_m)\nabla C + \theta v C \\
&= -\theta D \nabla C + \theta v C
\end{aligned}
$$

which, for uniform flow in $\hat{k}$, is

$$
= \left(-\theta D_{xx}\frac{\partial C}{\partial x}\right)\hat{\imath} + \left(-\theta D_{yy}\frac{\partial C}{\partial y}\right)\hat{\jmath} + \left(-\theta D_{zz}\frac{\partial C}{\partial z} + \theta v_z C\right)\hat{k}, \qquad (4.1)
$$

where

$$
\begin{aligned}
J_{dis} &= \text{Total Dispersive Mass Flux } [kg/m^2/s] \\
J_{adv} &= \text{Advective Mass Flux } [kg/m^2/s] \\
\tau &= \text{Toruosity } [-] \\
\theta &= \text{Porosity } [\%] \\
D_m &= \text{Molecular diffusion coefficient } [m^2/s] \\
D_{mdis} &= \text{Coefficient of mechanical dispersivity} [m^2/s] \\
D &= \text{Effective Dispersion Coefficient } [m^2/s] \\
C &= \text{Concentration } [kg/m^3] \\
v &= \text{Fluid Velocity in the medium } [m/s].
\end{aligned}
$$

Solutions to this equation can be categorized by their boundary conditions and those boundary conditions serve as the interfaces between components in the Cyder library of nuclide transport models.
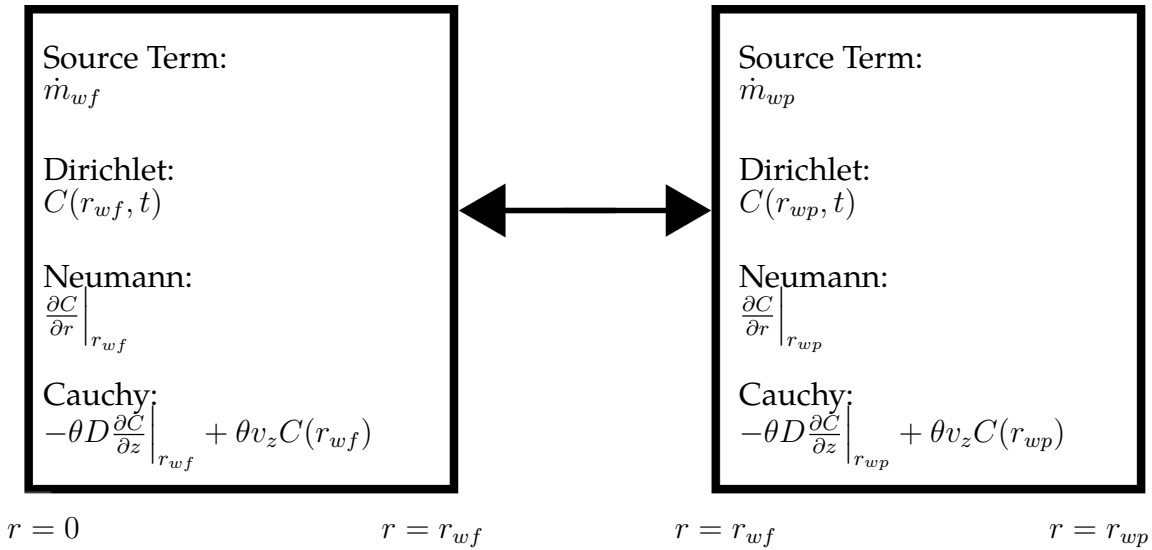
Figure 4.1: The boundaries between components (in this case, waste form (wf) and waste package (wp) components) are robust interfaces defined by Source Term, Dirichlet, Neumann, and Cauchy boundary conditions.

In addition to a specified source term (the zeroth type boundary condition, perhaps), the first, specified-head or Dirichlet type boundary conditions define a specified species concentration on some section of the boundary of the representative volume,

$$
C(\vec{r}, t) = C_0(\vec{r}, t) \ \text{ for } \vec{r} \in \Gamma. \tag{4.2}
$$

The second type, specified-flow or Neumann type boundary conditions describe a full set of concentration gradients at the boundary of the domain,

$$\frac{\partial C(\vec{r}, t)}{\partial r} = \theta D \vec{J}(t) \ \text{ for } \vec{r} \in \Gamma \tag{4.3}$$

where

$$
\begin{aligned}
\vec{r} &= \text{ position vector} \\
\Gamma &= \text{ domain boundary} \\
\vec{J}(t) &= \text{ solute mass flux } [kg/m^2 \cdot s].
\end{aligned}
$$

The third, head-dependent mixed boundary condition or Cauchy type, defines a solute flux along a boundary,

$$-D \frac{\partial C}{\partial z} + v_z C = v_z C(\vec{r}, t) \ \text{ for } \vec{r} \in \Gamma. \tag{4.4}$$

The spatial concentration throughout the volume is sufficient to fully describe implementation of the following nuclide transport models within Cyder. This is supported by the implementation in which vertical advective velocity is uniform throughout the system and in which parameters such as the dispersion coefficient are known for each component. Since this is the case in Cyder, description of the Dirichlet condition is sufficient to fully define calculation of the Neumann and Cauchy type conditions.

Degradation Rate Radionuclide Transport Model

The degradation rate model, simulating the fractional degradation of the material containment properties, is the simplest of implemented models and is most appropriate for simplistic waste package failure modeling.

The materials that constitute the engineered barriers in a saturated repository environment degrade over time. The implemented model of this nuclide release behavior is based solely on a fractional degradation rate. This model incorporates the source term made available on the inner boundary into its available mass and defines the resulting boundary conditions at the outer boundary as solely a function of the degradation rate of that component.

This results in the following expression for the mass transfer, $m_{ij}(t)$, from cell i to cell j at time t:

$$\dot{m}_{ij}(t) = f_i(\cdots) m_i(t) \tag{4.5}$$

where

$$
\begin{aligned}
\dot{m}_{ij} &= \text{ the rate of mass transfer from i to j } [kg/s] \\
f_i &= \text{ fractional degradation rate in cell i } [1/s] \\
m_i &= \text{ mass in cell i } [kg] \\
t &= \text{ time } [s].
\end{aligned}
$$

For a situation as in Cyder and Cyclus, with discrete timesteps, the timesteps are assumed to be small enough to assume a constant rate m_{ij} over the course of the timestep. The mass transferred between discrete times t_{n-1} and t_n is thus a simple linear function of the transfer rate in (4.5),

$$
\begin{aligned}
m_{ij}^n &= \int_{t_{n-1}}^{t_n} \dot{m}_{ij}(t')dt' \\
&= f_i(\cdots)m_i^{n-1}\left(t_n - t_{n-1}\right).
\end{aligned}
\tag{4.6}
$$

The concentration boundary condition must also be defined at the outer boundary to support parent components that utilize the Dirichlet boundary condition. For the degradation model, which incorporates no diffusion or advection, the concentration, C_{ij} at the boundary between cells i and j is the average concentration in the saturated pore volume,

$$
\begin{aligned}
C_{ij}^n &= \frac{m_i^n}{V_{vi}} \\
&= \frac{\text{solute mass in cell i}}{\text{void volume in cell i}}.
\end{aligned}
\tag{4.7}
$$

For the case in which all engineered barrier components are represented by degradation rate models, the source term at the outermost edge will be solely a function of the original central source and the degradation rates of the components.

To support parent components that utilize the Cauchy boundary condition, the degradation model assumes that the fluid velocity is constant across the cell as is the concentration. Thus,

$$
-\theta_i D_{zz}\frac{\partial C}{\partial z}\hat{k} + \theta_i v_z C\hat{k} = \theta_{i0}v_0 C_0\hat{k}
$$

$$
\begin{aligned}
\theta_i &= \text{ porosity in cell i } [-] \\
D_{zz} &= \hat{k} \text{ component diffusion tensor component in } \hat{k} \text{ direction } [m^2/s] \\
C_i &= \text{ concentration in cell i } [kg/m^3] \\
v_z &= \text{ velocity in } \hat{k} \text{ direction } [m/s]
\end{aligned}
$$

reduces to

$$\theta_i^n v_z^n C_i^n = \theta_i^{n-1} v_z^{n-1} C_i^{n-1}. \tag{4.8}$$

Mixed Cell Volume Radionuclide Transport Model

Slightly more complex and suited to representing waste form and buffer components, the mixed cell model incorporates solubility limited, congruent release under the influence of elemental solubility limits, sorption, diffusive behavior, and advective behavior. Abstraction results concerning the transition between primarily diffusive and primarily advective transport regimes were used for benchmarking and to iteratively improve accuracy in the development of this model.

A main nuclide transport component model used in this work is a mixed cell component module incorporating solubility and sorption effects as well as engineered material dissolution.

A graphical representation of the mixed cell model is given in Figures 4.2 and 4.3.
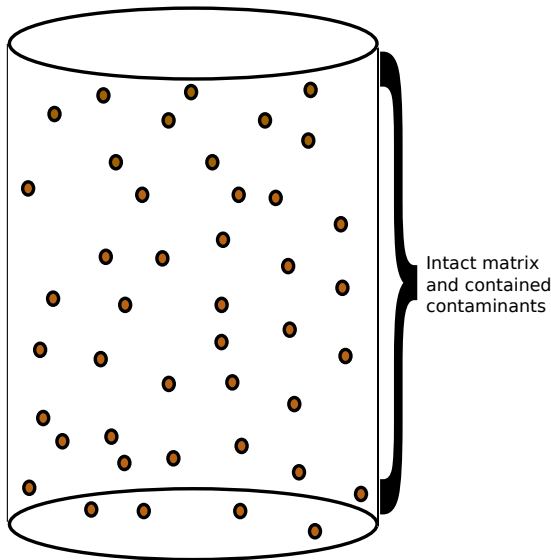
Figure 4.2: The control volume contains an intact material matrix. Contaminants are unavailable to neighboring subcomponents until dissolution has begun.
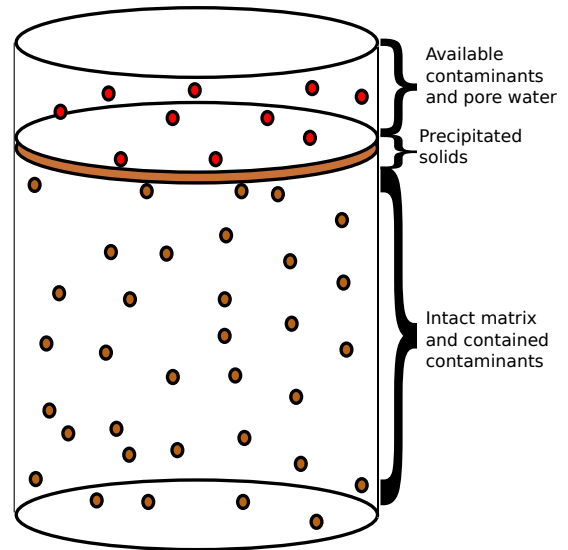
Figure 4.3: Once dissolution begins, the control volume contains a partially dissolved material matrix, contaminated pore water, and degraded and precipitated solids.

After some time degrading, the volume of free fluid can be expressed as

$$V_{ff}(t_n) = \theta V_T \int_{t_0}^{t_n} f(\cdots) dt. \tag{4.9}$$

The volume of the intact matrix can be expressed as

$$V_{im}(t_n) = V_T - V_T \int_{t_0}^{t_n} f(\cdots) dt. \tag{4.10}$$

Finally, the volume of the degraded and precipitated solids can be expressed as

$$V_{ps}(t_n) = (1 - \theta) V_T \int_{t_0}^{t_n} f(\cdots) dt. \tag{4.11}$$

This model assumes that all net influx to the cell enters the free fluid rather than the intact matrix. The total volumetric contaminant concentration in the intact matrix, can be expressed as

$$C_{im}(t_n) = C_0 \tag{4.12}$$

$$= \frac{m_0}{V_{im}(t_0)} \tag{4.13}$$

where

$$m_0 = \text{ total initial mass.}$$

The resulting contaminant mass in the intact matrix at time t_n is

$$m_{im}(t_n) = C_0 V_{im}(t_n)$$

$$= C_0 V_T \left(1 - \int_{t_0}^{t_n} f(\cdots) dt \right). \tag{4.14}$$

The contaminant mass in the free fluid is just the initial pore water concentration times the free fluid volume plus the time integral of net influx to the cell such that

$$C_{ffT}(t_n) = \left[C_0 + \frac{\int_{t_0}^{t_n} \dot{m}_i(t') dt'}{V_{ff}(t_n)} \right] \tag{4.15}$$

and

$$m_{ffT}(t_n) = C_{ff}(t_n) V_{ff}(t_n)$$

$$= \left[C_0 + \frac{\int_{t_0}^{t_n} \dot{m}_i(t') dt'}{V_{ff}(t_n)} \right] V_{ff}(t_n)$$

$$= C_0 V_{ff}(t_n) + \int_{t_0}^{t_n} \dot{m}_i dt'. \tag{4.16}$$

It is limited, however, by both solubility limitation and sorption.

Sorption

The mass in both the free fluid and in the intact matrix exists in both sorbed and non-sorbed phases. The relationship between the sorbed mass concentration in the solid phase (e.g. the pore walls),

$$s = \frac{\text{mass of sorbed contaminant}}{\text{mass of total solid phase}} \tag{4.17}$$

and the dissolved liquid concentration,

$$c = \frac{\text{mass of dissolved contaminant}}{\text{volume of total liquid phase}} \tag{4.18}$$

can be expressed by a number of isotherm models.

In this model, sorption is taken into account throughout the volume. In the intact matrix, the contaminant mass is distributed between the pore walls and the pore fluid by sorption. So too, contaminant mass released from the intact matrix by degradation is distributed between dissolved mass in the free fluid and sorbed mass in the degraded and precipitated solids.

To solve for the boundary conditons in this model, the amount of non-sorbed contaminant mass in the free fluid must be found. This value, m_{ffl}, can be expressed in terms of the total degraded contaminant mass and the contaminant mass in the degraded and precipitated solid,

$$m_{ffl} = m_{ffT} - m_{psc}. \tag{4.19}$$

The mass of contaminant sorbed into the degraded and precipitated solids can be found using a linear isotherm model [74], characterized by the relationship

$$s_i = K_{di}c_i \tag{4.20}$$

where

$$
\begin{aligned}
s_i &= \text{ the solid concentration of isotope i } [kg/kg] \\
K_{di} &= \text{ the distribution coefficient of isotope i} [m^3/kg] \\
c_i &= \text{ the liquid concentration of isotope i } [kg/m^3].
\end{aligned}
$$

Thus, from (4.17),

$$
\begin{aligned}
s_{i,ps} &= \frac{\text{contaminant mass in degraded and precipitated solids}}{\text{total mass of degraded and precipitated solids}} \\
&= \frac{m_{psc}}{m_{psT}} \\
&= \frac{m_{psc}}{m_{psm} + m_{psc}}
\end{aligned}
$$

where

$$m_{psm} = \text{noncontaminant mass in degraded and precipitated solids } [kg]$$
$$= \rho_b V_{ps}$$
$$m_{psc} = \text{contaminant mass in degraded and precipitated solids } [kg]$$
$$\rho_b = \text{bulk (dry) density of the medium } [kg/m^3].$$

<div align="right">(4.21)</div>

The following expression results, giving contaminant mass in the degraded and precipitated solids in terms of the sorption coefficient,

$$
\begin{aligned}
m_{psc} &= s_{ps} m_{psT} \\
&= K_d C_{ffl} m_{psT} \\
&= \frac{K_d m_{ffl} m_{psT}}{V_{ff}} \\
&= \frac{K_d}{V_{ff}} (m_{ffT} - m_{psc}) m_{psT} \\
&= \frac{K_d}{V_{ff}} (m_{ffT} - m_{psc})(m_{psm} + m_{psc}) \\
&= \frac{K_d}{V_{ff}} (m_{ffT} m_{psm} - m_{psc} m_{psm} + m_{ff} m_{psc} - m_{psc}^2) \\
&= \frac{K_d}{V_{ff}} (m_{ffT} m_{psm} + (m_{ffT} - m_{psm}) m_{psc} - m_{psc}^2)
\end{aligned}
$$

which, rearranged, becomes

$$0 = m_{psc}^2 + \left(-m_{ffT} + m_{psm} + \frac{V_{ff}}{K_d} \right) m_{psc} - m_{ffT} m_{psm}$$

and is solved using the quadratic formula, such that

$$m_{psc} = \frac{m_{ffT} - m_{psm} - \frac{V_{ff}}{K_d}}{2} \pm \frac{\sqrt{\left(-m_{ffT} + m_{psm} + \frac{V_{ff}}{K_d} \right)^2 - 4 m_{ffT} m_{psm}}}{2}$$

which, again rearranged, becomes

$$
= \frac{1}{2} \left(m_{ffT} - m_{psm} - \frac{V_{ff}}{K_d} \right)
$$
$$
\pm \frac{1}{2} \sqrt{ m_{ffT}^2 + 2 m_{ffT} \left(m_{psm} - \frac{V_{ff}}{K_d} \right) + \left(m_{psm} + \frac{V_{ff}}{K_d} \right)^2 }.
$$

<div align="right">(4.22)</div>

Plugging (4.22) into (4.19) results in the following expression for m_{ffl} in terms of known quantities

$$m_{ffl} = m_{ffT} - \frac{1}{2}\left(m_{ffT} - m_{psm} - \frac{V_{ff}}{K_d}\right)$$
$$\mp \frac{1}{2}\sqrt{m_{ffT}^2 + 2m_{ffT}\left(m_{psm} - \frac{V_{ff}}{K_d}\right) + \left(m_{psm} + \frac{V_{ff}}{K_d}\right)^2}. \tag{4.23}$$

Solubility

In addition to engineered barriers, contaminant transport is constrained by the solubility limit [35],

$$m_{s,i} \leq V_w C_{sol,i}, \tag{4.24}$$

where

$$m_{s,i} = \text{ solubility limited mass of isotope i in volume } V_w [kg]$$
$$V_w = \text{ volume of the solution } [m^3]$$
$$C_{sol,i} = \text{ solubility limit, the maximum concentration of i } [kg/m^3].$$

The desired boundary conditions can be expressed in terms of m_{ffl}. First, the Dirichlet boundary condition is

$$C(x, y, z, t) = \frac{m_{ffl}(t)}{V_{ff}(t)} \forall (x, y, x) \in \Gamma. \tag{4.25}$$

From this boundary condition in combination with global advective velocity data, all other boundary conditions can be found.

Lumped Parameter Radionuclide Transport Model

The response function model implemented interchangeable piston flow, exponential, and dispersion response functions [55]. For systems in which the flow is sufficiently slow to be assumed constant over a timestep, it is possible to model a system of volumes as a connected lumped parameter models (Figure 4.4).

The method by which each lumped parameter component is modeled is according to a relationship between the incoming concentration, $C_{in}(t)$, and the outgoing concentration, $C_{out}(t)$,

$$C_{out}(t) = \int_{-\infty}^{t} C_{in}(t')g(t - t')e^{-\lambda(t-t')}dt' \tag{4.26}$$
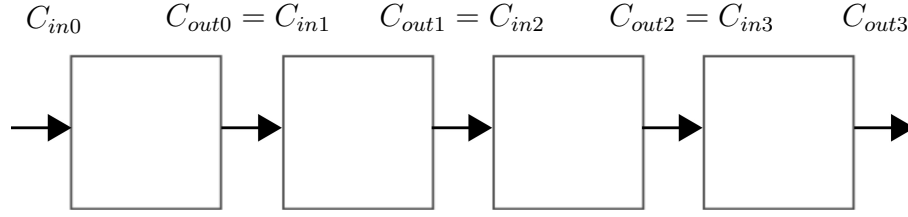
Figure 4.4: A system of volumes can be modeled as lumped parameter models in series.

equivalently

$$C_{out}(t) = \int_0^\infty C_{in}(t - t')g(t')e^{-\lambda t'}dt' \tag{4.27}$$

where

$$
\begin{aligned}
t' &= \text{ time of entry } [s] \\
t - t' &= \text{ transit time } [s] \\
g(t - t') &= \text{ response function, a.k.a. transit time distribution}[-]] \\
\lambda &= \text{ radioactive decay constant, 1 to neglect}[s^{-1}].
\end{aligned}
$$

Selection of the response function is usually based on experimental tracer results in the medium at hand. However, some functions used commonly in chemical engineering applications [55] include the Piston Flow Model (PFM),

$$g(t') = \delta(t' - t_t)) \tag{4.28}$$

the Exponential Model (EM)

$$g(t') = \frac{1}{t_t}e^{-\frac{t'}{t_t}} \tag{4.29}$$

and the Dispersion Model (DM),

$$g(t') = \left(\frac{Pe\, t_t}{4\pi t'}\right)^{\frac{1}{2}}\frac{1}{t'}e^{-\frac{Pe\, t_t\left(1 - \frac{t'}{t_t}\right)^2}{4t'}}, \tag{4.30}$$

where

$$
\begin{aligned}
Pe &= \text{ Peclet number for mass diffusion } [-] \\
t_t &= \text{ mean tracer age } [s] \\
&= t_w \text{ if there are no stagnant areas} \\
t_w &= \text{ mean residence time of water } [s] \\
&= \frac{V_m}{Q} \\
&= \frac{z}{v_z} \\
&= \frac{z\theta_e}{q}
\end{aligned}
$$

in which

$$
\begin{aligned}
V_m &= \text{ mobile water volume } [m^3] \\
Q &= \text{ volumetric flow rate } [m^3/s] \\
z &= \text{ average travel distance in flow direction } [m] \\
v_z &= \text{ mean water velocity} [m/s] \\
q &= \text{ Darcy Flux } [m/s] \\
\theta_e &= \text{ effective (connected) porosity } [\%].
\end{aligned}
$$

The latter of these, the Dispersion Model satisfies the one dimensional advection-dispersion equation, and is therefore the most physically relevant for this application. The solutions to these for constant concentration at the source boundary are given in [55],

$$
C(t) = \begin{cases}
PFM & C_0 e^{-\lambda t_t} \\
EM & \frac{C_0}{1 + \lambda t_t} \\
DM & C_0 e^{\frac{Pe}{2}\left(1 - \sqrt{1 + \frac{4\lambda t_t}{Pe}}\right)}.
\end{cases}
\tag{4.31}
$$

One Dimensional Permeable Porous Medium Radionuclide Transport Model

Finally, abstraction results informed modifications to the implementation of an analytic solution to the one dimensional advection-dispersion equation with finite domain and Cauchy and Neumann boundary conditions at the inner and outer boundaries, respectively.

Various solutions to the advection dispersion equation (4.1) have been published for both the first and third types of boundary conditions. The third, Cauchy type, is mass conservative, and will be the primary kind of boundary condition used at the source for this model.

The conceptual model in Figure 4.5 represents solute transport in one dimension with unidirectional flow upward (a conservative assumption) and a semi-infinite boundary condition in the positive flow direction. The solution is given (Leij et. al, [50]) and described below.
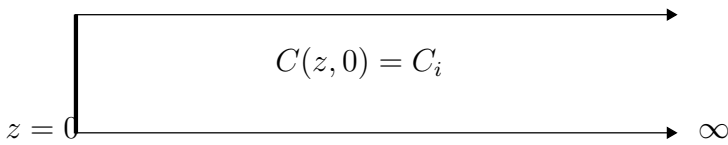
$$-D\frac{\partial C}{\partial z}\Big|_{z=0} + v_z C = \begin{cases} v_z C_0 & t < t_0 \\ 0 & t > t_0 \end{cases} \qquad\qquad \frac{\partial C}{\partial z}\Big|_\infty = 0$$

$$C(z,0) = C_i$$

$$z = 0 \qquad\qquad\qquad\qquad\qquad\qquad\qquad \infty$$

Figure 4.5: A one dimensional, semi-infinite model, unidirectional flow, solution with Cauchy and Neumann boundary conditions

For the boundary conditions,

$$-D\frac{\partial C}{\partial z}\Big|_{z=0} + v_z c = \begin{cases} v_z C_0 & (0 < t < t_0) \\ 0 & (t > t_0) \end{cases}, \tag{4.32}$$

$$\frac{\partial C}{\partial z}\Big|_{z=\infty} = 0 \tag{4.33}$$

and the initial condition,

$$C(z,0) = C_i, \tag{4.34}$$

the solution is given as

$$C(z,t) = \frac{C_0}{2}\left[\operatorname{erfc}\left[\frac{L - v_z t}{2\sqrt{D_L t}}\right] + \frac{1}{2}\left(\frac{v_z^2 t}{\pi D_L}\right)^{1/2} e^{\frac{-(L-v_z t)^2}{4 D_L t}} \right.$$

$$\left. - \frac{1}{2}\left(1 + \frac{v_z L}{D_L} + \frac{v_z^2 t}{D_L}\right) e^{\frac{v_z L}{D_L}} \operatorname{erfc}\left[\frac{L - V_z t}{2\sqrt{D_L t}}\right]\right]. \tag{4.35}$$

Implications For Waste Form Modeling

Though the Waste Form Component can be modeled by any of the available Nuclide-Models, the Degradation Rate based or Mixed Cell radionuclide transport models are

preferred for modeling of the Waste Form Component. This is because, in repository performance assessments, waste form dissolution is typically modeled as instantaneous or rate based. Dissolution related release is historically modeled as congruent, solubility limited, or both, with some radionuclides becoming immediately accessible, and some tending to remain in the fuel matrix.

Implications For Waste Package Modeling

Though the Waste Package Component can be modeled by any of the available Nuclide-Models, the simple Degradation Rate based model is strongly preferred. Waste package time to failure is dependent on water contact and heat, but is historically modeled probabilistically, or at a constant rate. Accordingly, waste package degradation in repository performance is either neglected entirely, instantaneous and complete (a delay before full release), or partial and constant (a constantly present hole in the package).

Implications For Buffer Modeling

Diffusion is the primary mechanism for nuclide transport through the buffer Component of the repository system. While the buffer may degrade, the near field has historically been modeled in as much hydrologic detail as possible. For this reason, the Lumped Parameter or One Dimensional Permeable Porous Medium nuclide transport models are preferred.

Implications for Geologic Environment Modeling

In most of the saturated, low permeability environments being considered, diffusion is the primary mechanism for nuclide transport through the geologic medium Component of the repository system. While the near field may degrade, the far field should be modeled in detail if possible. For this reason, the One Dimensional Permeable Porous Medium nuclide transport model is preferred.

4.2   Thermal Transport in Cyder

An algorithm and supporting database for rapid thermal repository capacity calculation was implemented in Cyder. This algorithm employs a Specific Temperature Change (STC) method [70, 69] and has resulted from combining detailed spent nuclear fuel composition data [20] with a detailed thermal repository performance analysis tool from Lawrence Livermore National Laboratory (LLNL) and the UFD campaign [32]. By abstraction of and benchmarking against these detailed thermal models, Cyder captures the dominant physics of thermal phenomena affecting repository capacity in various geologic media and as a function of spent fuel composition.

Abstraction based on detailed computational thermal repository performance calculations with the LLNL analytic model has resulted in implementation of the STC estimation algorithm and a supporting reference dataset. This method is capable of rapid estimation of temperature increase near emplacement tunnels as a function of waste composition, limiting radius, r_{lim}, waste package spacing, S, near field thermal conductivity, K_{th}, and near field thermal diffusivity, α_{th}.

Specific Temperature Change Method

Introduced by Radel, Wilson et al., the STC method uses a linear approximation to arrive at the thermal loading density limit [69, 70]. Since the thermal response in a system with a long term transient response is strong function of the transient decay power, it is also a strong function of the isotopic composition of the waste. Thus, the time dependent temperature change, ΔT, at the limiting radius, r_{lim}, can be approximated as proportional to the mass loading density. First, ΔT is determined for a limiting loading density of the particular material composition then it is normalized to a single kilogram of that material, Δt, the so called STC.

$$\Delta T(r_{lim}) = m \cdot \Delta t(r_{lim}) \tag{4.36}$$

where

$$\begin{aligned}
\Delta T &= \text{ Temperature change due to m } [^\circ K] \\
m &= \text{ Mass of heat generating material } [kg] \\
\Delta t &= \text{ Temperature change due to 1 kg } [^\circ K] \\
r_{lim} &= \text{ Limiting radius } [m].
\end{aligned}$$

For an arbitrary waste stream composition, scaled curves, Δt_i, calculated in this manner for individual isotopes can be superimposed for each isotope to arrive at an approximate total temperature change.

$$\Delta T(r_{lim}) \sim \sum_i m_i \Delta t_i(r_{lim}) \tag{4.37}$$

where

$$\begin{aligned}
i &= \text{ An isotope in the material } [-] \\
m_i &= \text{ mass of isotope i } [kg] \\
\Delta t_i &= \text{ Specifc temperature change due to } i \ [^\circ K].
\end{aligned}$$

Supporting Thermal Response Dataset

To support this calculation in Cyder, a reference data set of temperature change curves was calculated. Repeated runs of a detailed analytic model over the range of values in Table 4.1 determined STC values over a range of thermal heat limit radii, r_{lim}, thermal diffusivity values, α_{th}, thermal conductivity values, K_{th} and waste package spacings, S. Linear interpolation across the discrete parameter space provides a simple thermal reference dataset for use in Cyder.

<div align="center">

Thermal Cases

Parameter	Symbol	Units	Value Range
Diffusivity	α_{th}	$[m^2 \cdot s^{-1}]$	$1.0 \times 10^{-7} - 3.0 \times 10^{-6}$
Conductivity	K_{th}	$[W \cdot m^{-1} \cdot K^{-1}]$	$0.1 - 4.5$
Spacing	S	$[m]$	2, 5, 10, 15, 20, 25, 50
Radius	r_{lim}	$[m]$	0.1, 0.25, 0.5, 1, 2, 5
Isotope	i	$[-]$	$^{241,243}Am,$ $^{242,243,244,245,246}Cm,$ $^{238,240,241,242}Pu$ $^{134,135,137}Cs$ ^{90}Sr

</div>

Table 4.1: A thermal reference dataset of STC values as a function of each of these parameters was generated by repeated parameterized runs of the LLNL MathCAD model[32, 31].

The analytic model used to populate the reference dataset was created at LLNL for the UFD campaign. In this tool, heat limited thermal response is calculated analytically for each geology, for many waste package loading densities, and for many fuel cycle options [34, 31, 32]. It employs an analytic model from Carslaw and Jaeger and is implemented in MathCAD [19, 67]. The integral solver in the MathCAD toolset is the primary calculation engine for the analytic MathCAD thermal model, which relies on superposition of point, finite-line, and line source integral solutions.

Figure 4.6 demonstrates the scaling of an STC curve according to equation (4.36) to represent the heat from $25.9g$ of initial ^{242}Cm using the reference data set.

The supporting database was limited to some primary heat contributing isotopes present in traditional spent nuclear fuel, H, such that the superposition in equation (4.37) becomes

$$\Delta T(r_{lim}, S, K_{th}, \alpha_{th}) \sim \sum_{i \in H} m_i \Delta t_i(r_{lim}, S, K_{th}, \alpha_{th}) \tag{4.38}$$
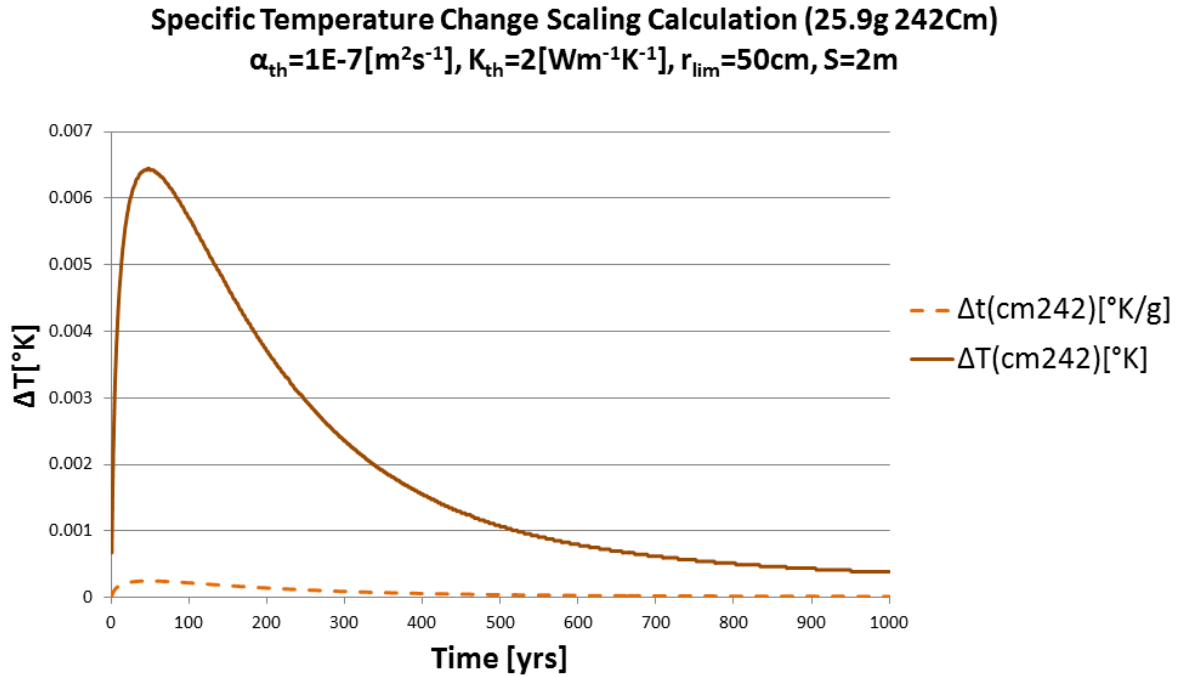
Figure 4.6: As a demonstration of the calculation procedure, the temperature change curve for one initial gram of ^{242}Cm and is scaled to represent $25.9g$, approximately the ^{242}Cm inventory per MTHM in 51GWd burnup UOX PWR fuel.

where

$$
\begin{aligned}
H &= \text{set of high heat isotopes } [-] \\
S &= \text{uniform waste package spacing } [m] \\
K_{th} &= \text{thermal conductivity } [W \cdot m^{-1} \cdot K^{-1}] \\
\alpha_{th} &= \text{thermal diffusivity } [m^2 \cdot s^{-1}]
\end{aligned}
$$

$$(4.39)$$

The use of this superposition is demonstrated in Figure 4.7.

The primary outcome of this work is a mulitdimensional database of repository temperature change per mass of high heat contributing isotopes supporting the implementation of the STC method in Cyder.

A validation effort concerning this tool was performed to assess the validity of the STC method for the purpose of repository thermal response estimation. Comparison of the results of this method with the LLNL model [32] gave appropriately accurate results and demonstrated the way in which inaccuracies from neglected low heat contributing nuclides are bounded. Figure 4.8 shows the results of one example validation exercise
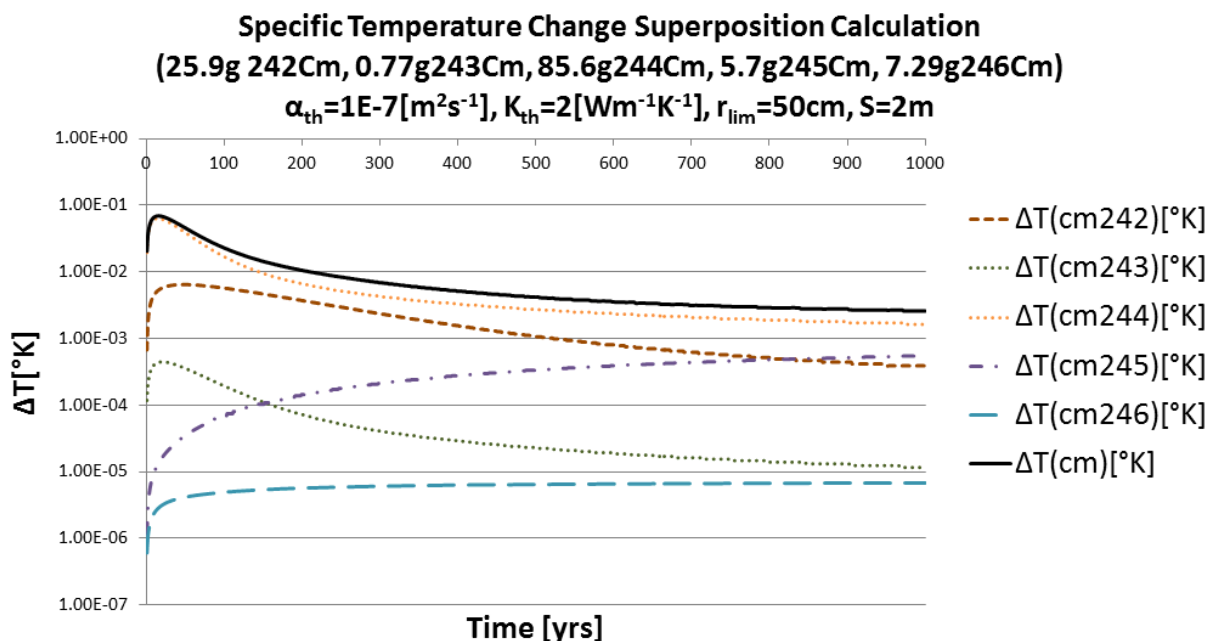
Figure 4.7: As a demonstration of the calculation procedure, scaled temperature change curves for five curium isotopes are superimposed to achieve a total temperature change (note log scale).

comparing the combined scaling and superposition calculations demonstrated in Figures 4.6 and 4.7 respectively. This particular validation example, containing no neglected nuclides, demonstrates an average error of 1.1% and a maximum error of 4.4%.

In addition to this validation effort, continual verification of code behavior is enabled by a suite of unit tests packaged with the tool. These tests may continually be performed to evaluate the implemented behavior of units of functionality within the interpolation and specific temperature change algorithms even as the code is improved in the future.

Specific Temperature Change to LLNL Comparison
(25.9g 242Cm, 0.77g243Cm, 85.6g244Cm, 5.7g245Cm, 7.29g246Cm)
α_{th}=1E-7[m^2s^{-1}], K_{th}=2[$Wm^{-1}K^{-1}$], r_{lim}=50cm, S=2m
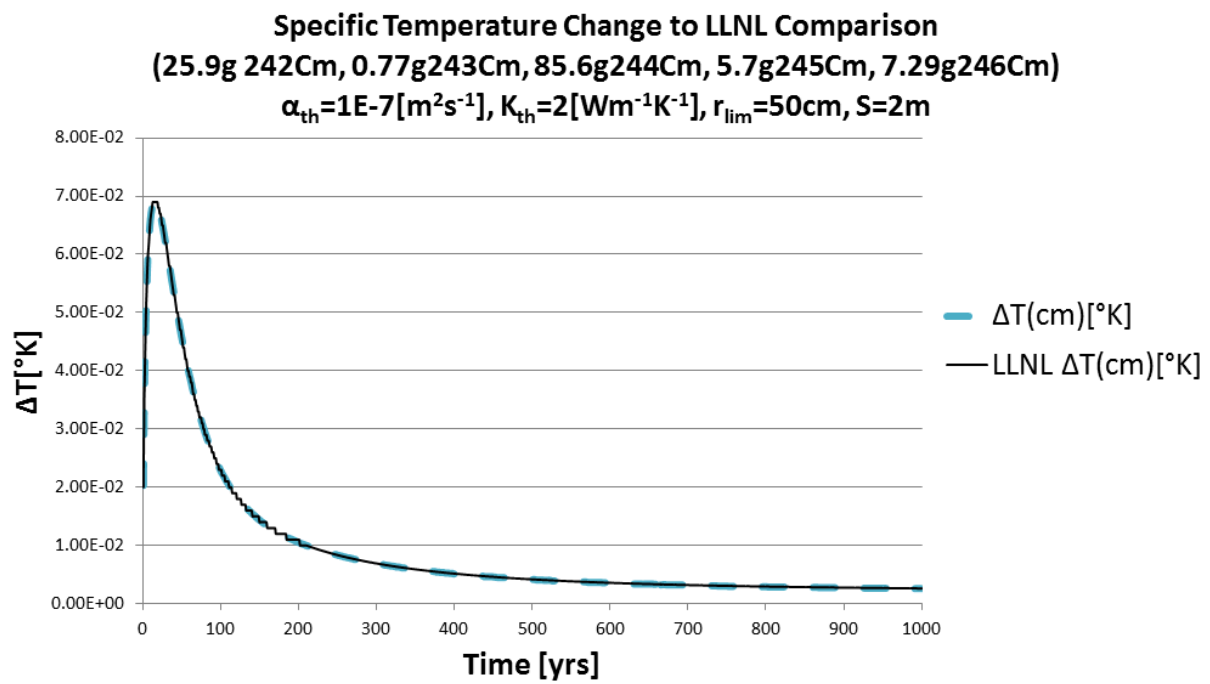
Figure 4.8: This comparison of STC calculated thermal response from Cm inventory per MTHM in 51GWd burnup UOX PWR fuel compares favorably with results from the analytical model from LLNL.

5 DEMONSTRATION CASES AND BENCHMARKING

5.1 Nuclide Model Base Cases

No Release

Degradation Rate Model

Mixed Cell Model

Lumped Parameter Model

One Dimensional Advecitive Dispersive Model

Basic Transport

Degradation Rate Model

Mixed Cell Model

Lumped Parameter Model

One Dimensional Advecitive Dispersive Model

5.2 Nuclide Model Benchmarks

As described in Section 4.1, hydrologic contaminant transport in Cyder is implemented with four interchangeable methods in a modular software design. These modeling options alternately optimize speed and fidelity in representations of barrier components within the repository concept (i.e. waste form, waste package, buffer, near field geology, and far field geology)[41]. Simplistic models include a congruent release component degradation model and a mixed cell control volume model. For systems in which the flow can be assumed constant, a medium fidelity lumped parameter dispersion model is implemented. Also implemented is a Leij et al. solution to the advection dispersion equation for Cauchy boundary condition [50, 30].

Analyses in Table 5.1 were conducted to compare the performance of these radionuclide transport models with more detailed results from the Clay Generic Disposal Sytem Environment (GDSE).

Radionuclide Transport Benchmark Cases

Parameter	Symbol	Units	Value Range
Disposal Inventory			
Hydraulic Reference Diffusivity	$\alpha_{h,ref}$	$[m^2 s]$	$10^8 - 10^{15}$
Hydraulic Conductivity	K_h	$[m \cdot s^{-1}]$	$10^{-13} - 10^{-3}$
Advective Water Velocity	v_{adv}	$[m \cdot s^{-1}]$	$2 \times 10^{-16} - 2 \times 10^{-12}$
Sorption & Behavior	$K_{d,i}$	$[m^3 \cdot kg^{-1}]$	Reducing - Oxidizing
Solubility Limitation	$C_{sol,i}$	$[kg \cdot m^{-3}3]$	Reducing - Oxidizing
WF Degradation Rate			
WP Failure Time			

Table 5.1: The sensitivity analyses conducted in this work covered a range of thermal and hydrologic geology parameters in the context of canonical fuel cycle choices.

Case I : Diffusion Coefficient and Inventory Sensitivity

Case II : Vertical Advective Velocity and Diffusion Coefficient Sensitivity

Case III : Solubility Sensitivity

Case IV : Sorption Sensitivity

Case V : Waste Form Degradation Rate and Inventory Sensitivity

Case VI : Waste Package Failure Time and Diffusion Coefficient Sensitivity

5.3   Thermal Transport Base Cases

5.4   Thermal Benchmarking

For dynamic thermal capacity analysis in Cyder, a transient model utilizes a linear approximation of heat based capacity quickly for each arbitrary waste stream offered to

the repository. As described in section 4.2, this relies on a thermal reference database of repository heat evolution curves covering the thermal coefficient range of the main geologies of interest and over a range of realistic waste package spacings.

Analyses in Table 5.2 were conducted to compare the performance of these thermal models with more detailed results from the LLNL analytical MathCAD model.

Heat Transport Benchmarking Cases

Parameter	Symbol	Units	Value Range
Disposal Inventory			
Thermal Diffusivity	α_{th}	$[m^2 \cdot s^{-1}]$	$1.0 \times 10^{-7} - 3.0 \times 10^{-6}$
Thermal Conductivity	K_{th}	$[W \cdot m^{-1} \cdot K^{-1}]$	$0.1 - 4.5$
Package Spacing	S	$[m]$	2-50
Thermal Limiting Radius	r_{lim}	$[m]$	0.1-5

Table 5.2: The sensitivity analyses conducted in this work covered a range of thermal and hydrologic geology parameters in the context of canonical fuel cycle choices.

5.5 System Level Cases

6 CONCLUSIONS

6.1 Contributions

This work has provided a repository anaylsis module for fuel cycle analysis that is the first of its kind. That is, it provides the first generic geology repository model integrated dynamically within a fuel cycle simulation code.

The Cyder source code in which these models are implemented as well as associated documentation are freely available to interested researchers and potential model developers. The application programming interface to this software library is intentionally general, facilitating the incorporation of the models presented here within external software tools in need of a multicomponent repository model.

Furthermore, this work contributes to an expanding ecosystem of computational models available for use with the Cyclus fuel cycle simulator. This hydrologic nuclide transport library, by virtue of its capability to modularly integrate with the Cyclus fuel cycle simulator has laid the foundation for integrated disposal option analysis in the context of fuel cycle options.

6.2 Suggested Future Work

A   RADIONUCLIDE TRANSPORT SENSITIVITY ANALYSIS

The four GDSMss developed by the UFD campaign facilitate sensitivity analysis of the long-term post-closure performance of geologic repositories in generic media with respect to various key processes and parameters [21]. Processes and parameters expected to be influential to repository performance include the rate of waste form degradation, timing of waste package failure, and various coupled geochemical and hydrologic characteristics of the natural system including diffusion, solubility, and advection.

The results here provide an overview of the relative importance of processes that affect the repository performance of simplified generic disposal concepts. This work is not intended to give an assessment of the performance of a disposal system. Rather, it is intended to generically identify properties and parameters expected to influence repository performance in each geologic envrionment.

A.1   Approach

This analysis utilized four GDSMs developed by the UFD campaign to represent clay, granite, salt, and deep borehole repository concepts. Each GDSM performs detailed calculations of radionuclide transport within its respective geology [21].

The radionuclide transport calculations for the geologically distinct models are performed within the GoldSim simulation platform. GoldSim is a commercial simulation environment [? ?]. Probabilistic elements of the GoldSim modelling framework enable the models to incorporate simple probabilistic Features, Events, and Processes (FEPs) that affect repository performance including waste package failure, waste form dissolution, and an optional vertical advective fast pathway [21].

The GoldSim framework and its contaminant transport module provide a simulation framework and radionuclide transport toolset that the GDSMs have utilized to simulate chemical and physical attenuation processes including radionuclide solubility, dispersion phenomena, and reversible sorption [? ?].

A.2   Mean of the Peak Annual Dose

In this analysis, repository performance is quantified by radiation dose to a hypothetical receptor. Specifically, this sensitivity analysis focuses on parameters that affect the mean of the peak annual dose. The mean of the peak annual dose,

$$D_{MoP,i} = \frac{\sum_{r=1}^{N} \max\left[D_{r,i}(t)|_{\forall t} \right]}{N} \tag{A.1}$$

where

$$D_{MoP,i} = \text{mean of the peak annual dose due to isotope i}[mrem/yr]$$
$$D_i(t) = \text{annual dose in realization r at time t due to isotope i } [mrem/yr]$$
$$N = \text{Number of realizations,}$$

is a conservative metric of repository performance. The mean of the peak annual dose should not be confused with the peak of the mean annual dose,

$$D_{PoM,i} = \max \left[\frac{\sum_{r=1}^{N} D_{r,i}(t)|_{\forall t}}{N} \right] \tag{A.2}$$

$$= \text{peak of the mean annual dose due to isotope i } [mrem/yr].$$

The mean of the peak annual dose rate given in equation (A.1) captures trends as well as the peak of the mean annual dose rate given in equation (A.2). However, the mean of the peaks metric, $D_{MoP,i}$, was chosen in this analysis because it is more conservative since it is able to capture temporally local dose maxima and consistently reports higher dose values than the peak of the means, $D_{PoM,i}$.

A.3   Sampling Scheme

The multiple barrier system modeled in the clay GDSM calls for a multi-faceted sensitivity analysis. The importance of any single component or environmental parameter must be analyzed in the context of the full system of barrier components and environmental parameters. Thus, this analysis has undertaken an analysis strategy to develop a many dimensional overview of the key factors in modeled repository performance.

To address this, both individual and dual parametric studies were performed. Individual parameter studies varied a single parameter of interest in detail over a broad range of values. Dual parameter sensitivity studies were performed for pairs of parameters expected to exhibit some covariance. For each parameter or pair of parameters, forty simulation groups varied the parameter or parameters within the range considered. Example tables of the resulting forty simulation groups for individual and dual parametric study configurations appear in Tables A.1 and A.2 respectively.

For each simulation group, a 100 realization simulation was completed. Each realization held the parameters being analyzed as constant and sampled stochastic values for uncertain parameters not being studied. A sampling scheme developed in previous generic disposal media modeling was implemented in this model in order to ensure that the each 100 realization simulation sampled identical values for uncertain parameters [21?].

In order to independently analyze the dose contributions from radioisotope groups, four cases,

Individual Parameter Study

	P_1	Group 1
	P_2	Group 2
	P_3	Group 3
P	.	.
	.	.
	.	.
	P_{40}	Group 40

Table A.1: For an individual one group of 100 realizations was run for each each discrete value, P_i, within the range considered for P.

Dual Parameter Study

		Q_1	Q_2	Q_3	Q_4	Q_5
				Q		
	P_1	Group 1	Group 2	Group 3	Group 4	Group 5
	P_2	Group 6	Group 7	Group 8	Group 9	Group 10
	P_3	Group 11	Group 12	Group 13	Group 14	Group 15
P	P_4	Group 16	Group 17	Group 18	Group 19	Group 20
	P_5	Group 21	Group 22	Group 23	Group 24	Group 25
	P_6	Group 26	Group 27	Group 28	Group 29	Group 30
	P_7	Group 31	Group 32	Group 33	Group 34	Group 35
	P_8	Group 36	Group 37	Group 38	Group 39	Group 40

Table A.2: The simulation groups for a dual simulation sample each parameter within the range over which it was considered.

- Americium and its daughters,

- Plutonium and its daughters,

- Uranium and its daughters,

- Neptunium, its daughters, and fission products

were run independently. This allowed an evaluation of the importance of daughter production from distinct actinide chains.

A.4   Clay

These analyses were performed using the Clay GDSM developed by the UFD campaign[21]. The Clay GDSM is built on the GoldSim software and tracks the movement of key radionuclides through the natural system and engineered barriers [? ?].

The disposal concept modeled by the Clay GDSM includes an Engineered Barrier System (EBS) which can undergo rate based dissolution and barrier failure. Releases from the EBS enter near field and subsequently far field host rock regions in which

diffusive and advective transport take place, attenuated by solubility limits as well as sorption and dispersion phenomena.

The Clay GDSM models a single waste form, a waste package, additional EBSs, an Excavation Disturbed Zone (EDZ), and a far field zone using a batch reactor mixing cell framework. This waste unit cell is modeled with boundary conditions such that it may be repeated assuming an infinite repository configuration. The waste form and engineered barrier system are modeled as well-mixed volumes and radial transport away from the cylindrical base case unit cell is modeled as one dimensional. Two radionuclide release pathways are considered. One is the nominal, undisturbed case, while the other is a fast pathway capable of simulating a hypothetical disturbed case [21].

Vertical Advective Velocity

Transport out of the EBS and through the permeable, porous geosphere involves advection, diffusion, and hydraulic dispersion phenomena. Advection is transport driven by bulk water velocity, while diffusion is the result of Brownian motion across concentration gradients. The method by which the dominant solute transport mode (diffusive or advective) is determined for a particular porous medium is by use of the dimensionless Peclet number,

$$Pe = \frac{nvL}{\alpha nv + D_{eff}},$$
$$= \frac{\text{advective rate}}{\text{diffusive rate}}$$

(A.3)

where

$$n = \text{solute accessible porosity } [\%]$$
$$v = \text{advective velocity } [m \cdot s^{-1}]$$
$$L = \text{transport distance } [m]$$
$$\alpha = \text{dispersivity } [m]$$
$$D_{eff} = \text{effective diffusion coefficient } [m^2 \cdot s^{-1}].$$

For a high Pe number, advection is the dominant transport mode, while diffusive or dispersive transport dominates for a low Pe number [74].

In this analysis, the threshold between primarily diffusive and primarily advective transport was investigated by varying the vertical advective velocity in conjunciton with the diffusion coefficient. It was expected that for the low diffusion coefficients and low advective velocities usually found in clay media, the model should behave entirely in the diffusive regime, but as the vertical advective velocity grows, system behavior should increasingly approach the advective regime.

Parametric Range

The diffusion coefficient was altered as in section A.4 and the vertical advective velocity of the far field was altered as well.

From Table 5.5-1 of the Argile Safety Evaluation by ANDRA, the vertical hydraulic gradient is 0.4, while the hydraulic conductivity is $5.0 \times 10^{14}[m/s]$. The resulting vertical advective velocity is then $2.0 \times 10^{-14}[m/s]$, which is $6.31 \times 10^{-7}[m/yr]$ [8].

As in section A.4, in order to isolate the effect of the far field behavior, the waste form degradation rate was set to be very high as were the solubility and advective flow rate through the EBS. This guarunteed that in the first few time steps, the far field was the primary barrier to release.

The forty runs are a combination of the five values of the vertical advective velocity and eight magnitudes of relative diffusivity (see Table A.3).

		Vertical Advective Velocity [m/yr]				
		6.31E-08	6.31E-07	6.31E-06	6.31E-05	6.31E-04
		Groupings				
Reference Diffusivity (m^2/s)	1.E-08	1	2	3	4	5
	1.E-09	6	7	8	9	10
	1.E-10	11	12	13	14	15
	1.E-11	16	17	18	19	20
	1.E-12	21	22	23	24	25
	1.E-13	26	27	28	29	30
	1.E-14	31	32	33	34	35
	1.E-15	36	37	38	39	40

Table A.3: Vertical advective velocity and diffusion coefficient simulation groupings.

To capture the importance of the vertical advective velocity, a range was chosen to span a number of orders of magnitude between 6.31×10^{-8} and $6.31 \times 10^{-4}[m/yr]$. The relative diffusivity was simultaneously varied over the eight magnitudes between 10^{-8} and $10^{-15}[m^2/s]$. It is worth noting that both the relative diffusivity and the vertical advective velocity are functions of porosity in the host rock and are therefore expected to vary together.

Results

For isotopes of interest, higher advective velocity and higher diffusivity lead to higher means of the peak annual dose. However, the relationship between diffusivity and advective velocity adds depth to the notion of a boundary between diffusive and advective regimes.

The highly soluble and non-sorbing elements, I and Cl were expected to exhibit behavior that is highly sensitive to advection in the system in the advective regime but less sensitive to advection in the diffusive regime.

In Figures A.1, A.2, A.3, and A.4 , ^{129}I and ^{36}Cl are more sensitive to vertical advective velocity for lower vertical advective velocities. This demonstrates that for vertical advective velocities $6.31 \times 10^{-6}[m/yr]$ and above, lower reference diffusivities are ineffective at attenuating the mean of the peak doses for soluble, non-sorbing elements.

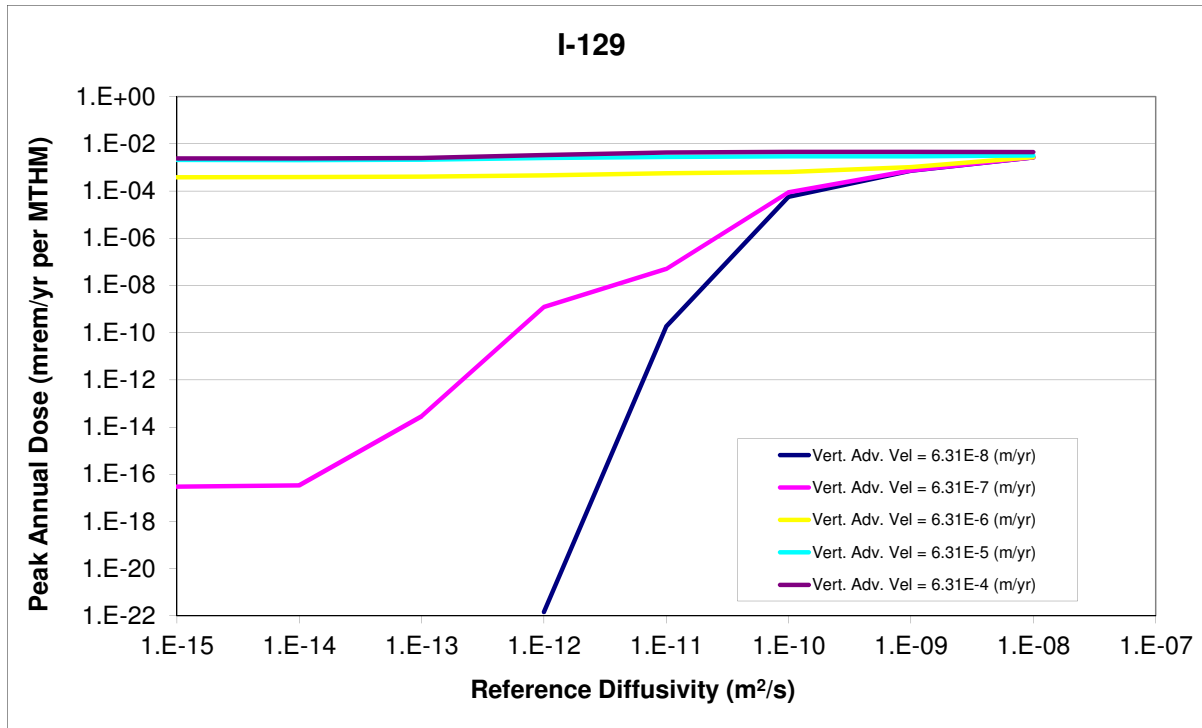Figure A.1: ^{129}I reference diffusivity sensitivity.

The solubility limited and sorbing elements, Tc and Np, in Figures A.5, A.6, A.7, and A.8 show a very weak influence on peak annual dose rate for low reference diffusivities, but show a direct proportionality between dose and reference diffusivity above a threshold. For ^{99}Tc, for example, that threshold occurs at $1 \times 10^{-11}[m^2/s]$.

Dose contribution from ^{99}Tc has a proportional relationship with vertical advective velocity above a regime threshold at $6.31 \times 10^{-5}[m/yr]$, above which the system exhibits sensitivity to advection.

The convergence of the effect of the reference diffusivity and vertical advective velocity for the cases above shows the effect of dissolved concentration (solubility) limits and sorption. Se is non sorbing, but solubility limited. The results from ^{79}Se in Figure A.9 and A.10 show that for low vertical advective velocity, the system is diffusion dominated. However, for high vertical advective velocity, the diffusivity remains important even in the advective regime as spreading facilitates transport in the presence of solubility limited transport.
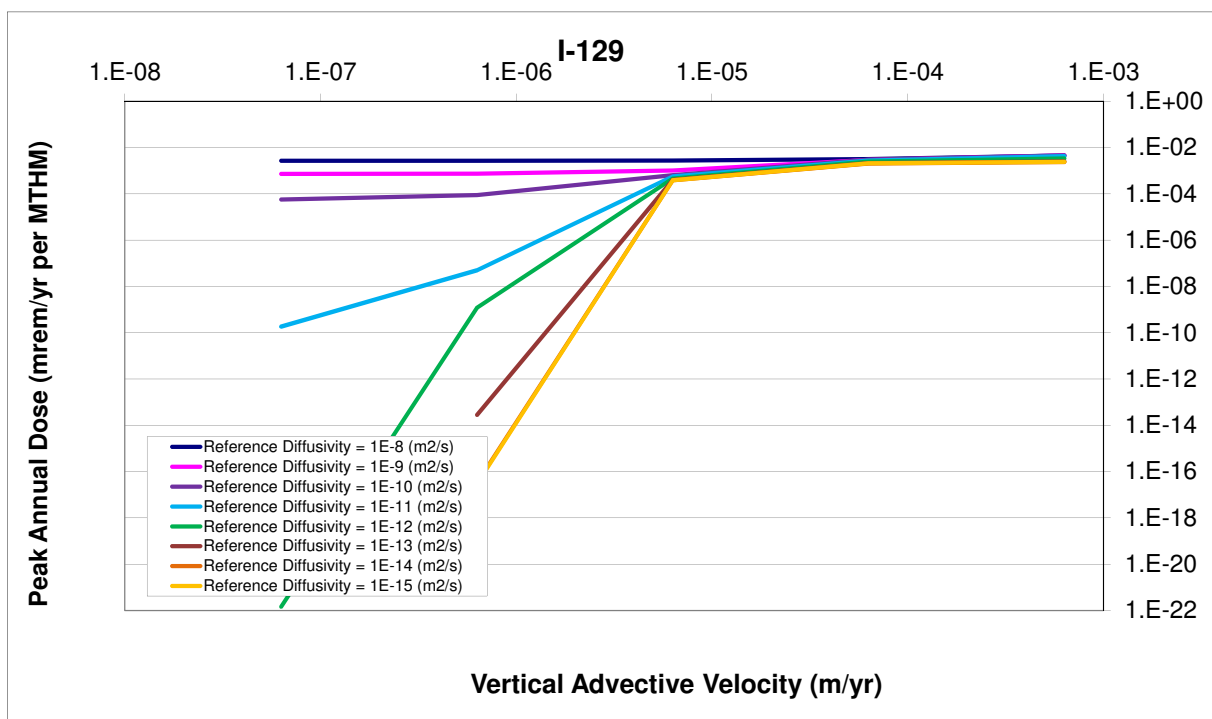
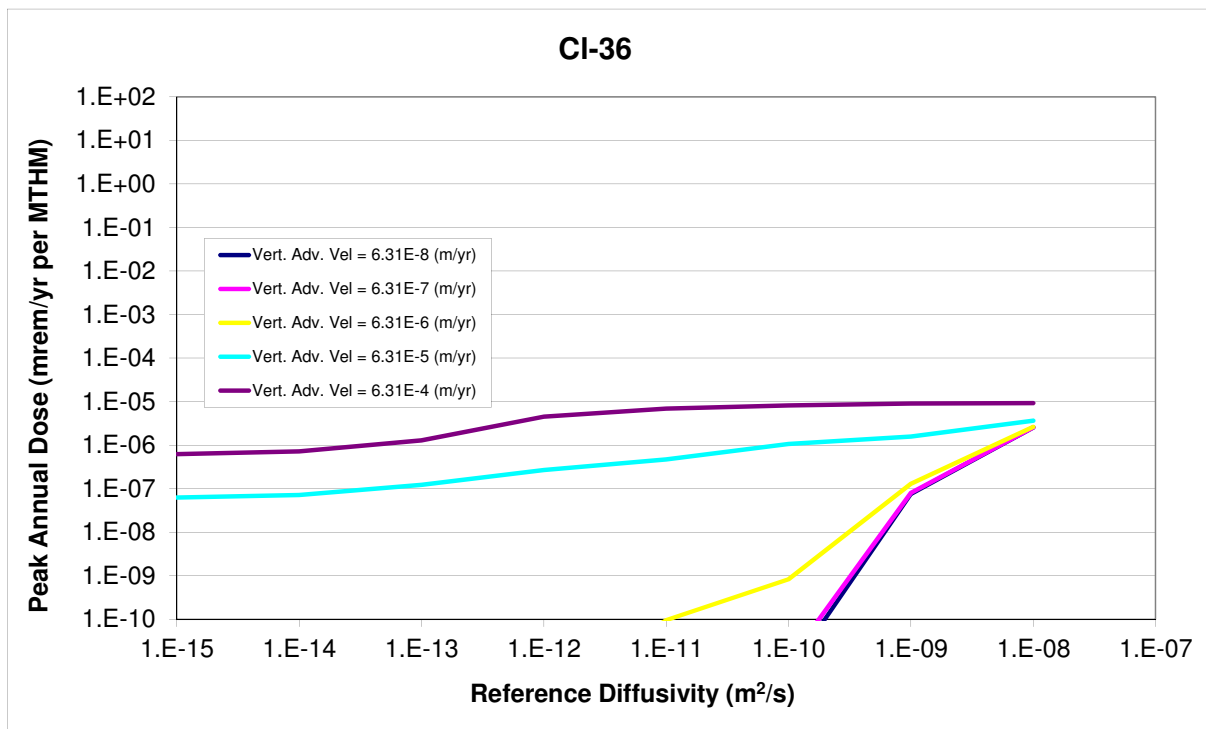Figure A.2: ^{129}I vertical advective velocity sensitivity.

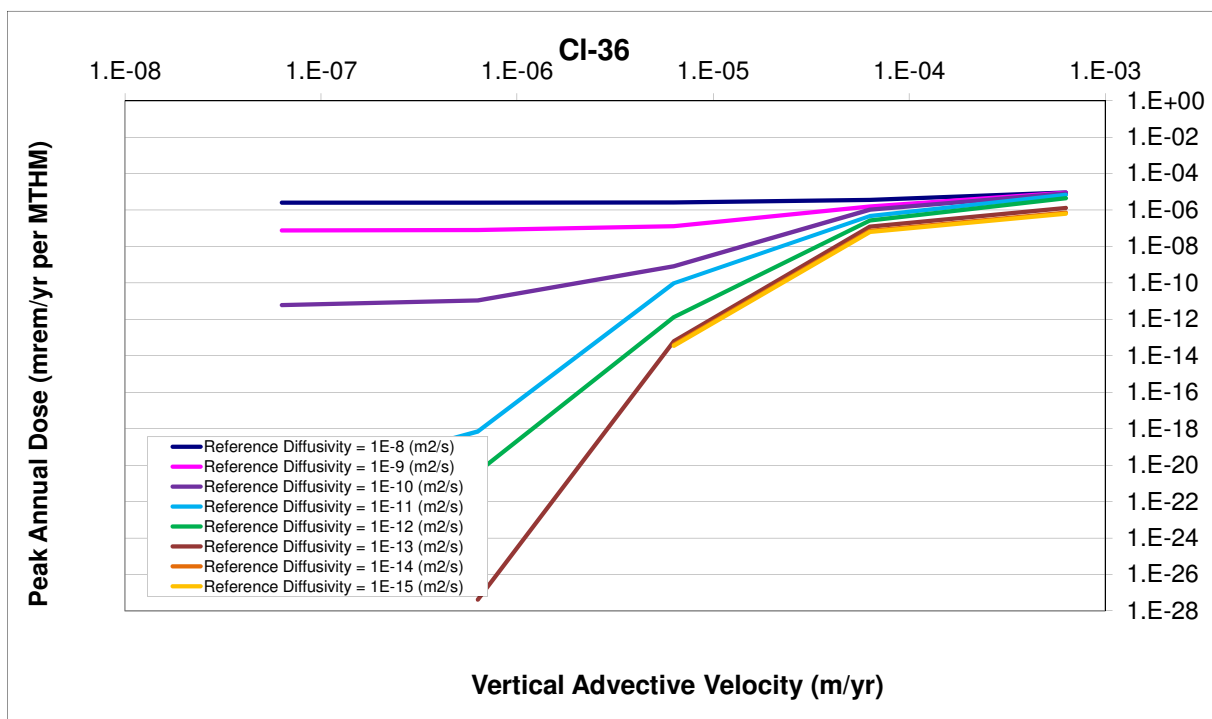Figure A.3: ^{36}Cl reference diffusivity sensitivity.

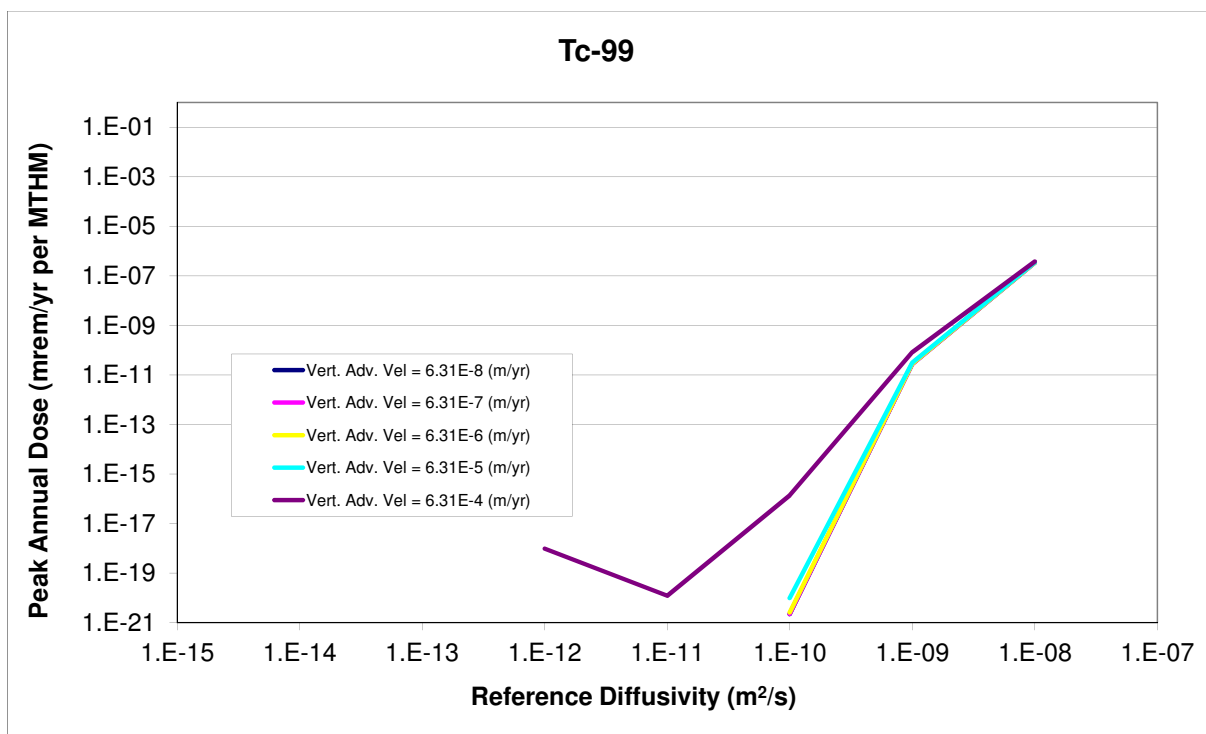Figure A.4: ^{36}Cl vertical advective velocity sensitivity.

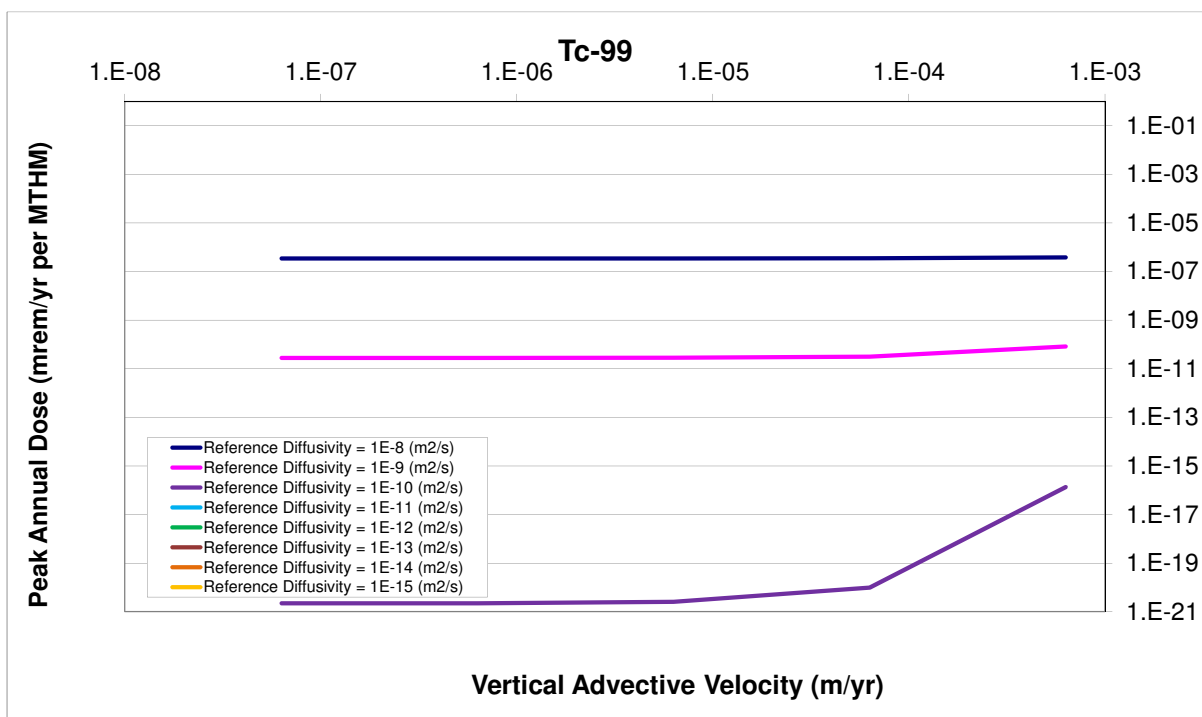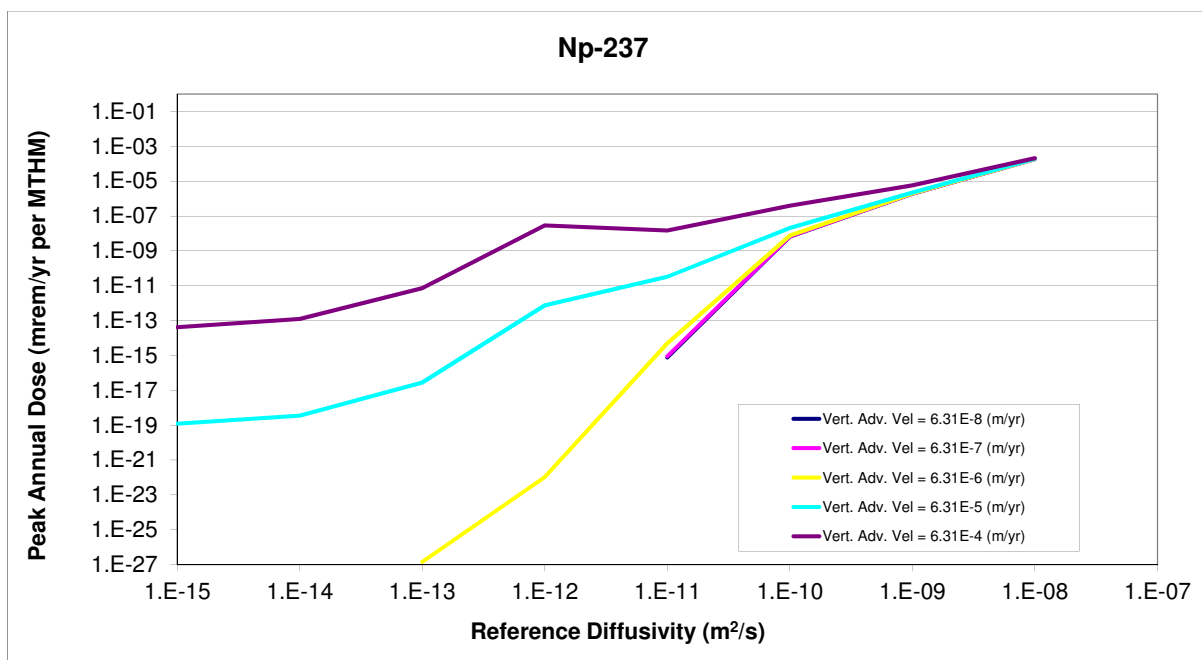Figure A.5: ^{99}Tc reference diffusivity sensitivity.

Tc-99

Peak Annual Dose (mrem/yr per MTHM)

1.E-08 1.E-07 1.E-06 1.E-05 1.E-04 1.E-03

1.E-01
1.E-03
1.E-05
1.E-07
1.E-09
1.E-11
1.E-13
1.E-15
1.E-17
1.E-19
1.E-21

Reference Diffusivity = 1E-8 (m2/s)
Reference Diffusivity = 1E-9 (m2/s)
Reference Diffusivity = 1E-10 (m2/s)
Reference Diffusivity = 1E-11 (m2/s)
Reference Diffusivity = 1E-12 (m2/s)
Reference Diffusivity = 1E-13 (m2/s)
Reference Diffusivity = 1E-14 (m2/s)
Reference Diffusivity = 1E-15 (m2/s)

Vertical Advective Velocity (m/yr)

Figure A.6: ^{99}Tc vertical advective velocity sensitivity.

Np-237

Peak Annual Dose (mrem/yr per MTHM)

1.E-01
1.E-03
1.E-05
1.E-07
1.E-09
1.E-11
1.E-13
1.E-15
1.E-17
1.E-19
1.E-21
1.E-23
1.E-25
1.E-27

1.E-15 1.E-14 1.E-13 1.E-12 1.E-11 1.E-10 1.E-09 1.E-08 1.E-07

Vert. Adv. Vel = 6.31E-8 (m/yr)
Vert. Adv. Vel = 6.31E-7 (m/yr)
Vert. Adv. Vel = 6.31E-6 (m/yr)
Vert. Adv. Vel = 6.31E-5 (m/yr)
Vert. Adv. Vel = 6.31E-4 (m/yr)

Reference Diffusivity (m²/s)

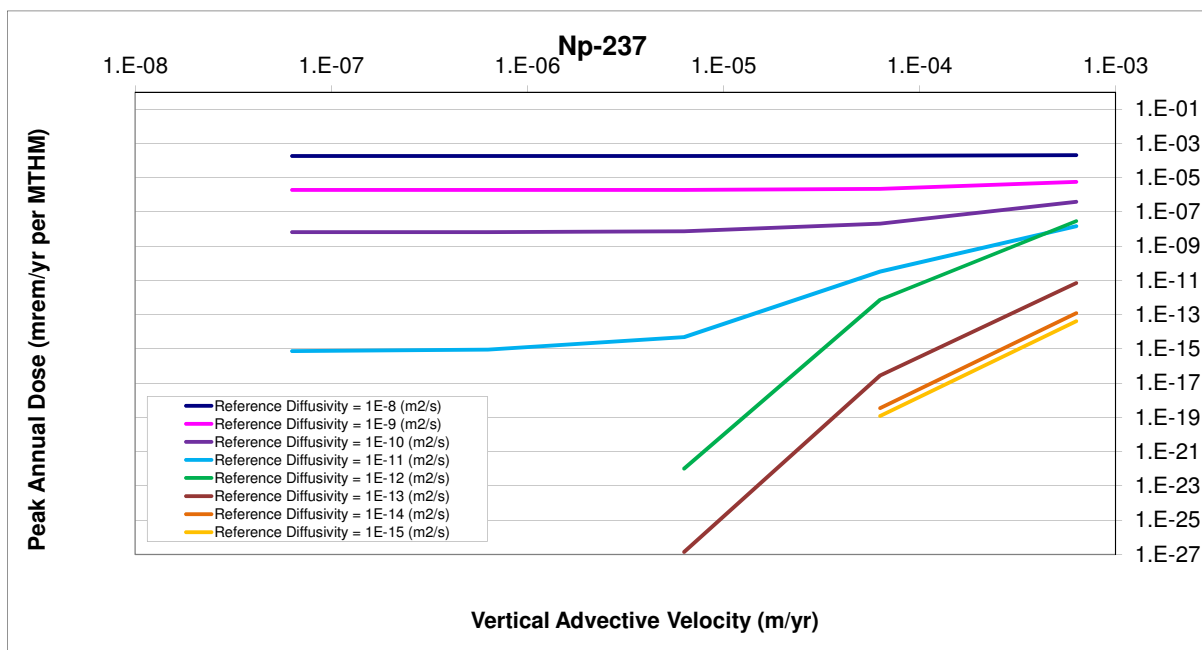Figure A.7: ^{237}Np reference diffusivity sensitivity.

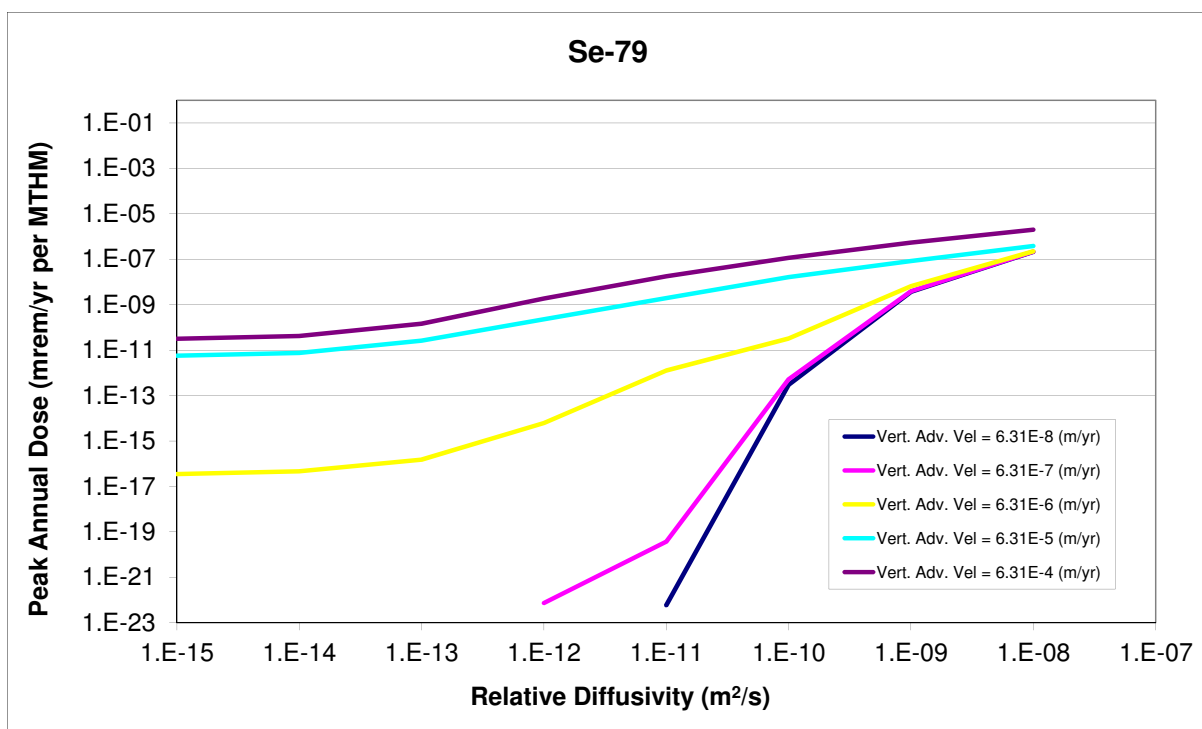Figure A.8: ^{237}Np vertical advective velocity sensitivity.
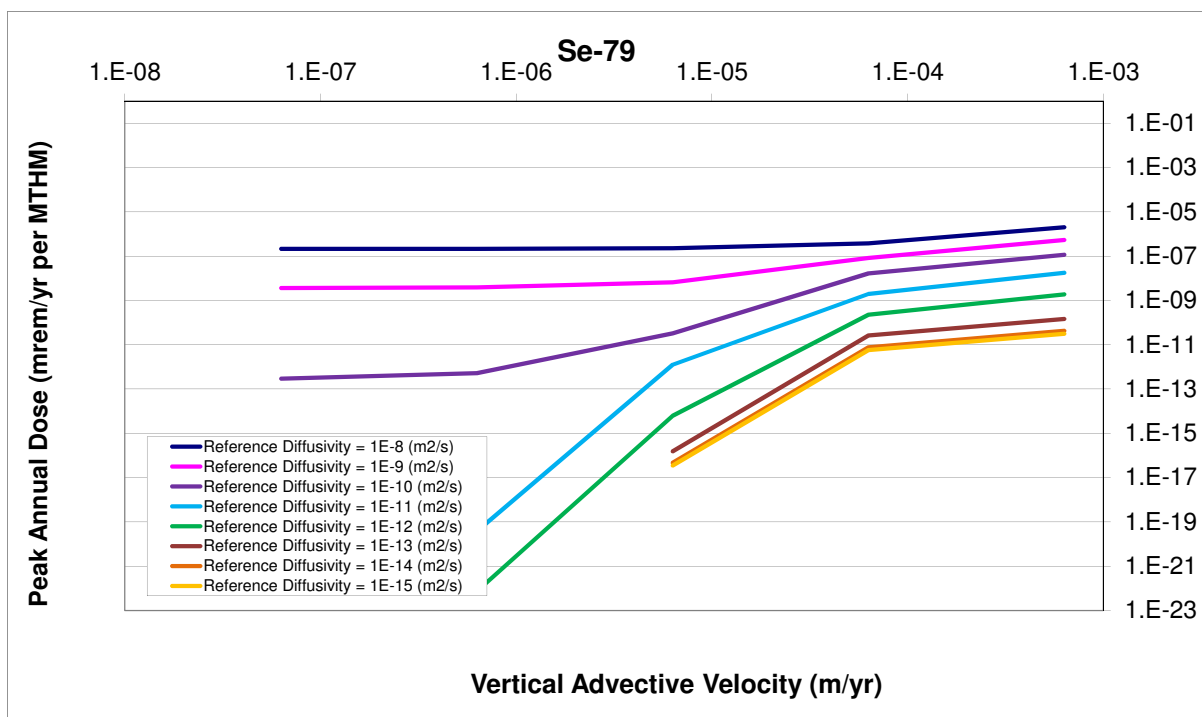

Figure A.9: ^{79}Se reference diffusivity sensitivity.

Figure A.10: ^{79}Se vertical advective velocity sensitivity.

Diffusion Coefficient of Far Field

In clay media, diffusion dominates far field hydrogeologic transport due to character-istically low hydraulic head gradients and permeability. Thus, the effective diffusion coefficient is a parameter to which repository performance in clay media is expected to be very sensitive.

The sensitivity of the peak dose to the reference diffusivity of the host rock was analyzed. In this model, the reference diffusivity of the medium was the input parameter used to vary the effective diffusivity in a controlled manner. In GoldSim's transport module, the effective diffusion coefficient is defined as

$$D_{eff} = n\tau D_{ref} D_{rel} \tag{A.4}$$

$$
\begin{aligned}
D_{eff} &= \text{ effective diffusion coefficient } [m^2/s], \\
D_{rel} &= \text{ relative diffusivity for each isotope in water } [\%], \\
D_{ref} &= \text{ reference diffusivity in water } [m^2/s], \\
\tau &= \text{ tortuosity} [\%], \\
n &= \text{ porosity} [\%].
\end{aligned}
$$

$$\tag{A.5}$$

The reference diffusivity was altered while the porosity and the tortuosity were both set to 1. Thus, the simulation rendered the effective diffusivity equal to the product of the reference diffusivity and the relative diffusivity (set to 1 for all isotopes). This allowed the diffusivity to be controlled directly for all isotopes.

The waste inventory total mass was also altered for each value of the reference diffusivity. That is, the radionuclide inventory in a reference Metric Ton of Heavy Metal (MTHM) of commercial spent nuclear fuel was multiplied by a scalar mass factor. It was expected that changing these two parameters in tandem would capture the importance of diffusivity in the far field to the repository performance as well as a threshold at which the effect of waste inventory dissolution is attenuated by solubility limits.

Finally, in order to isolate the effect of the far field behavior, the waste form degrada-tion rate was set to be very high as were the solubility and advective flow rate through the EBS. This guaranteed that contaminant flowthrough in the near field was unhindered, leaving the far field as the dominant barrier to release.

Parametric Range

The forty runs corresponded to eight values of relative diffusivity and five values of inventory mass multiplier. That is, the reference diffusivity was varied over the eight magnitudes between 10^{-8} and 10^{-15} $[m^2/s]$. The Mass Factor, the unitless inventory multiplier, was simultaneously varied over the five magnitudes between 10^{-4} and $10^1 [-]$. That is, the radionuclide inventory was varied between 10^{-4} and 10^1 of that in one MTHM

of spent nuclear fuel (SNF), which is expected to cover the full range of inventories in current wasteforms.

		Mass Factor				
		0.001	0.01	0.1	1	10
		Groupings				
Reference Diffusivity (m²/s)	1.E-08	1	2	3	4	5
	1.E-09	6	7	8	9	10
	1.E-10	11	12	13	14	15
	1.E-11	16	17	18	19	20
	1.E-12	21	22	23	24	25
	1.E-13	26	27	28	29	30
	1.E-14	31	32	33	34	35
	1.E-15	36	37	38	39	40

Table A.4: Diffusion coefficient and mass factor simulation groupings.

Results

The peak doses due to highly soluble, non-sorbing elements such as I and Cl, are proportional to the radionuclide inventory and largely directly proportional to the relative diffusivity. This can be seen for the cases of ^{129}I and ^{36}Cl in Figures A.11, A.12, A.13 and A.14.

Long lived ^{129}I and ^{36}Cl are assumed to have near complete solubility, so in Figures A.11 and A.13, the effect of a solubility limited attenuation regime is not seen. Even for very low diffusivities, the diffusion length of the far field is the primary barrier. In Figures A.12 and A.14 it is clear that in the absence of solubility limitation and sorption, the peak dose is directly proportional to mass factor.

Both Cl and I are soluble and non-sorbing. The amount of ^{129}I in the SNF inventory is greater than the amount of ^{36}Cl, so a difference in magnitudes are expected, however, the trends should be the same. Since the halflife of ^{36}Cl, $3 \times 10^5 [yr]$, is much shorter than the half life of ^{129}I, $1.6 \times 10^7 [yr]$, a stronger proportional dependence on mass factor is seen for Cl due to its higher decay rate.

With the exception of those dose-contributors assumed to be completely soluble, two regimes were visible in the results of this analysis. In low diffusion coefficient regime, the diffusive pathway through the homogeneous permeable porous medium in the far field continues to be a dominant barrier to nuclide release for normal (non-intrusive) repository conditions.

In the second regime, for very high diffusion coefficients, the effects of additional attenuation phenomena in the natural system can be seen. The dependence of peak annual dose on mass factor was consistently directly proportional for all isotopic groups.
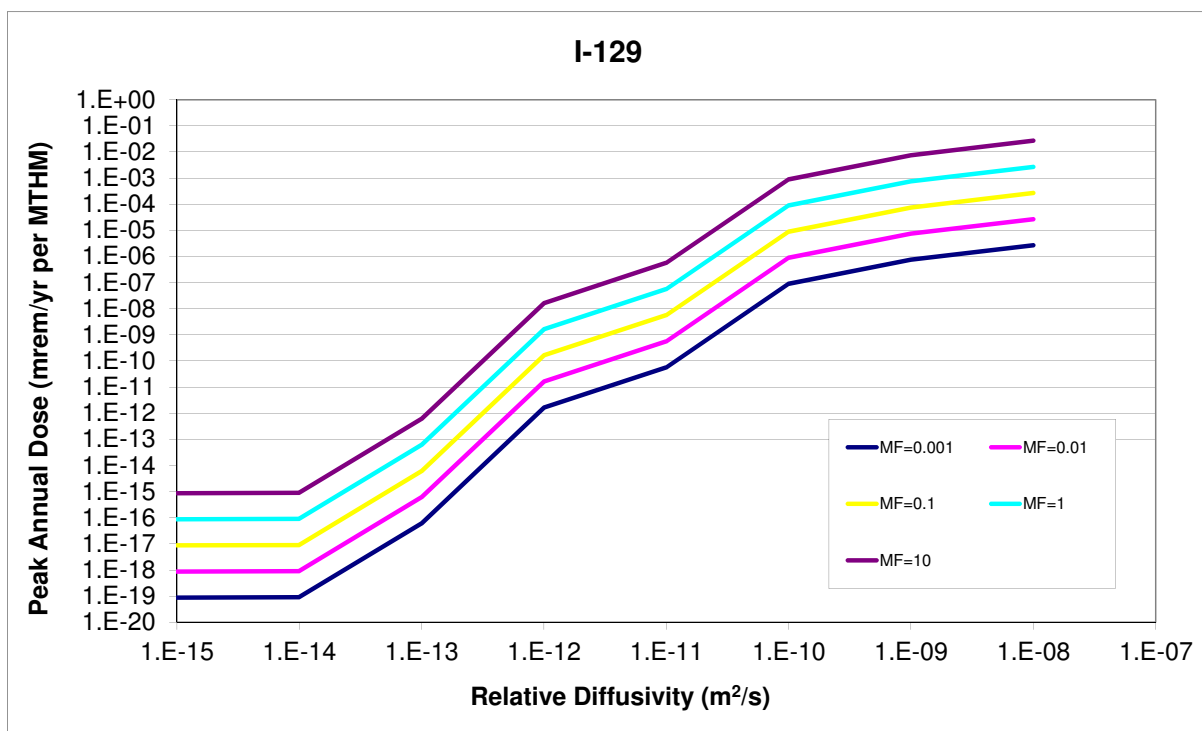
Figure A.11: ^{129}I relative diffusivity sensitivity.

The peak doses due to solubility limited, sorbing elements such as Np and Tc demonstrate two major regimes. In the first regime, for low values of mass factor, the mean of the peak annual dose rates is directly proportional to both reference diffusivity and mass factor. For higher values of mass factor, the sensitivity to reference diffusivity and mass factor are both attenuated at higher values. The attenuation in these regimes is due to natural system attenuation, most notably, sorption.

^{237}Np and ^{99}Tc exhibit a strong proportional relationship between diffusivity and dose in Figures A.15 and A.17. This relationship is muted as diffusivity increases. Both are directly proportional to mass factor until they reach the point of attenuation by their solubility limits, as can be seen in Figures A.16 and A.18.
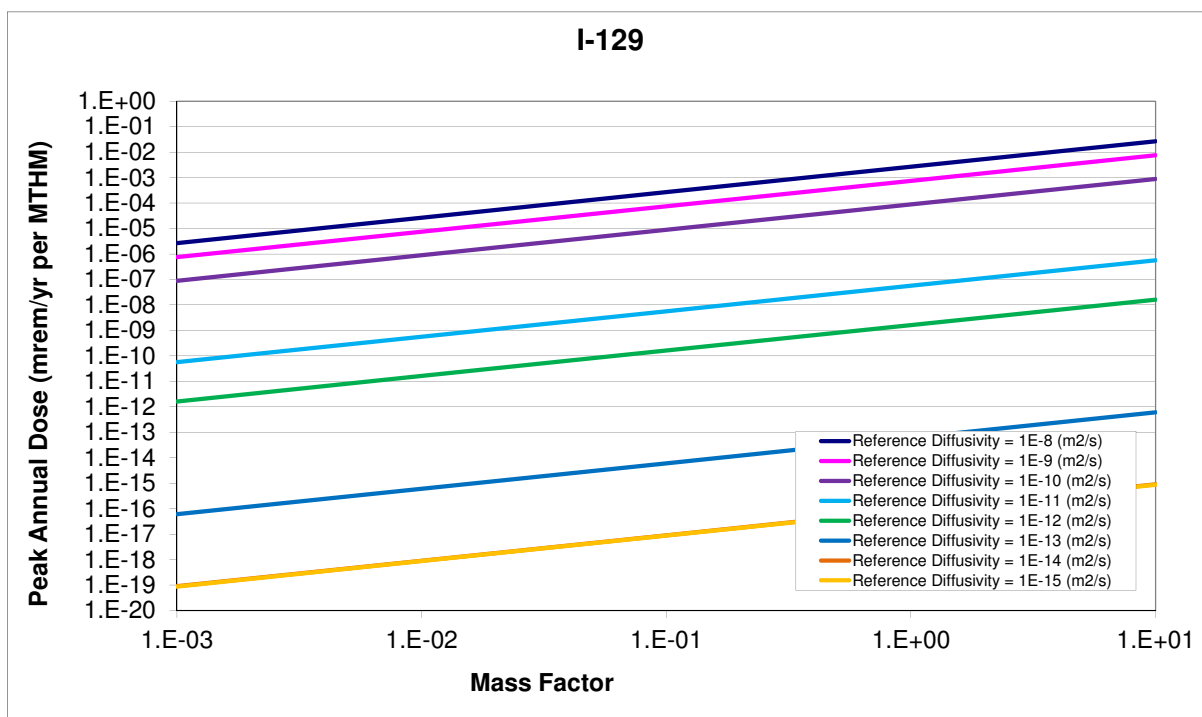
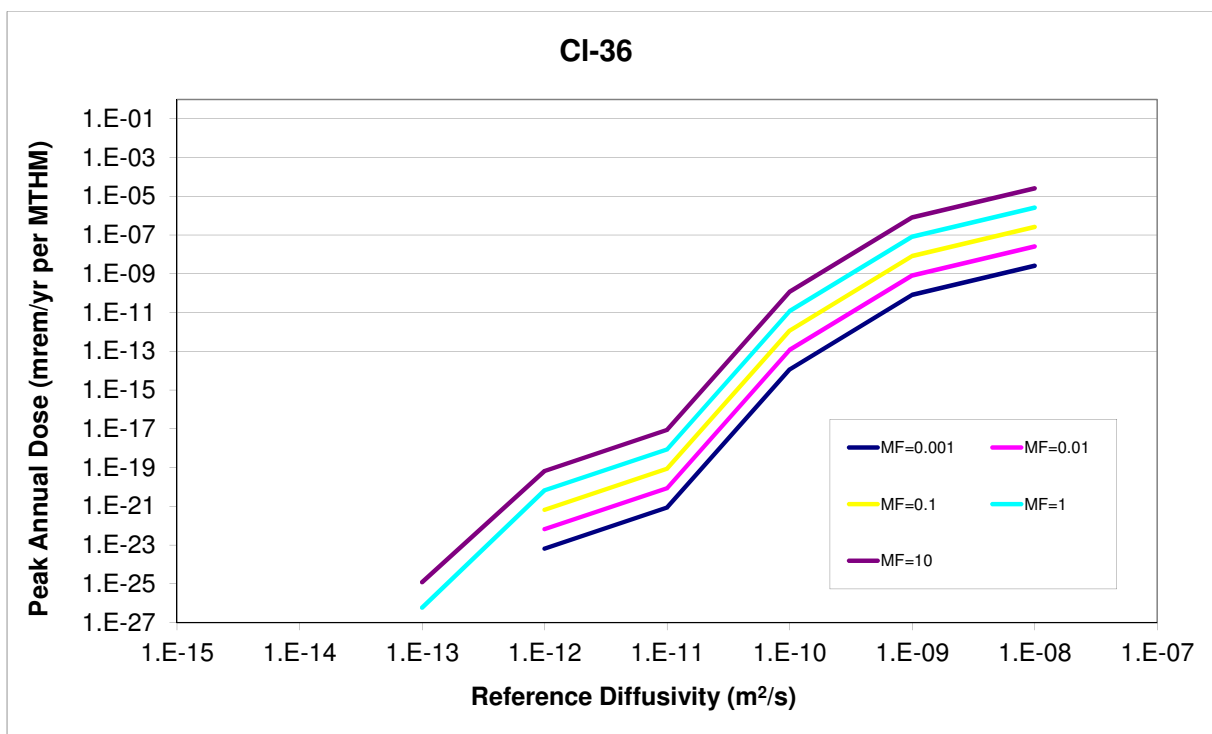Figure A.12: ^{129}I mass factor sensitivity.

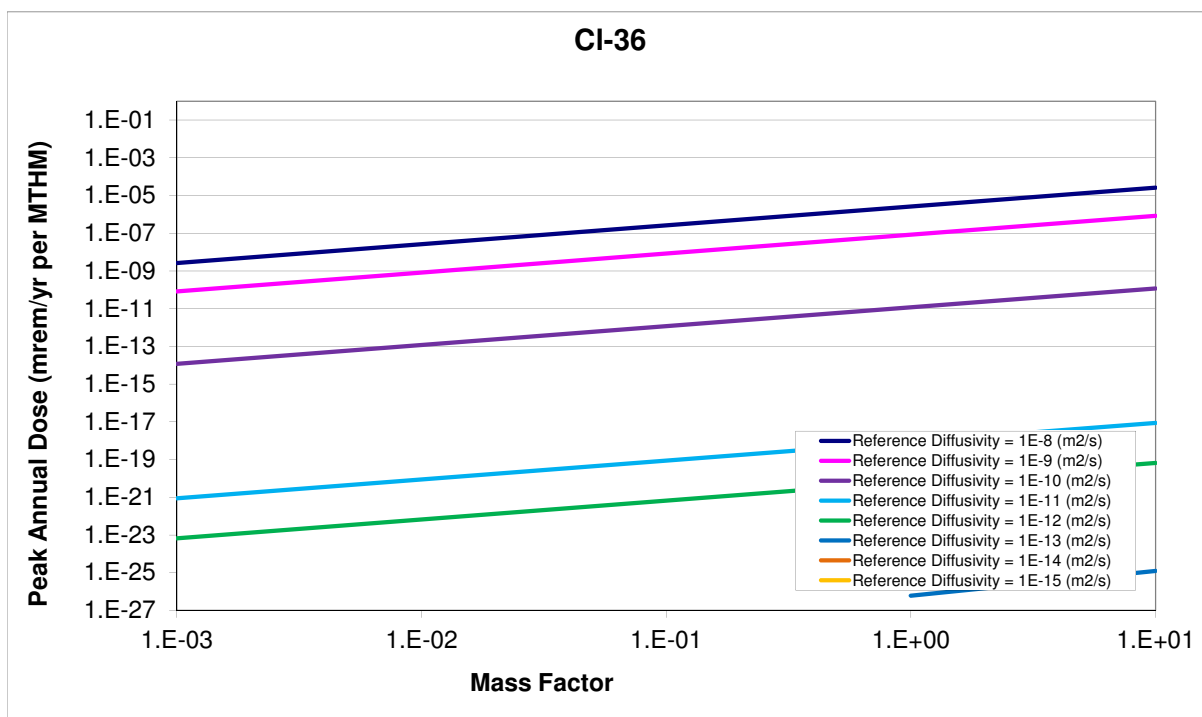Figure A.13: ^{36}Cl relative diffusivity sensitivity.

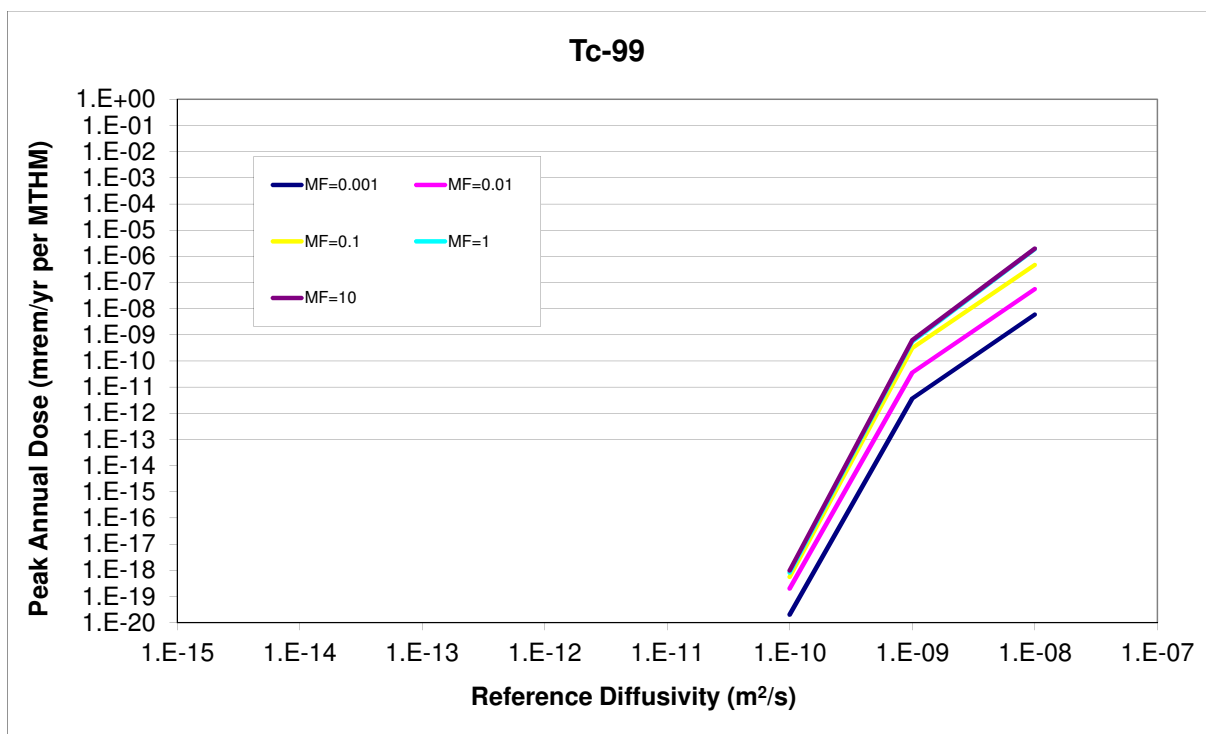Figure A.14: ^{36}Cl mass factor sensitivity.

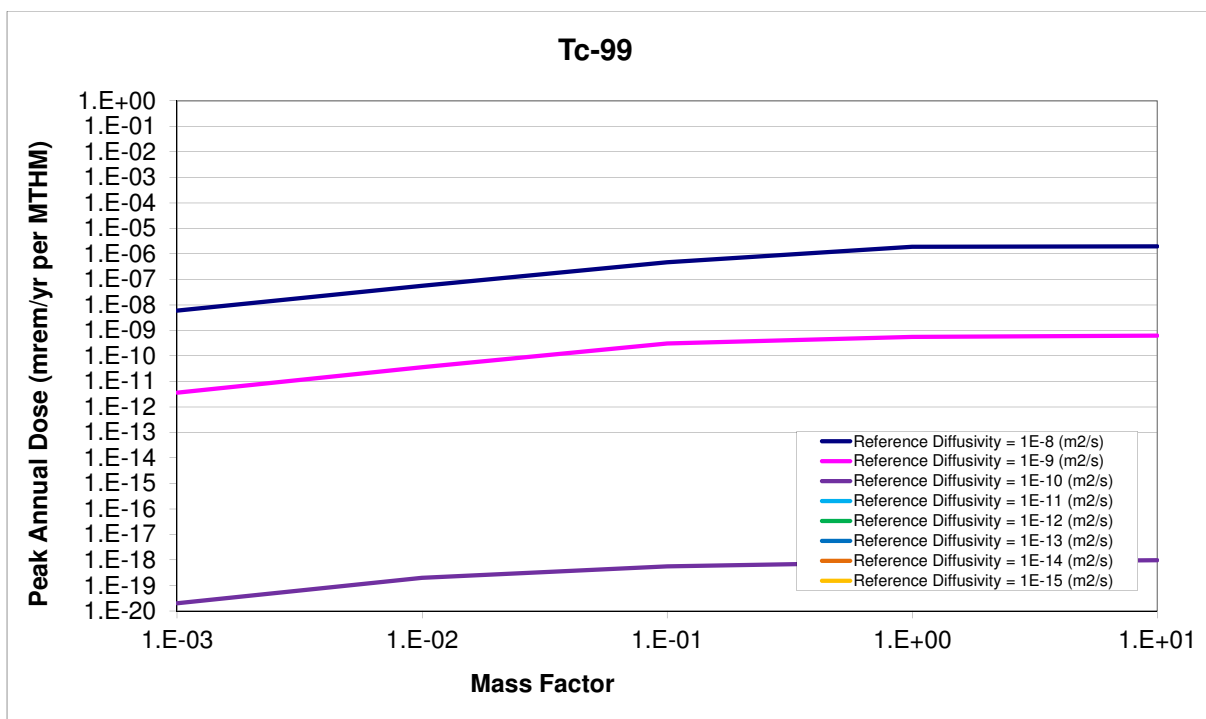Figure A.15: ^{99}Tc relative diffusivity sensitivity.
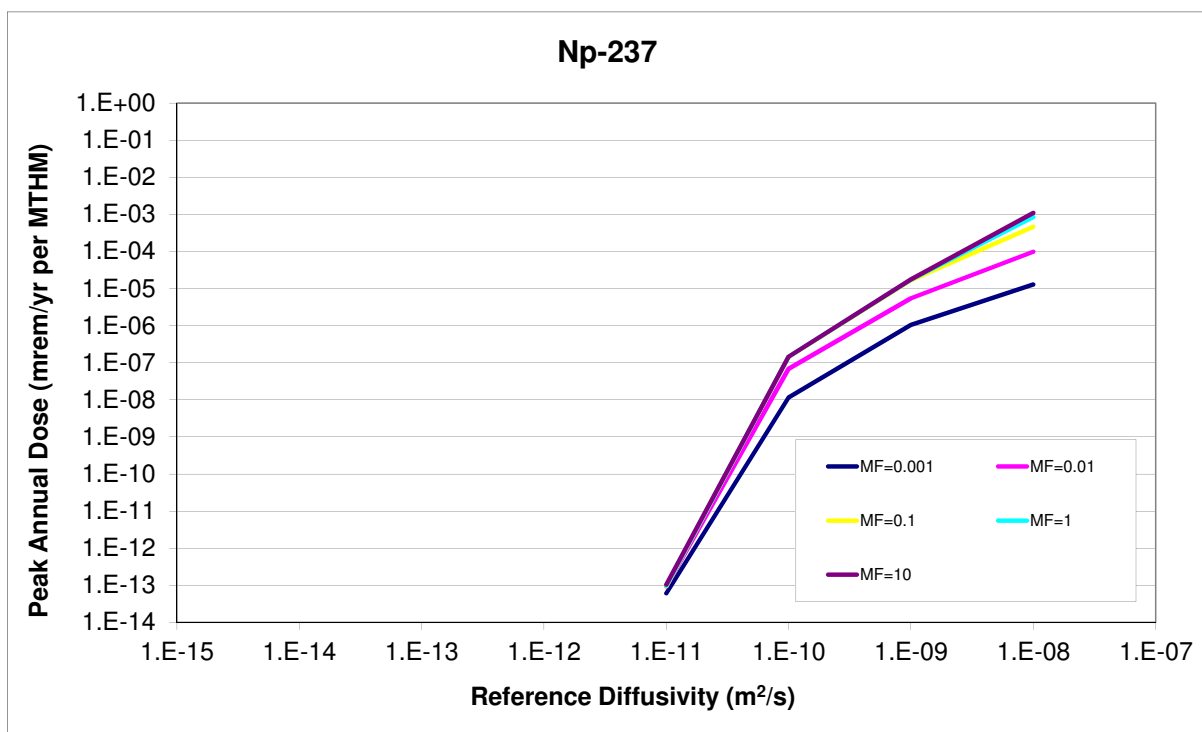
Figure A.16: ^{99}Tc mass factor sensitivity.

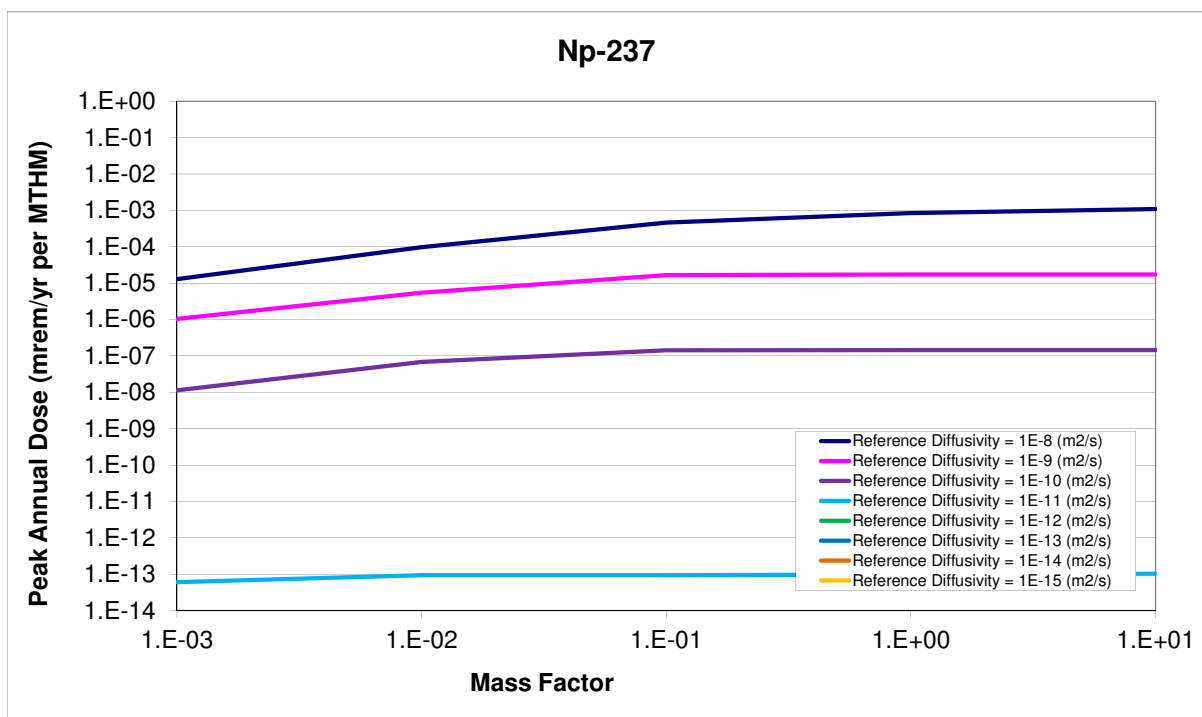Figure A.17: ^{237}Np relative diffusivity sensitivity.

Figure A.18: ^{237}Np mass factor sensitivity.

Solubility Coefficients

This study varied the solubility coefficients for each isotope in the simulation to help inform the effect of reprocessing on repository benefit for the clay repository scenario. The importance of the actinide contribution relative to the contribution from ^{129}I, ^{79}Se, and ^{99}Tc was of particular interest.

The dissolution behavior of a solute in an aqueous solutions is called its solubility. This behavior is limited by the solute's solubility limit, described by an equilibrium constant that depends upon temperature, water chemistry, and the properties of the element. The solubility constant for ordinary solutes, K_s gives units of concentration, $[kg/m^3]$, and can be determined algebraically by the law of mass action which gives the partitioning at equilibrium between reactants and products. For a reaction

$$cC + dD = yY + zZ, \tag{A.6}$$

where

$$c, d, y, z = \text{ amount of respective constituent } [mol]$$
$$C, D = \text{ reactants } [-]$$
$$Y, Z = \text{ products } [-],$$

the law of mass action gives

$$K = \frac{(Y)^y (Z)^z}{(C)^c (D)^d} \tag{A.7}$$

where

$$(X) = \text{ the equilibrium molal concentration of X } [mol/m^3]$$
$$K = \text{ the equilibrium constant } [-].$$

The equilibrium constant for many reactions are known, and can be found in chemical tables. Thereafter, the solubility constraints of a solution at equilibrium can be found algebraically. In cases of salts that dissociate in aqueous solutions, this equilibrium constant is called the salt's solubility product K_{sp}.

This equilibrium model, however, is only appropriate for dilute situations, and nondilute solutions at partial equilibrium must be treated with an activity model by substituting the activities of the constituents for their molal concentrations,

$$[X] = \gamma_x (X) \tag{A.8}$$

where

$$[X] = \text{ activity of X } [-]$$
$$\gamma_x = \text{ activity coefficient of X} [-]$$
$$(X) = \text{ molal concentration of X} [mol/m^3]$$

such that

$$IAP = \text{ Ion Activity Product } [-].$$
$$= \frac{[Y]^y [Z]^z}{[C]^c [D]^d} \tag{A.9}$$
$$\tag{A.10}$$

The ratio between the IAP and the equilibrium constant (IAP/K) quantifiesn the departure from equilibrium of a solution. This information is useful during the transient stage in which a solute is first introduced to a solution. When $IAP/K < 1$, the solution is undersaturated with respect to the products. When, conversely, $IAP/K > 1$, the solution is oversaturated and precipitation of solids in the volume will occur.

Parametric Range

The solubility coefficients were varied in this simulation using a multiplier. The reference solubilities for each element were multiplied by the multiplier for each simulation group. This technique preserved relative solubility among elements. Forty values of solubility coefficient multiplier were used to change the far field solubility. This did not alter any of the solubility in the EDZ, WF, or Fast Path solubilities.

The values of the solubility multiplier were deliberately varied over many magnitudes, from 1^{-9} through 5×10^{10}. This multiplier multiplied the most likely values of solubility for each element, so the relative solubility between elements was preserved.

Results

The results for varying the solubility coefficient were very straightforward. For solubility limits below a certain threshold, the dose releases were directly proportional to the solubility limit, indicating that the radionuclide concentration saturated the groundwater up to the solubility limit near the waste form. For solubility limits above the threshold, however, further increase to the limit had no effect on the peak dose. This demonstrates the situation in which the solubility limit is so high that even complete dissolution of the waste inventory into the pore water is insufficient to reach the solubility limit.

In Figures A.19 and A.20, it is clear that for solubility constants lower than a threshold, the relationship between peak annual dose and solubility limit is strong.
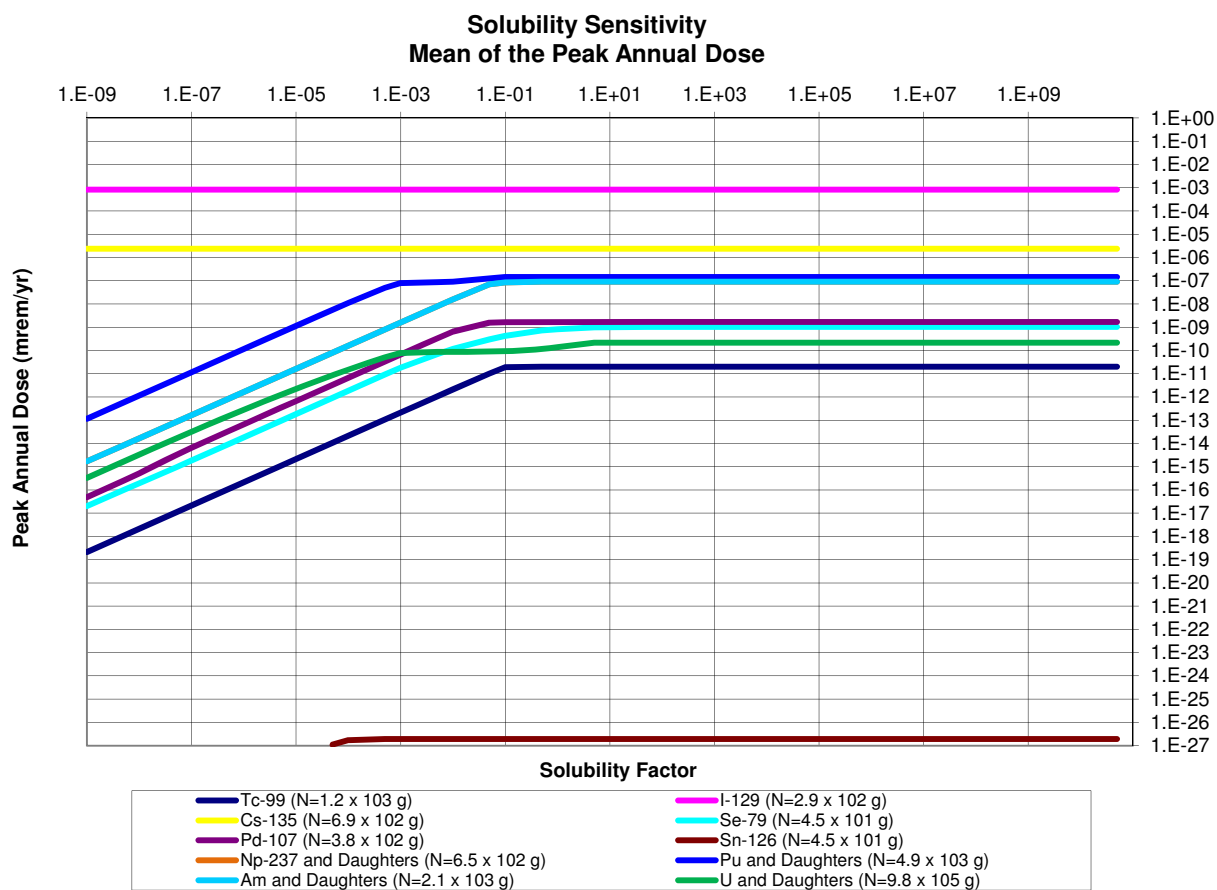
Figure A.19: Solubility factor sensitivity. The peak annual dose due to an inventory, N, of each isotope.
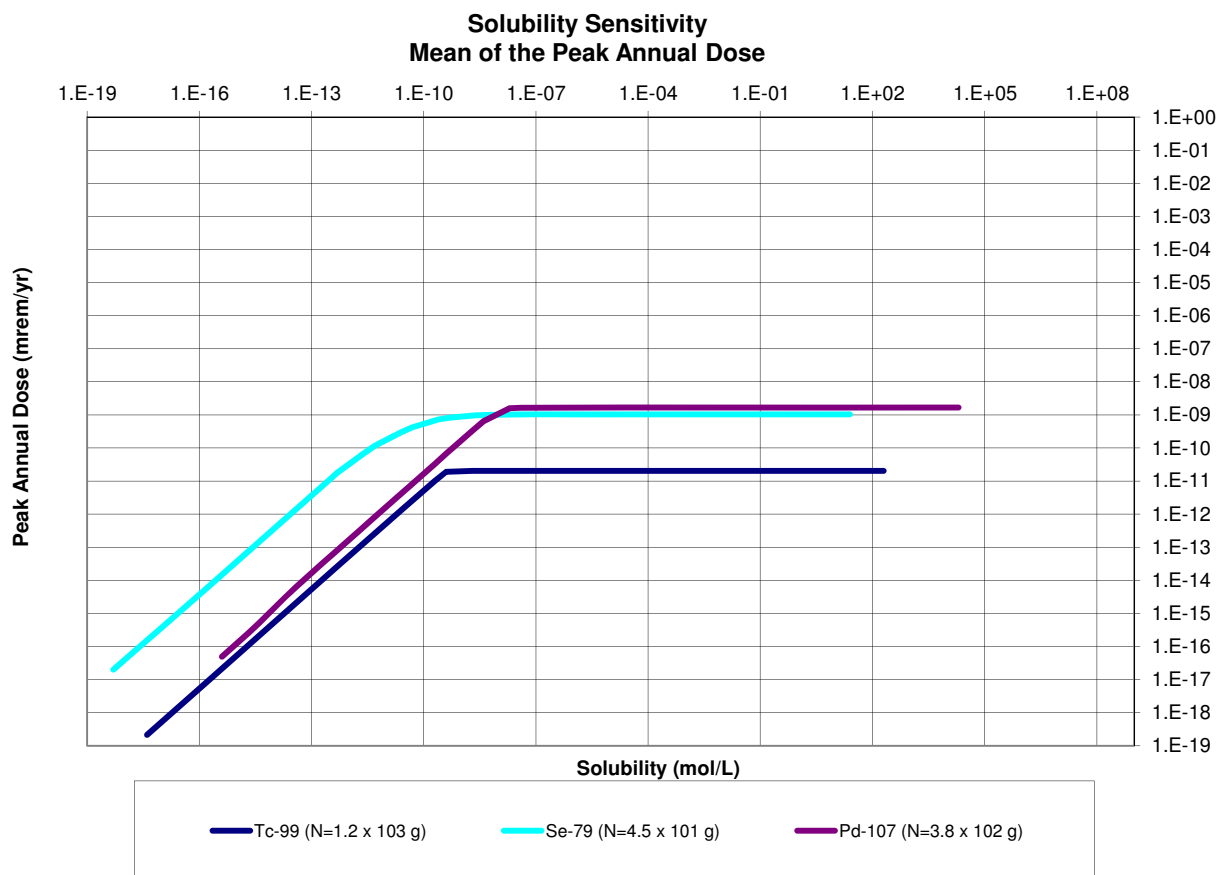
Figure A.20: Solubility limit sensitivity. The peak annual dose due to an inventory, N, of each isotope.

The Partition Coefficient

This analysis investigated the peak dose rate contribution from various radionuclides to the partition coefficient of those radionuclides.

The partition or distribution coefficient, K_d, relates the amount of contaminant adsorbed into the solid phase of the host medium to the amount of contaminant adsorbed into the aqueous phase of the host medium. It is a common empirical coefficient used to capture the effects of a number of retardation mechanisms. The coefficient K_d, in units of $[m^3 \cdot kg^{-1}]$, is the ratio of the mass of contaminant in the solid to the mass of contaminant in the solution.

The retardation factor, R_f, which is the ratio between velocity of water through a volume and the velocity of a contaminant through that volume, can be expressed in terms of the partition coefficient,

$$R_f = 1 + \frac{\rho_b}{n_e} K_d \tag{A.11}$$

where

$$\rho_b = \quad \text{bulk density} [kg \cdot m^{-3}]$$

and

$$n_e = \quad \text{effective porosity of the medium} [\%].$$

Parametric Range

The parameters in this model were all set to the default values except a multiplier applied to the partitioning K_d coefficients.

The multiplier took the forty values $1 \times 10^{-9}, 5 \times 10^{-8}, \cdots 5 \times 10^{10}$ Only the far field partition coefficients were altered by this factor. Partition coefficients effecting the EDZ and fast pathway were not changed.

Results

The expected inverse relationship between the retardation factor and resulting peak annual dose was found for all elements that were not assumed to be effectively infinitely soluble. In the low retardation coefficient cases, a regime is established in which the peak annual dose is entirely unaffected by changes in retardation coefficient. For large values of retardation coefficient, the sensitivity to small changes in the retardation coefficient increases dramatically. In that sensitive regime, the change in peak annual dose is inversely related to the retardation coefficient. Between these two regimes was a transition regime, in which the K_d factor ranges from 1×10^{-5} to $5 \times 10^0 [-]$.

It is clear from Figures A.21 and A.22 that for retardation coefficients greater than a threshold, the relationship between peak annual dose and retardation coefficient is a strong inverse one.
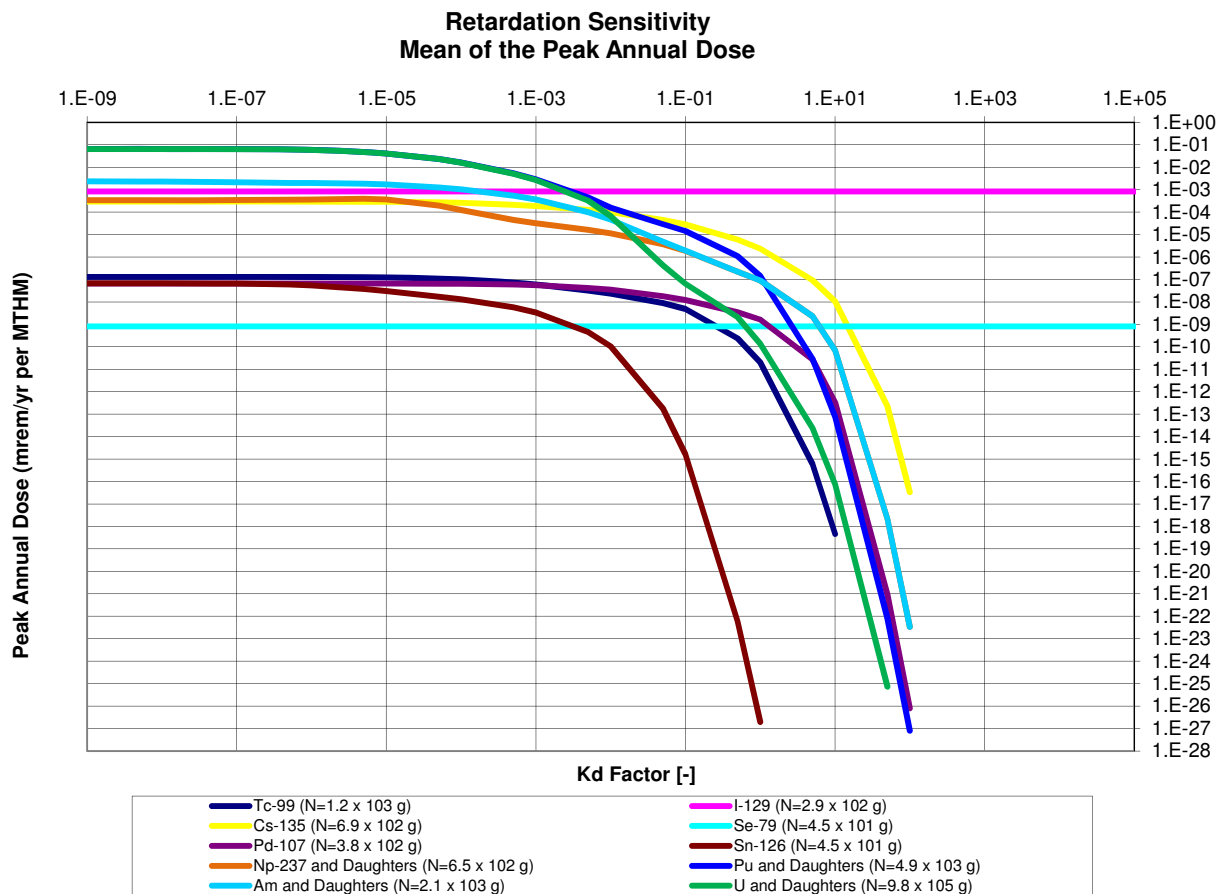

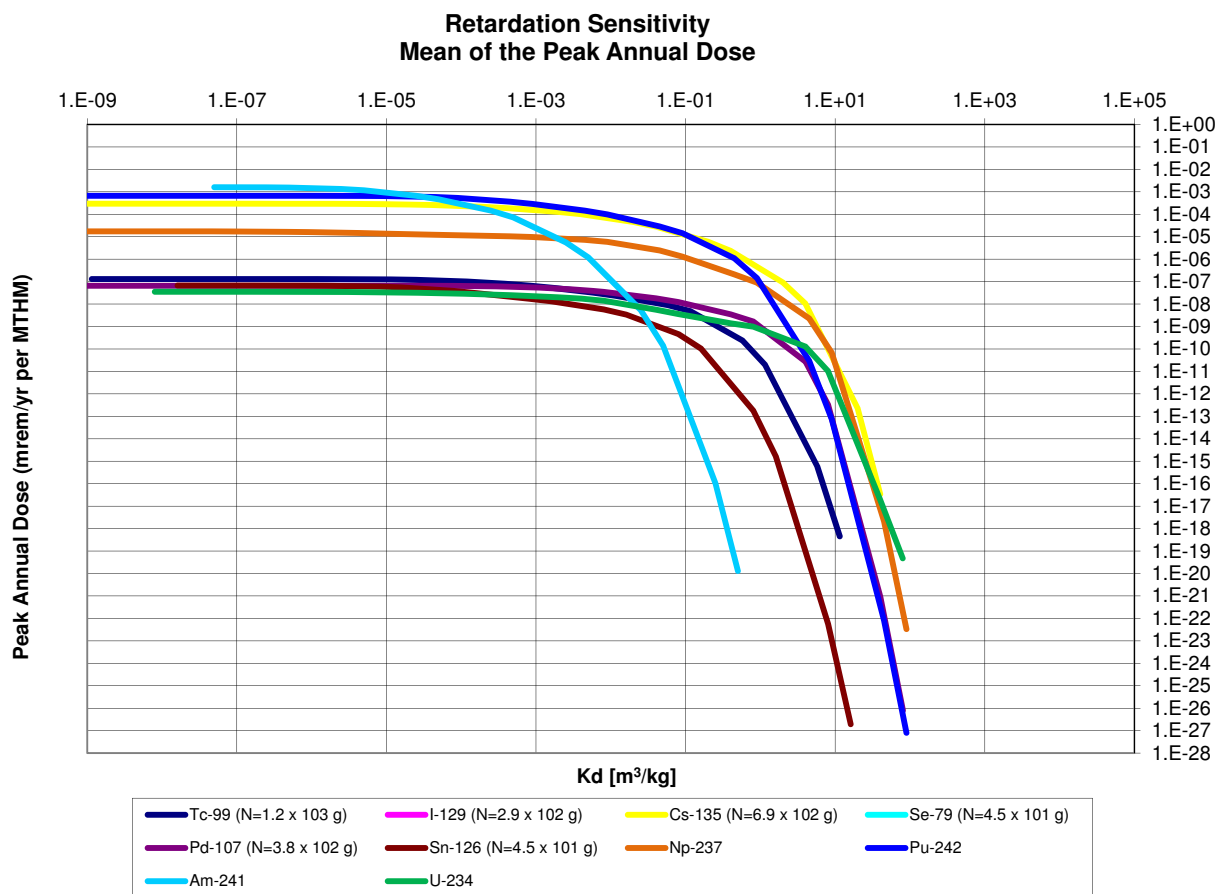Figure A.21: K_d factor sensitivity. The peak annual dose due to an inventory, N, of each isotope.

Figure A.22: K_d sensitivity. The peak annual dose due to an inventory, N, of each isotope.

Waste Form Degradation Rate

The sensitivity of peak dose rate to the waste form degradation rate was determined with respect to varying inventories of waste.

The sensitivity of repository performance to waste form degradation rate was expected to vary according to the waste inventory. For cases in which the dominant dose contributing radionuclides have half-lives much shorter than the expected waste form lifetime, the waste form degradation rate is not expected to have an effect. So too, for cases in which the primary barrier to release, the slow diffusive pathway, dominates overall repository performance, the waste form engineered barrier was expected to have a negligible effect on repository performance in comparison.

In the case of a clay repository, the effect of the long time scale of the diffusive release pathway was to dampen the potential effect of high waste form degradation rates.

Parametric Range

These runs varied the waste form degradation rate and the waste inventory mass factor. There were forty runs corresponding to eight values of the waste form degradation rate and five values of the mass factor.

The waste form degradation rate was varied over the eight magnitudes between 10^{-9} and $10^{-2}[1/yr]$. The inventory mass factor was varied over the five magnitudes between 0.001 and $10.0[-]$.

Results

These results show two regimes. In the first regime, the mean of the peak annual dose rates is directly proportional to both the mass factor and the fractional waste form degradation rate. For some radionuclides, attenuation occurs for high values of both parameters as the release of radionuclides is limited by dispersion parameters. This phenomenon can be seen in the figures below in which transition between regimes for higher degradation rates happens at lower mass factors than transition between regimes for lower degradation rates.

Safety indicators for post closure repository performance have been developed by the UFD campaign which utilize the inventory multiplier that was varied in this study [**?**]. These indicators are normalized by a normalization factor (100 mrem/yr) recommended by the International Atomic Energy Agency (IAEA) as the limit to "relevant critical members of the public" [**?**]. The functional form for this safety indicator for a single waste category, high level waste (HLW), is just

$$SI_G = \left(\frac{\sum_{i=1}^{N} D_{G,i}(I_i, F_d)}{100 mrem/yr} \right) [GWe/yr]. \tag{A.12}$$

where

$$SI_G = \text{Safety indicator for disposal in media type G}[GWe/yr]$$
$$N = \text{Number of key radionuclides considered in this indicator}$$
$$D_{G,i} = \text{Peak dose rate from isotope i in media type G}[mrem/yr]$$
$$F_d = \text{Fractional waste form degradation rate}[1/yr].$$

Tables A.5, A.6, and A.7 report the safety indicators for various independent isotopes and, where applicable, their daughters.

		Inventory Factor				
		0.001	0.01	0.1	1	10
		I-129 (N=2.9 x 10² g)				
Degradation Rate	1.E-09	3.E-11	3.E-10	3.E-09	3.E-08	3.E-07
	1.E-08	3.E-10	3.E-09	3.E-08	3.E-07	3.E-06
	1.E-07	2.E-09	2.E-08	2.E-07	2.E-06	2.E-05
	1.E-06	8.E-09	8.E-08	8.E-07	8.E-06	8.E-05
	1.E-05	1.E-08	1.E-07	1.E-06	1.E-05	1.E-04
	1.E-04	1.E-08	1.E-07	1.E-06	1.E-05	1.E-04
	1.E-03	1.E-08	1.E-07	1.E-06	1.E-05	1.E-04
	1.E-02	1.E-08	1.E-07	1.E-06	1.E-05	1.E-04
		Cl-36 (N=1 g)				
Degradation Rate	1.E-09	1.E-15	1.E-14	1.E-13	1.E-12	1.E-11
	1.E-08	1.E-14	1.E-13	1.E-12	1.E-11	1.E-10
	1.E-07	1.E-13	1.E-12	1.E-11	1.E-10	1.E-09
	1.E-06	9.E-13	9.E-12	9.E-11	9.E-10	9.E-09
	1.E-05	3.E-12	3.E-11	3.E-10	3.E-09	3.E-08
	1.E-04	4.E-12	4.E-11	4.E-10	4.E-09	4.E-08
	1.E-03	4.E-12	4.E-11	4.E-10	4.E-09	4.E-08
	1.E-02	4.E-12	4.E-11	4.E-10	4.E-09	4.E-08

Table A.5: Safety indicators for soluble, non-sorbing nuclides.

		Inventory Factor				
		0.001	0.01	0.1	1	10
		Pd-107 (N=3.8 x 10² g)				
Degradation Rate	1.E-09	2.E-16	2.E-15	2.E-14	2.E-13	2.E-12
	1.E-08	2.E-15	2.E-14	2.E-13	2.E-12	1.E-11
	1.E-07	2.E-14	2.E-13	2.E-12	8.E-12	3.E-11
	1.E-06	5.E-14	5.E-13	3.E-12	2.E-11	3.E-11
	1.E-05	5.E-14	5.E-13	4.E-12	2.E-11	3.E-11
	1.E-04	5.E-14	5.E-13	4.E-12	2.E-11	3.E-11
	1.E-03	5.E-14	5.E-13	4.E-12	2.E-11	3.E-11
	1.E-02	5.E-14	5.E-13	4.E-12	2.E-11	3.E-11
		Sn-126 (N=4.5 x 10¹ g)				
Degradation Rate	1.E-09	0.E+00	0.E+00	0.E+00	0.E+00	0.E+00
	1.E-08	0.E+00	0.E+00	0.E+00	0.E+00	0.E+00
	1.E-07	0.E+00	0.E+00	0.E+00	0.E+00	2.E-29
	1.E-06	0.E+00	0.E+00	0.E+00	2.E-29	5.E-29
	1.E-05	0.E+00	0.E+00	1.E-29	3.E-29	5.E-29
	1.E-04	0.E+00	0.E+00	1.E-29	3.E-29	5.E-29
	1.E-03	0.E+00	0.E+00	1.E-29	3.E-29	5.E-29
	1.E-02	0.E+00	0.E+00	1.E-29	3.E-29	5.E-29
		Zr-93 & Nb-93				
Degradation Rate	1.E-09	1.E-17	1.E-16	1.E-15	1.E-14	1.E-13
	1.E-08	1.E-16	1.E-15	1.E-14	1.E-13	7.E-13
	1.E-07	1.E-15	1.E-14	1.E-13	6.E-13	3.E-12
	1.E-06	4.E-15	4.E-14	3.E-13	1.E-12	4.E-12
	1.E-05	6.E-15	6.E-14	4.E-13	2.E-12	4.E-12
	1.E-04	6.E-15	6.E-14	4.E-13	2.E-12	4.E-12
	1.E-03	7.E-15	6.E-14	4.E-13	2.E-12	4.E-12
	1.E-02	7.E-15	6.E-14	4.E-13	2.E-12	4.E-12
		Tc-99 (N=1.2 x 10³ g)				
Degradation Rate	1.E-09	2.E-18	2.E-17	2.E-16	2.E-15	2.E-14
	1.E-08	2.E-17	2.E-16	2.E-15	2.E-14	1.E-13
	1.E-07	2.E-16	2.E-15	2.E-14	1.E-13	2.E-13
	1.E-06	1.E-15	1.E-14	1.E-13	2.E-13	2.E-13
	1.E-05	5.E-15	5.E-14	1.E-13	2.E-13	2.E-13
	1.E-04	7.E-15	5.E-14	1.E-13	2.E-13	2.E-13
	1.E-03	7.E-15	5.E-14	1.E-13	2.E-13	2.E-13
	1.E-02	7.E-15	5.E-14	1.E-13	2.E-13	2.E-13
		Cs-135 (N=6.9 x 10² g)				
Degradation Rate	1.E-09	6.E-14	6.E-13	6.E-12	6.E-11	6.E-10
	1.E-08	6.E-13	6.E-12	6.E-11	6.E-10	6.E-09
	1.E-07	5.E-12	5.E-11	5.E-10	5.E-09	5.E-08
	1.E-06	2.E-11	2.E-10	2.E-09	2.E-08	2.E-07
	1.E-05	3.E-11	3.E-10	3.E-09	3.E-08	3.E-07
	1.E-04	4.E-11	4.E-10	4.E-09	4.E-08	4.E-07
	1.E-03	4.E-11	4.E-10	4.E-09	4.E-08	4.E-07
	1.E-02	4.E-11	4.E-10	4.E-09	4.E-08	4.E-07
		Se-79 (N=4.5 x 10¹ g)				
Degradation Rate	1.E-09	2.E-14	2.E-13	2.E-12	5.E-12	8.E-12
	1.E-08	2.E-13	2.E-12	5.E-12	8.E-12	8.E-12
	1.E-07	2.E-12	5.E-12	8.E-12	8.E-12	8.E-12
	1.E-06	5.E-12	8.E-12	8.E-12	8.E-12	8.E-12
	1.E-05	6.E-12	8.E-12	8.E-12	8.E-12	8.E-12
	1.E-04	6.E-12	8.E-12	8.E-12	8.E-12	8.E-12
	1.E-03	6.E-12	8.E-12	8.E-12	8.E-12	8.E-12
	1.E-02	6.E-12	8.E-12	8.E-12	8.E-12	8.E-12

Table A.6: Safety indicators for solubility limited and sorbing nuclides.

Degradation Rate	Inventory Factor				
	0.001	0.01	0.1	1	10
Np-237 and Daughters (N=6.5 x 10^2 g)					
1.E-09	3.E-13	3.E-12	3.E-11	3.E-10	9.E-10
1.E-08	3.E-12	3.E-11	3.E-10	9.E-10	9.E-10
1.E-07	3.E-11	3.E-10	9.E-10	9.E-10	9.E-10
1.E-06	1.E-10	8.E-10	9.E-10	9.E-10	9.E-10
1.E-05	2.E-10	8.E-10	9.E-10	9.E-10	9.E-10
1.E-04	2.E-10	8.E-10	9.E-10	9.E-10	1.E-09
1.E-03	2.E-10	8.E-10	9.E-10	9.E-10	1.E-09
1.E-02	2.E-10	8.E-10	9.E-10	9.E-10	1.E-09
Pu and Daughters (N=4.9 x 10^3 g)					
1.E-09	4.E-15	4.E-14	4.E-13	3.E-12	2.E-11
1.E-08	4.E-14	3.E-13	3.E-12	2.E-11	2.E-10
1.E-07	3.E-13	2.E-12	2.E-11	2.E-10	2.E-09
1.E-06	2.E-12	2.E-11	2.E-10	1.E-09	9.E-09
1.E-05	4.E-12	4.E-11	4.E-10	3.E-09	1.E-08
1.E-04	5.E-12	5.E-11	5.E-10	3.E-09	1.E-08
1.E-03	5.E-12	5.E-11	5.E-10	3.E-09	1.E-08
1.E-02	5.E-12	5.E-11	5.E-10	3.E-09	1.E-08
Am and Daughters (N=2.1 x 10^3 g)					
1.E-09	3.E-13	3.E-12	3.E-11	3.E-10	9.E-10
1.E-08	3.E-12	3.E-11	3.E-10	9.E-10	9.E-10
1.E-07	3.E-11	3.E-10	9.E-10	9.E-10	9.E-10
1.E-06	1.E-10	8.E-10	9.E-10	9.E-10	9.E-10
1.E-05	2.E-10	8.E-10	9.E-10	9.E-10	9.E-10
1.E-04	2.E-10	8.E-10	9.E-10	9.E-10	1.E-09
1.E-03	2.E-10	8.E-10	9.E-10	9.E-10	1.E-09
1.E-02	2.E-10	8.E-10	9.E-10	9.E-10	1.E-09
U and Daughters (N=9.8 x 10^5 g)					
1.E-09	2.E-15	2.E-14	1.E-13	5.E-13	6.E-13
1.E-08	2.E-14	1.E-13	5.E-13	6.E-13	7.E-13
1.E-07	1.E-13	4.E-13	6.E-13	7.E-13	2.E-12
1.E-06	3.E-13	6.E-13	7.E-13	1.E-12	7.E-12
1.E-05	4.E-13	7.E-13	8.E-13	2.E-12	9.E-12
1.E-04	4.E-13	7.E-13	9.E-13	3.E-12	9.E-12
1.E-03	4.E-13	7.E-13	9.E-13	3.E-12	9.E-12
1.E-02	4.E-13	7.E-13	9.E-13	3.E-12	9.E-12

Table A.7: Safety indicators for the actinides and their daughters.

The peaks for highly soluble, non sorbing elements such as I and Cl are directly proportional to mass factor for most values of waste form degradation rates. This effect can be seen in Figures A.23, A.24, A.25, and A.26.

Highly soluble and non-sorbing ^{129}I demonstrates a direct proportionality between dose rate and fractional degradation rate until a turnover where other natural system parameters dampen transport. Highly soluble and non-sorbing ^{129}I domonstrates a direct proportionality to the inventory multiplier.
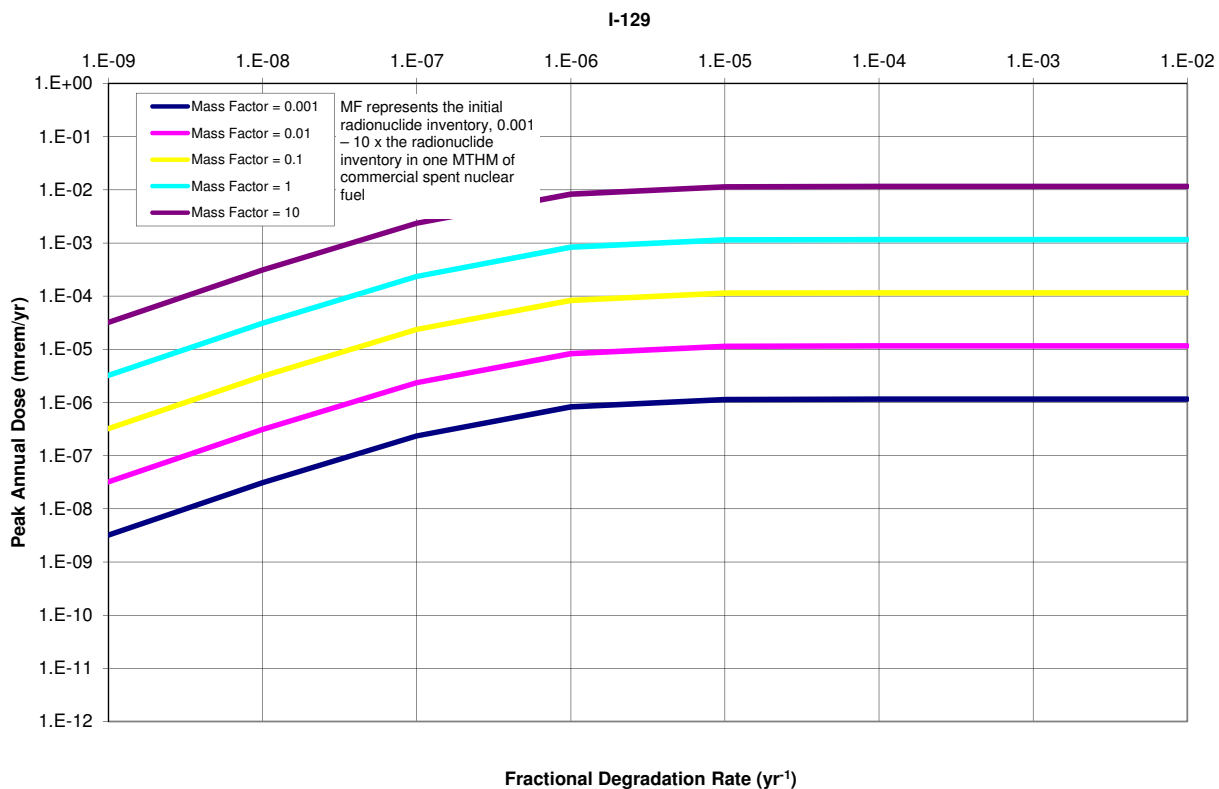
Figure A.23: ^{129}I waste form degradation rate sensitivity.
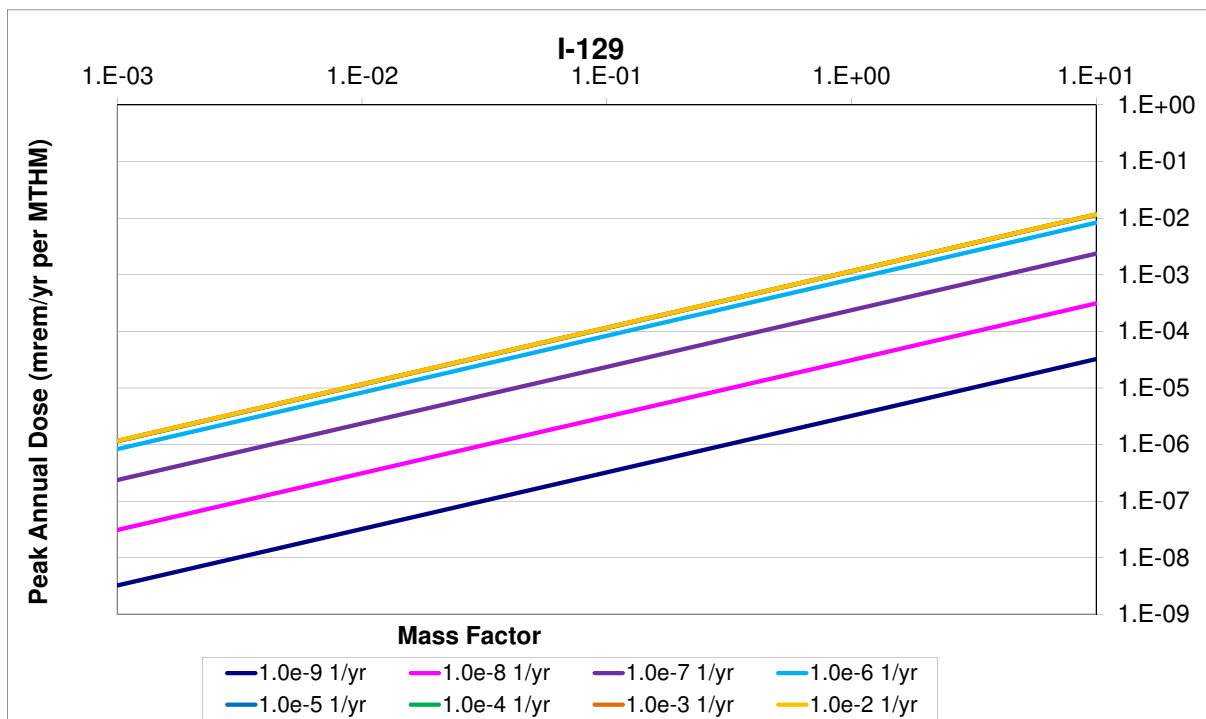
Figure A.24: ^{129}I inventory multiplier sensitivity.

Cl-36
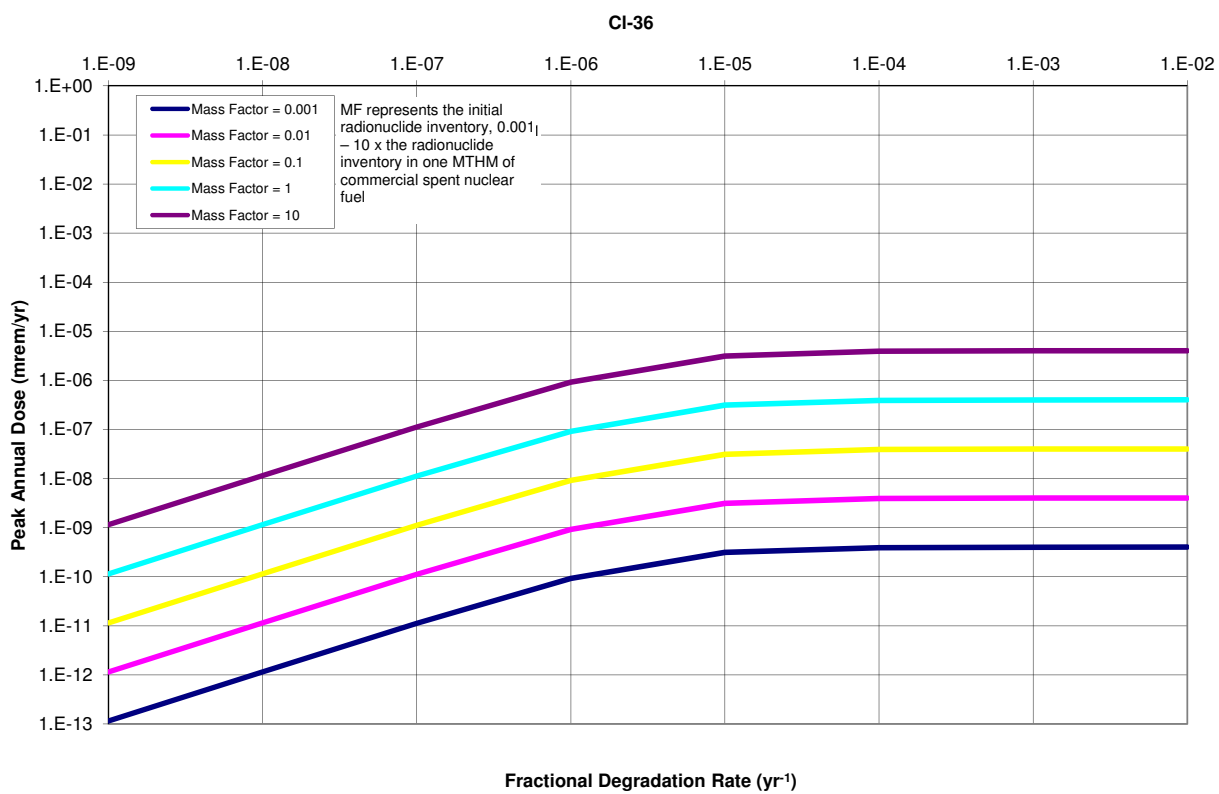
Figure A.25: ^{36}Cl waste form degradation rate sensitivity.
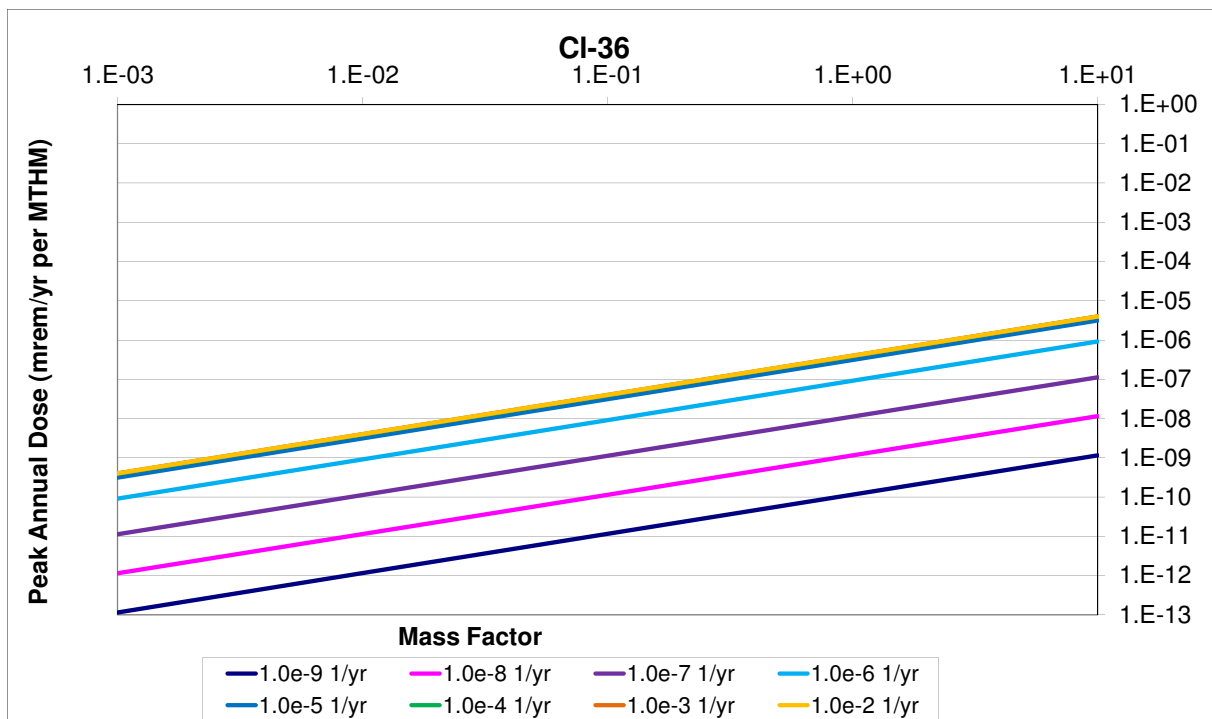
Figure A.26: ^{36}Cl inventory multiplier sensitivity.

The peaks for solubility limited, sorbing elements such as Tc and Np, on the other hand, have a more dramatic turnover. For very high degradation rates, the dependence on mass factor starts to round off due to attenuation by solubility limits, as can be seen in Figures A.29, A.30, A.27, and A.28.

Solubility limited and sorbing ^{99}Tc demonstrates a direct proportionality to fractional degradation rate until attuation by its solubility limit and other natural system parameters.
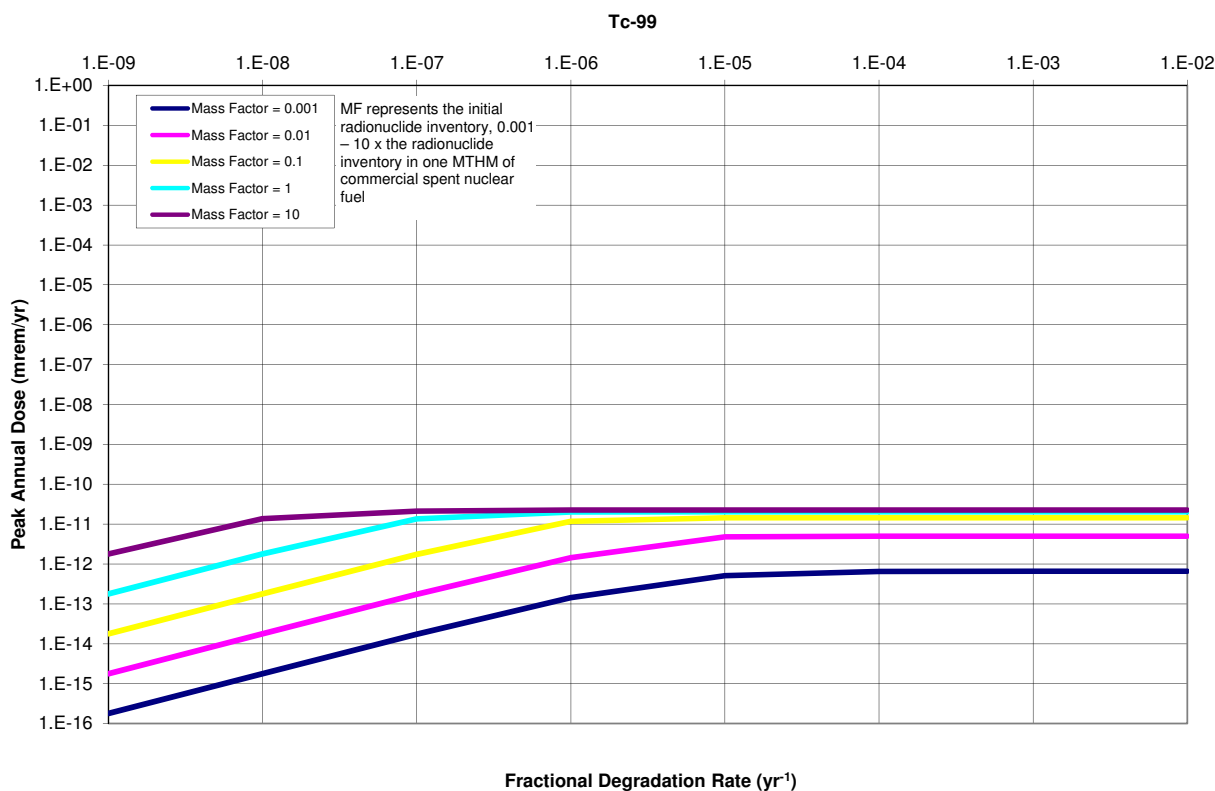
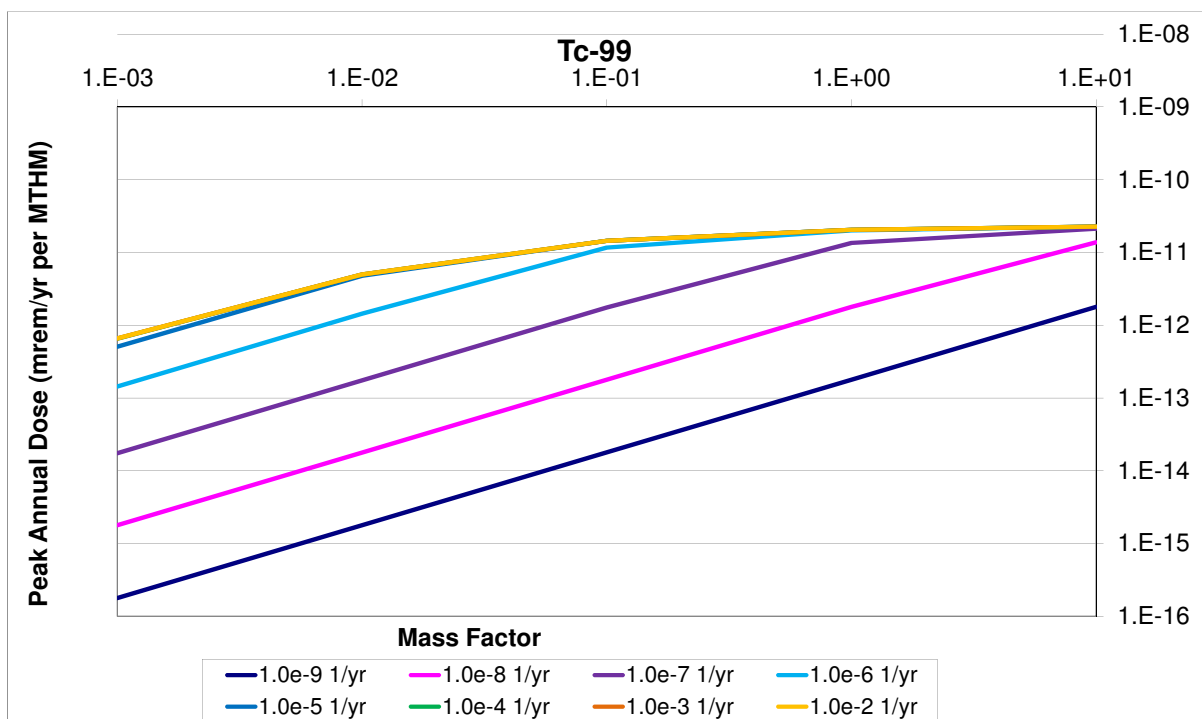Figure A.27: ^{99}Tc waste form degradation rate sensitivity.

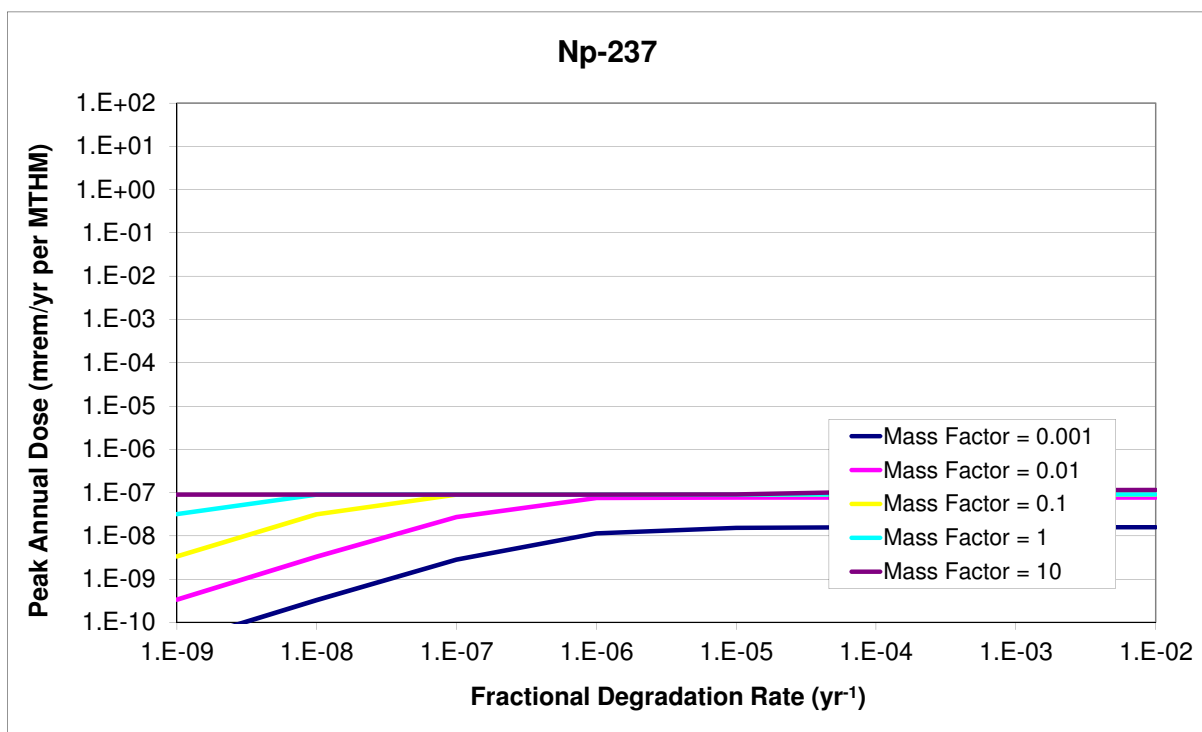Figure A.28: ^{99}Tc inventory multiplier sensitivity.

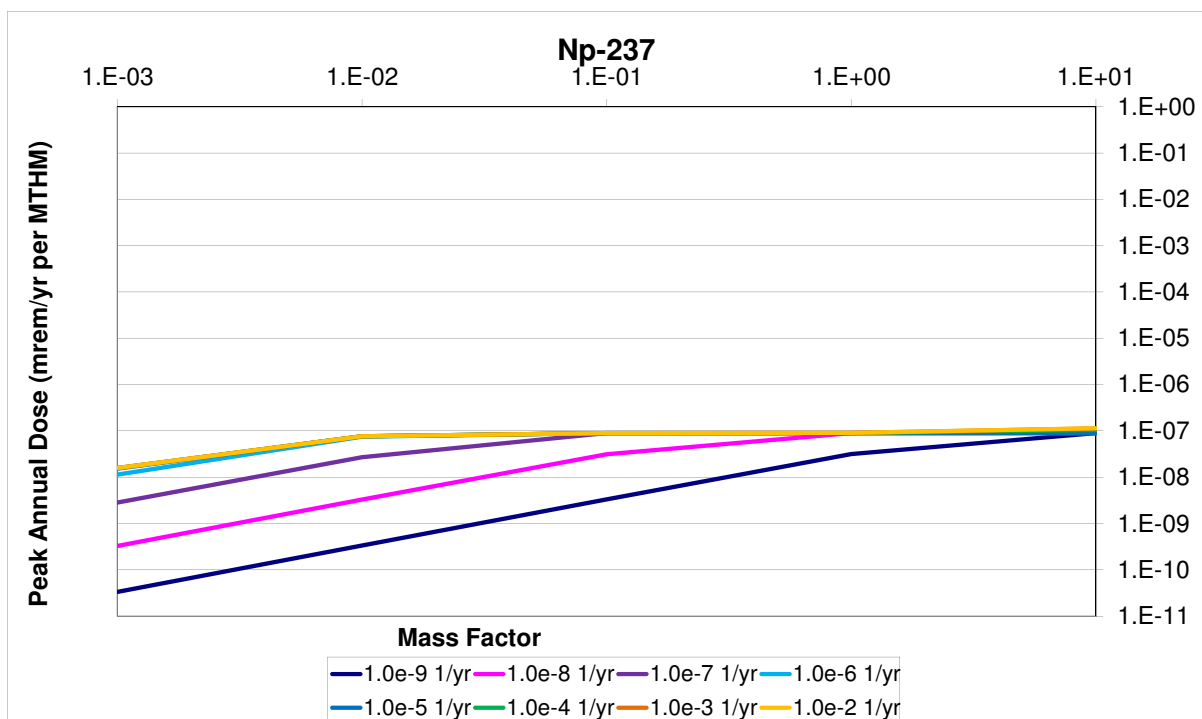Figure A.29: ^{237}Np waste form degradation rate sensitivity.

Figure A.30: ^{237}Np inventory multiplier sensitivity.

Waste Package Failure Time

The time of waste package failure was not expected to greatly effect the magnitude of the mean of the peak doses except for cases in which waste package failure times exceeded the half lives of dominant dose-contributing nuclides. That is, since the dominant dose-contributing radionuclides for the reference case are quite long lived (^{129}I, etc.), all but the longest reasonable waste package containment lifetime is overwhelmed by the half life of the dominant radionuclides. The long time scales of radionuclide release was expected to render the the waste package lifetime irrelevant if it was shorter than a million years.

Though the model contains a unit cell-type model, it is possible to determine, in post processing, the results of a simulation with temporally heterogeneous failures among waste packages. That is, by a weighted sum of the time histories of the no-fail case and the all-fail case, it is possible to mimic a time-varying failure among the many waste packages.

Parametric Range

To investigate the effect of the waste package failure time, it was varied over five magnitudes from one thousand to ten million years. Simultaneously, the reference diffusivity was varied over the eight magnitudes between 1×10^{-8} and 1×10^{-15} in order to determine the correlation between increased radionuclide mobility and the waste package lifetime.

Results

For the clay repository, the waste package failure time is entirely irrelevant until waste package failure times reach the million or ten million year time scale.
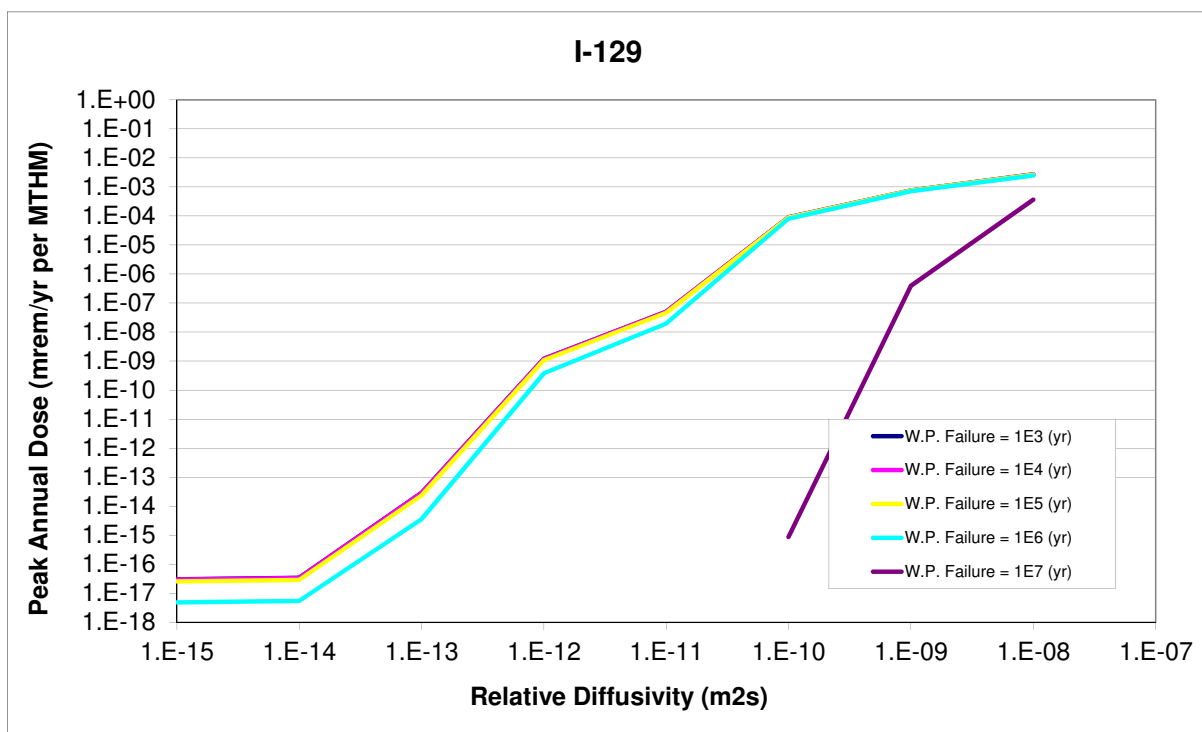
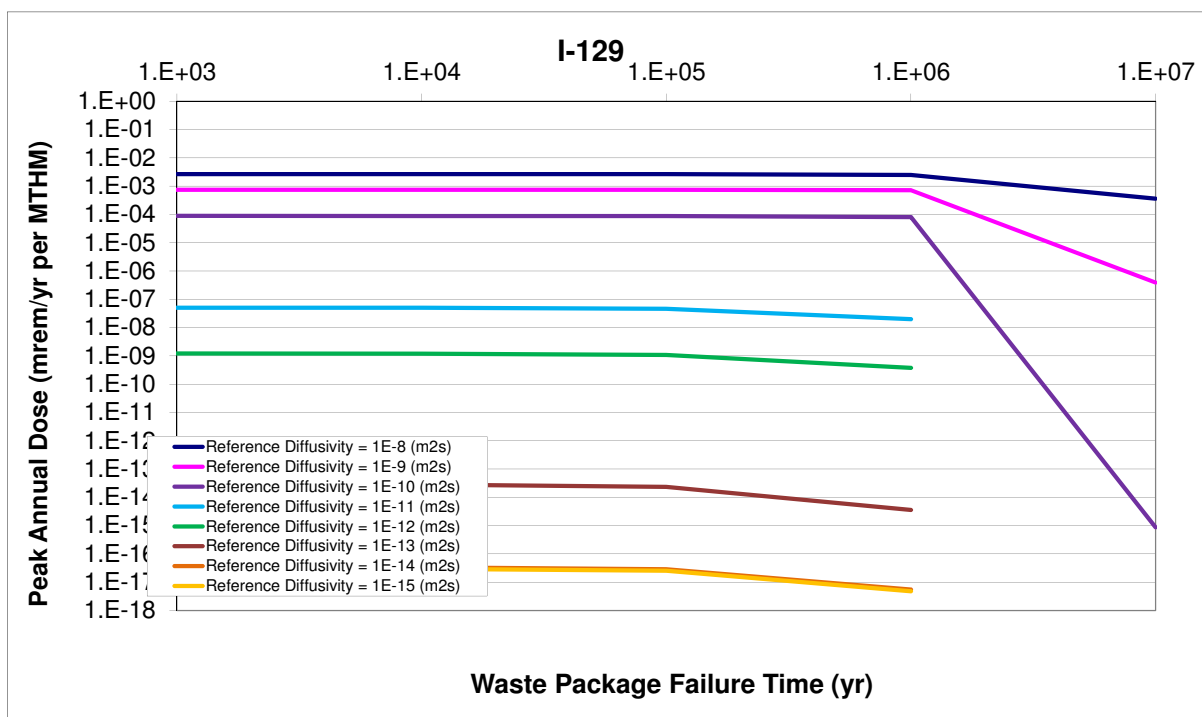Figure A.31: ^{129}I waste package failure time sensitivity.
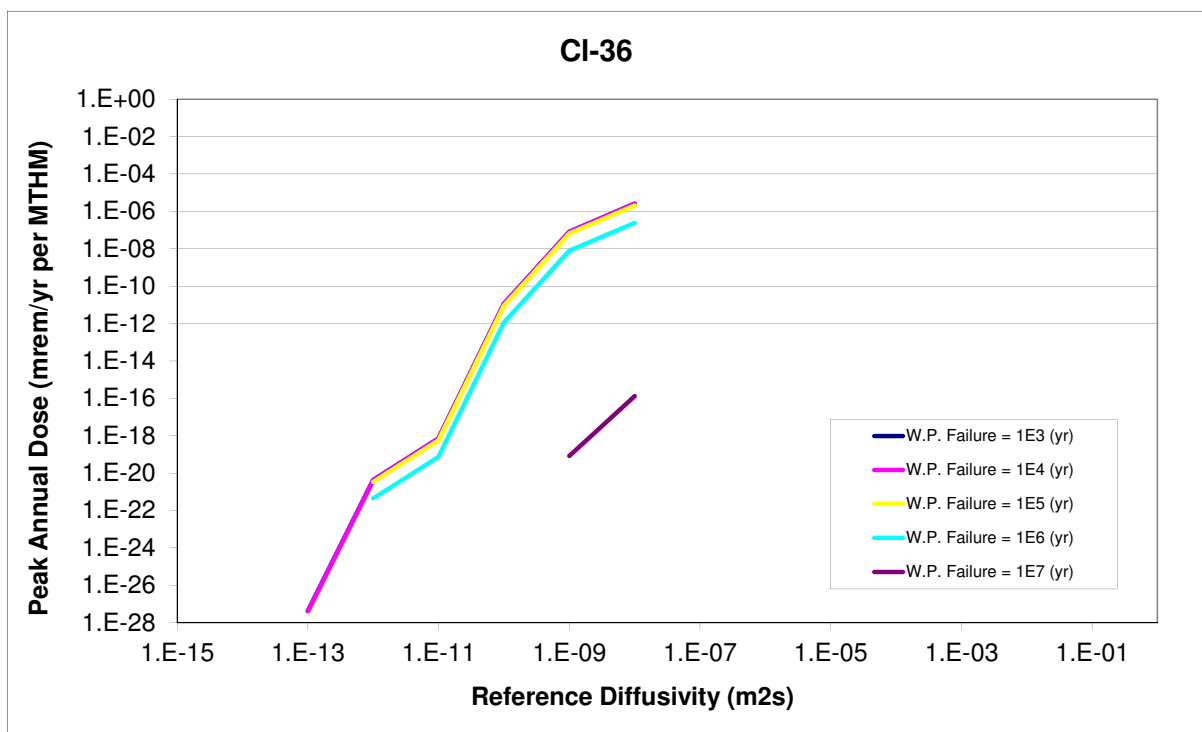
Figure A.32: ^{129}I waste package failure time sensitivity.

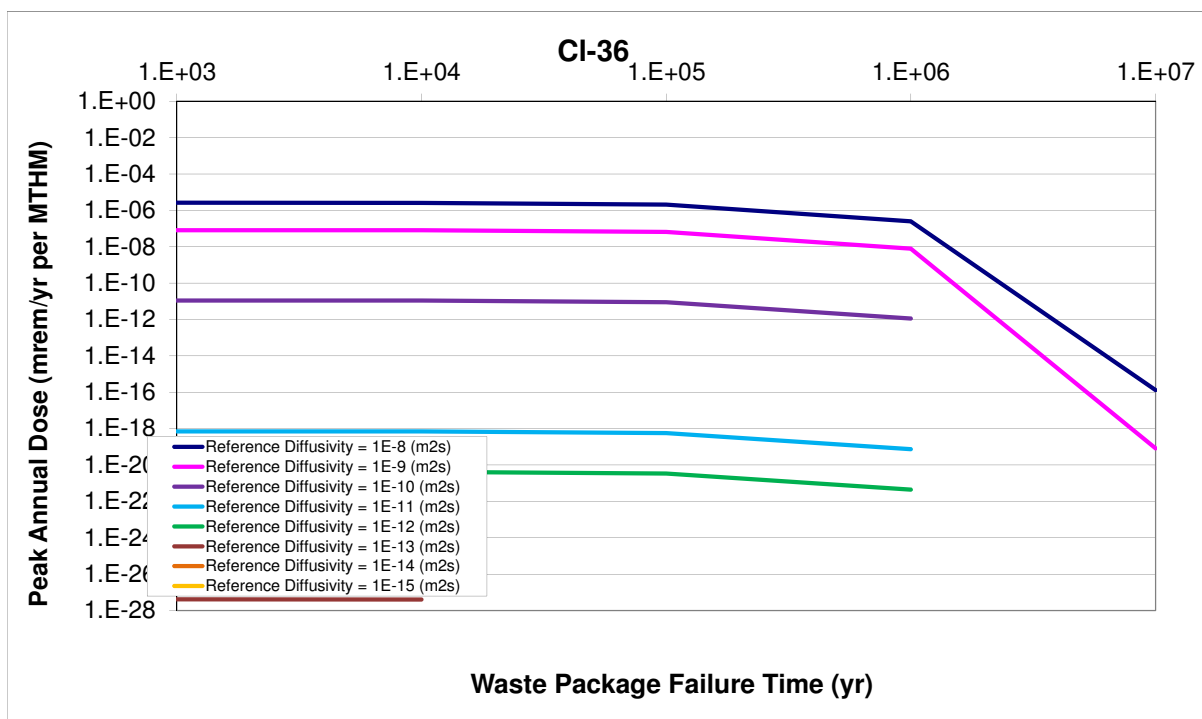Figure A.33: ^{36}Cl waste package failure time sensitivity.

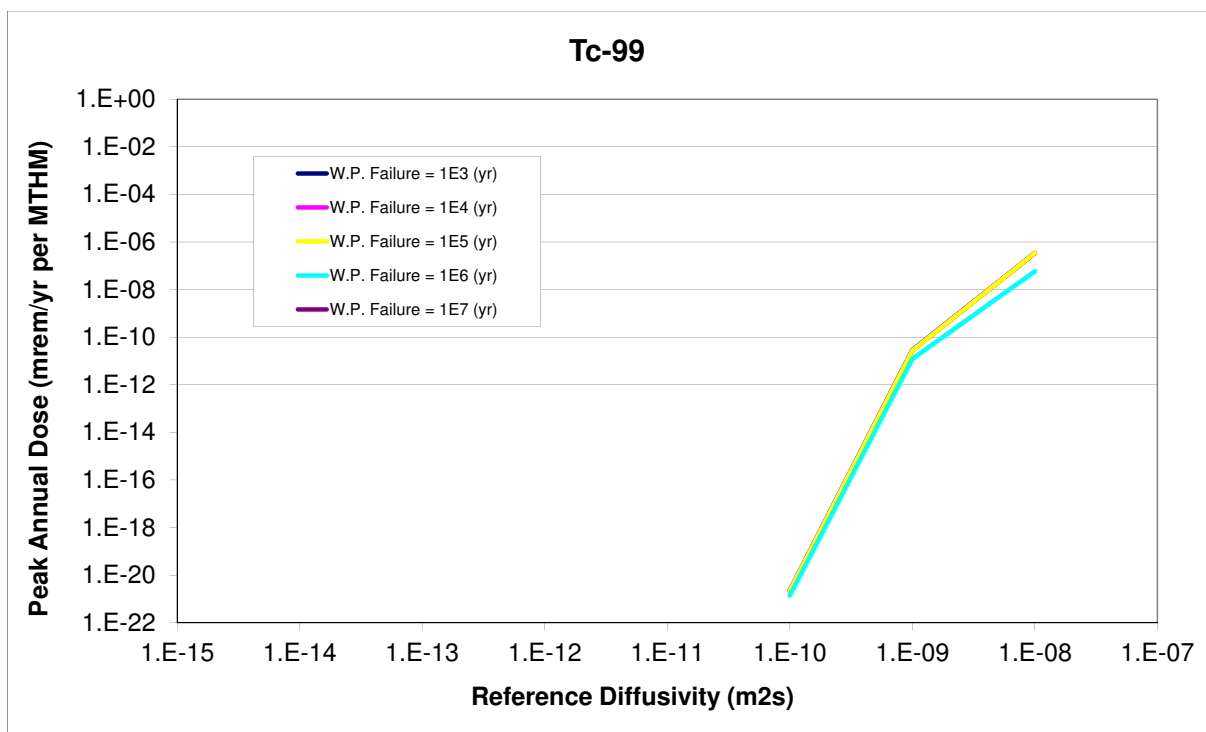Figure A.34: ^{36}Cl waste package failure time sensitivity.

Figure A.35: ^{99}Tc waste package failure time sensitivity.

Figure A.36: ^{99}Tc waste package failure time sensitivity.

Figure A.37: ^{237}Np waste package failure time sensitivity.

Figure A.38: ^{237}Np waste package failure time sensitivity.
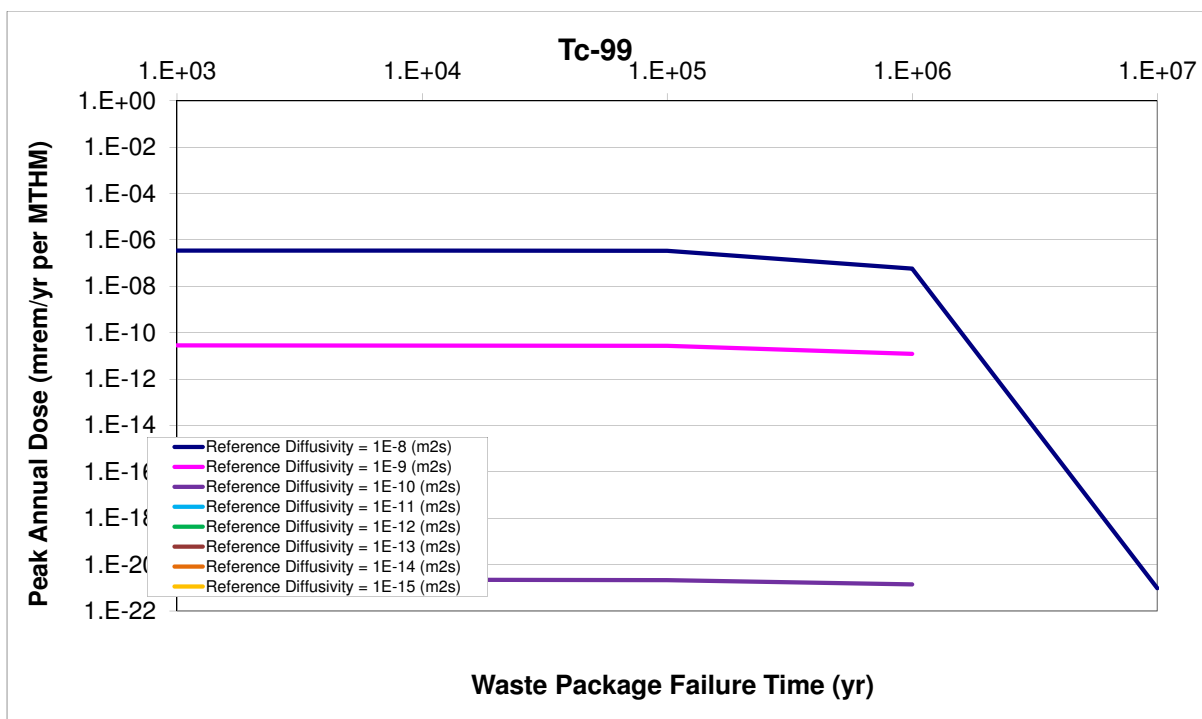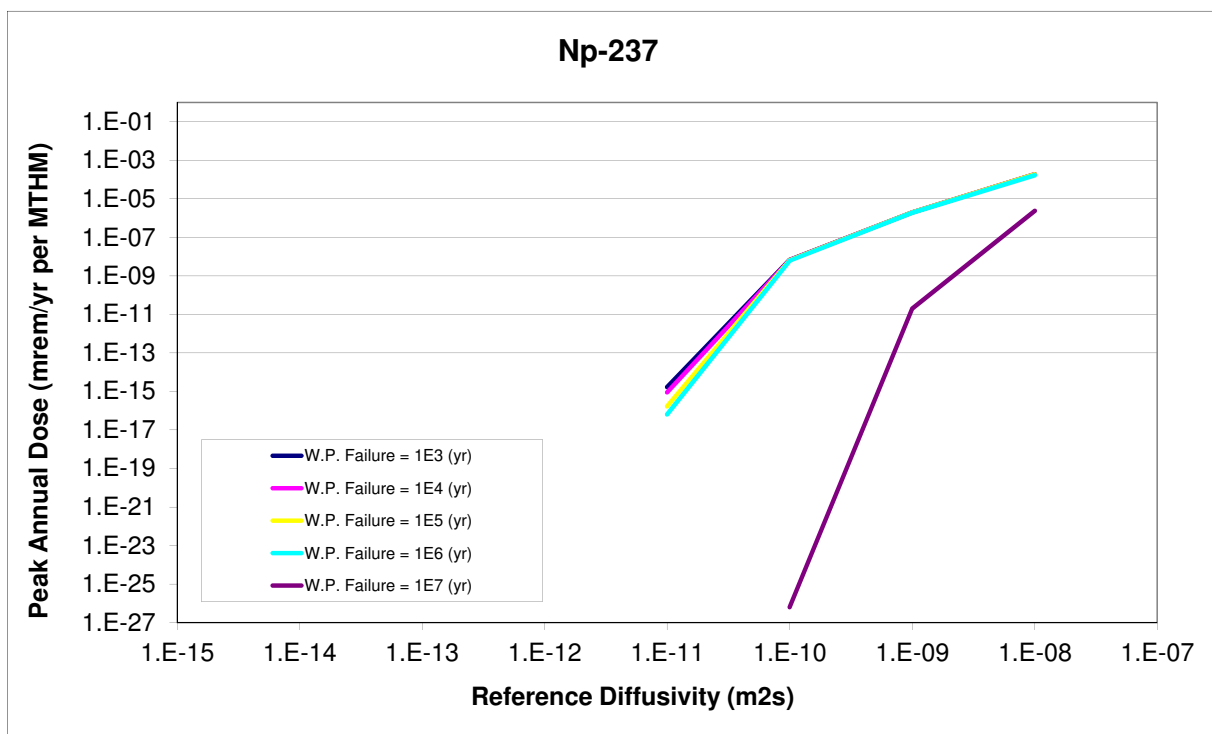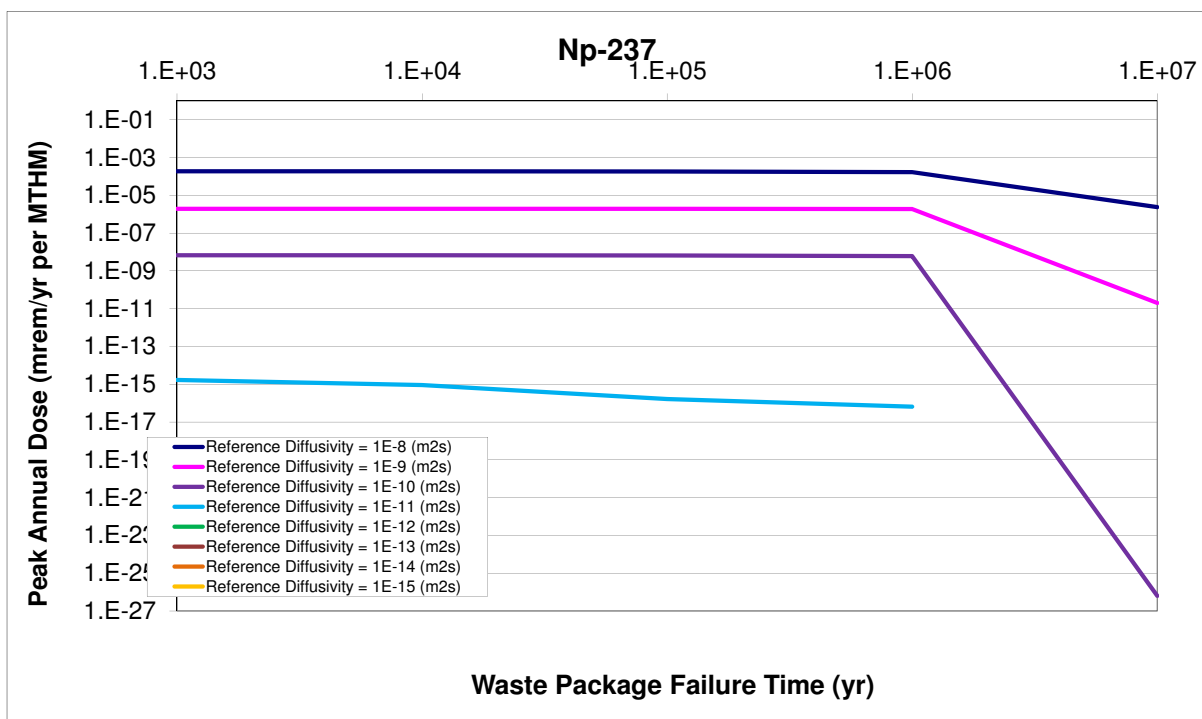
B THERMAL TRANSPORT SENSITIVITY ANALYSIS

B.1 Isotopic Thermal Sensitivity Study

B.2 Thermal Conductivity Sensitivity Study

B.3 Diffusivity Thermal Transport Sensitivity Study

B.4 Spacing Thermal Transport Sensitivity Studies

REFERENCES

[1] AB, Svensk karnbranslehantering. 2006. *Long-term safety for KBS-3 repositories at forsmark and laxemar-a first evaluation: Main report of the SR-Can project*. SKB.

[2] Abkowitz, Mark. 2010. Nuclear waste assessment system for technical evaluation - NUWASTE.

[3] Ahn, J. 1988. Mass transfer and transport of radionuclides in fractured porous rock. Tech. Rep., California Univ., Berkeley, CA.

[4] Ahn, J. 2004. An environmental impact measure for nuclear fuel cycle evaluation. *Journal of Nuclear Science and Technology* 41(3):296 – 306.

[5] Ahn, J. 2007. Environmental impact of yucca mountain repository in the case of canister failure. *Nuclear technology* 157(1):87 – 105.

[6] Ahn, J., D. Kawasaki, and P. L Chambre. 2002. Relationship among performance of geologic repositories, canister-array configuration, and radionuclide mass in waste. *Nuclear Technology* 140(1).

[7] Anderson, M. P, and W. W Woessner. 1992. *Applied groundwater modeling: simulation of flow and advective transport.*

[8] ANDRA. 2005. Argile: Evaluation de la faisabilite du stockage geologique en formation argileuse. Tech. Rep., ANDRA, Paris.

[9] ———. 2005. Granite: Evaluation de la faisabilite du stockage geologique en formation granite. Tech. Rep., ANDRA, Paris.

[10] Avila, R., J. Cervantes, and C. Estrada-Gasca. 2000. Transient thermal response in nuclear waste repositories. *Nuclear Engineering and Design* 198(3):307–316.

[11] Bateman, H. 1908. 1910. the solution of a system of differential equations occurring in the theory of radio-active transformations. In *Proc. cambridge philosophical soc*, vol. 15, 423.

[12] Berkowitz, Brian, Jacob Bear, and Carol Braester. 1988. Continuum models for contaminant transport in fractured porous formations. *Water Resources Research* 24(8):PP. 1225 – 1236.

[13] Blink, J. A., T. A. Buscheck, W. G. Halsey, and T. Wolery. 2010. Disposal systems evaluations and tool development-engineered barrier system evaluation (work package LL1015080425). Tech. Rep., Lawrence Livermore National Laboratory (LLNL), Livermore, CA.

[14] Boucher, Lionel. 2010. International comparison for transition scenario codes involving COSI, DESAE, EVOLCODE, FAMILY and VISION. CEA France.

[15] Bouvier, E., J. Ahn, and T. Ikegami. 2007. *Comparison of environmental impacts for PWR-UO{sub 2}, PWR-MOX and FBR*. LaGrange Park, IL: American Nuclear Society.

[16] Bracke, G., T. Beuth, K. Fischer-Appelt, J. Larue, and M. Navarro. 2008. Safety functions derived from geochemistry for safety analysis of final disposal of high-level radioactive waste. *Uranium, Mining and Hydrogeology* 771—778.

[17] Brady, P. V., B. W. Arnold, G. A. Freeze, P. N. Swift, S. J. Bauer, J. L. Kanney, R. P. Rechard, and J. S. Stein. 2009. Deep borehole disposal of high-level radioactive waste. *SAND2009-4401, Sandia National Laboratories*.

[18] Brewitz, Wernt, and Ulrich Noseck. 2002. Long-term performance of spent fuel in geological repositories. *Comptes Rendus Physique* 3(7-8):879–889.

[19] Carslaw, H. S., and J. C. Jaeger. 1959. Conduction of heat in solids. *Oxford: Clarendon Press, 1959, 2nd ed.* 1.

[20] Carter, J. T., A. J. Luptak, J. Gastelum, C. Stockman, and A. Miller. 2011. Fuel cycle potential waste inventory for disposition. Tech. Rep., FCR&D-USED-2010-000031, Rev. 3.

[21] Clayton, D, G Freeze, E Hardin, W.M. Nutt, J Birkholzer, H.H. Liu, and S Chu. 2011. Generic disposal system modeling - fiscal year 2011 progress report. Tech. Rep. FCRD-USED-2011-000184, U.S. Department of Energy, Sandia, NM.

[22] Diodato, D. M., and T. Center. 1994. A compendium of fracture flow modelsâĂŞ1994. *Work sponsored by US Department of Defense, United States Army, Europe, Combat Maneuver Training Center, Hohenfels, Germany*.

[23] DOE. 2008. The report to the president and the congress by the secretary of energy on the need for a second repository. Office of Civilian Radioactive Waste Management DOE/RW–0595, Department of Energy, Washington D.C.

[24] ———. 2010. Nuclear energy research & development roadmap: Report to congress.

[25] ———. 2013. Strategy for the management and disposal of used nuclear fuel and high-level radioactive waste. Tech. Rep., United States Department of Energy (DOE), Washington D.C., United States.

[26] DOE, US. 2002. Yucca mountain science and engineering report. *US Department of Energy, Las Vegas, NV DOE/RW-0539-1, Rev* 1.

[27] Durham, W. B., V. V. Mirkovich, and H. C. Heard. 1987. Thermal diffusivity of igneous rocks at elevated pressure and temperature. *Journal of Geophysical Research: Solid Earth* 92(B11):11615—11634.

[28] El-Wakil, Mohamed Mohamed. 1981. *Nuclear heat transport*. American Nuclear Society.

[29] Gaski, J. 1987. SINDA system improved numerical differencing analyzer.

[30] van Genuchten, M. T., and W. J. Alves. 1982. Analytical solutions of the one-dimensional convective-dispersive solute transport equation. *Technical Bulletin* 9(1661).

[31] Greenberg, H. R., M. Sharma, and M. Sutton. 2012. Investigations on repository near-field thermal modeling. Tech. Rep., Lawrence Livermore National Laboratory (LLNL), Livermore, CA.

[32] Greenberg, Harris, James Blink, Massimiliano Fratoni, Mark Sutton, and Amber Ross. 2012. Application of analytical heat transfer models of multi-layered natural and engineered barriers in potential high-level nuclear waste repositories. In *WM2012*. Phoenix, AZ. LLNL-CONF-511672.

[33] GuÃl̆rin, Laurent. 2009. *A benchmark study of computer codes for system analysis of the nuclear fuel cycle*, vol. MIT-NFC-TR-105.

[34] Hardin, E, J Blink, Harris Greenberg, Mark Sutton, Massimo Fratoni, Joe Carter, Mark Dupont, and Rob Howard. 2011. Generic repository design concepts and thermal analysis - 8.8.2011 draft. Tech. Rep. FCRD-USED-2011-000143, Department of Energy Office of Used Fuel Disposition, Sandia.

[35] Hedin, A. 2002. Integrated analytic radionuclide transport model for a spent nuclear fuel repository in saturated fractured rock. *Nuclear Technology* 138(2).

[36] Ho, C. K. 2000. Dual porosity vs. dual permeability models of matrix diffusion in fractured rock. Tech. Rep., Sandia National Laboratories, Albuquerque, NM (US); Sandia National Laboratories, Livermore, CA (US).

[37] Huff, Kathryn, and Theodore H. Bauer. 2012. Benchmarking a new closed-form thermal analysis technique against a traditional lumped parameter, finite-difference method. Technical Report FCRD-UFD-000142, Argonne National Laboratory (ANL), Argonne, IL, United States.

[38] ———. 2012. Numerical calibration of an analytical generic nuclear repository heat transfer model. In *Transactions of the american nuclear society*, vol. 106 of *Modeling and Simulation in the Fuel Cycle*, 260—263. Chicago, IL, United States: American Nuclear Society, La Grange Park, IL 60526, United States.

[39] Huff, Kathryn, and Mark Nutt. 2012. Key processes and parameters in a generic clay disposal system model. In *Transactions of the american nuclear society*, vol. 107 of *Environmental Sciences – General*, 208—211. San Diego, CA: the American Nuclear Society.

[40] Huff, Kathryn D. 2013. Cyder : A generic geology repository performance library.

[41] ———. 2013. Hydrologic nuclide transport models in cyder, a geologic disposal software library. In *WM2013*. Phoenix, AZ: Waste Management Symposium.

[42] Incropera, Frank. 2006. *Fundamentals of heat and mass transfer*. 6th ed. Hoboken N.J.: Wiley.

[43] Johnson, L., C. Ferry, C. Poinssot, and P. Lovera. 2005. Spent fuel radionuclide source-term model for assessing spent fuel performance in geological disposal. part i: Assessment of the instant release fraction. *Journal of Nuclear Materials* 346(1): 56âĂŞ65.

[44] Johnson, L., B. Kunz, C. Frei, Nagra, and Projekt Opalinuston. 2002. *Project opalinus clay: Safety report: Demonstration of disposal feasibility for spent fuel, vitrified high-level waste and long-lived intermediate-level waste (entsorgungsnachweis)*. Nagra, National cooperative for the Disposal of Radioactive Waste.

[45] Johnson, L. H., and Nagra. 2002. *Calculations of the temperature evolution of a repository for spent fuel, vitrified high-level waste and intermediate level waste in opalinus clay*. Nagra.

[46] Kawasaki, D., J. Ahn, P. L Chambre, and W. G Halsey. 2004. Congruent release of long-lived radionuclides from multiple canister arrays. *Nuclear technology* 148(2): 181 – 193.

[47] Kessler, J. H, J. Kemeny, F. King, A. M Ross, and B. Ross. 2006. Room at the mountain: Estimated maximum amounts of commercial spent nuclear fuel capable of disposal in a yucca mountain repository. Tech. Rep., The ASME Foundation, Inc., New York.

[48] Kim, J., Y. Lee, and M. Koo. 2007. Thermal properties of granite from korea. *AGU Fall Meeting Abstracts* 11:0576.

[49] Kossik, R.F., I. Miller, and S. Knopf. 2006. GoldSim graphical simulation environment user's guide.

[50] Leij, F. J., T. H. Skaggs, and M. T. Van Genuchten. 1991. Analytical solutions for solute transport in three-dimensional semi-infinite porous media. *Water resources research* 27(10):2719âĂŞ2733.

[51] von Lensa, W., R. Nabbi, and M. Rossbach. 2008. *RED-IMPACT impact of partitioning, transmutation and waste reduction technologies on the final nuclear waste disposal.* Forschungszentrum Julich.

[52] Li, J. 2006. A methodology to evaluate nuclear waste transmutation/fuel cycle systems.

[53] Li, J., M. Nicholson, W. C Proctor, M. S Yim, and D. McNelis. 2007. Examining repository loading options to expand yucca mountain repository capacity. In *Proceedings of GLOBAL*, 519 — 525.

[54] Li, Jun, M. S Yim, and D. McNelis. 2008. The specific temperature increase method for repository thermal analysis. *Transactions of the American Nuclear Society* 99:216 — 218.

[55] Maloszewski, Piotr, and Andrzej Zuber. 1996. Lumped parameter models for the interpretation of environmental tracer data. *Manual on mathematical models in isotope hydrology. IAEA-TECDOC-910* 9âĂŞ59.

[56] Miron, A., J. Valentine, J. Christenson, M. Hawwari, S. Bhatt, M. L Dunzik-Gougar, and M. Lineberry. 2009. Identification and analysis of critical gaps in nuclear fuel cycle codes required by the SINEMA program. Tech. Rep., University of Cincinnati.

[57] Nicholson, M. A. 2007. *Thermal loading and uncertainty analysis of high level waste in yucca mountain.* North Carolina State University.

[58] Nieland, J. D., K. D. Mellegard, Roger S. Schalge, and Hugh D. Kaiser. 2001. Storage of chilled natural gas in bedded salt storage caverns: Economic and technical feasibility. Topical Report RSI-1354 DE-AC26-97FT34350, United States Department of Energy National Energy Technology Laboratory 626 Cochrans Mill Road Pittsburgh, Pennsylvania 15236.

[59] No 115, IAEA Safety Series. 1996. International basic safety standards for protection against ionizing radiation and for the safety of radiation sources. *International Atomic Energy Agency, Vienna.*

[60] Nutt, Mark. 2011. Personal communication.

[61] Nutt, W. M. 2010. Used fuel disposition research and development roadmap-FY10 status. Tech. Rep., Argonne National Laboratory (ANL).

[62] OECD Nuclear Energy Agency. 2006. *Advanced nuclear fuel cycles and radioactive waste management.* OECD Publishing.

[63] ONDRAF-NIRAS. 2001. Technical overview of the SAFIR 2 report. Tech. Rep. Nirond 2001-05 E, Belgium.

[64] Papoulis, A., and S. U. Pillai. 2002. *Probability, random variables, and stochastic processes*. 4th ed. Series in Electrical and Computer Engineering, McGraw-Hill.

[65] Piet, S., T. Bjornard, B. Dixon, D. Gombert, C. Laws, and G. Matthern. 2007. Which elements should be recycled for a comprehensive fuel cycle? *Proc. Global 2007* 1595.

[66] Posiva. 2010. *Interim summary report of the safety case 2009*. POSIVA.

[67] ptc. 2010. MathCAD engineering calculations software.

[68] Pusch, R., L. Borgesson, and M. Erlstrom. 1987. *Alteration of isolating properties of dense smectite clay in repository environment as examplified by seven pre-quarternary clays*. Swedish Nuclear Fuel and Waste Management Co.

[69] Radel, T. E. 2007. *Repository modeling for fuel cycle scenario analysis*. University of Wisconsin – Madison.

[70] Radel, T. E, P. P.H Wilson, R. M. Grady, and T. H. Bauer. 2007. *Effect of separation efficiency on repository loading values in fuel cycle scenario analysis codes*. LaGrange Park, IL: American Nuclear Society.

[71] Radel, T.E., P.P.H. Wilson, T.H. Bauer, and R.M. Grady. 2007. Effect of separation efficiency on repository loading values in fuel cycle scenario analysis codes. In *GLOBAL 2007: Advanced nuclear fuel cycles and systems, september 9, 2007 - september 13, 2007*, 148–154. GLOBAL 2007: Advanced Nuclear Fuel Cycles and Systems, Boise, ID, United states: American Nuclear Society.

[72] Savoye, S., F. Goutelard, C. Beaucaire, Y. Charles, A. Fayette, M. Herbette, Y. Larabi, and D. Coelho. 2011. Effect of temperature on the containment properties of argillaceous rocks: The case study of callovo-oxfordian claystones. *Journal of Contaminant Hydrology*.

[73] Schneider, E., M. Knebel, and W. Schwenk-Ferrero. 2004. NFCSim scenario studies of german and european reactor fleets. Tech. Rep., LA-UR-04-4911, Los Alamos National Laboratory.

[74] Schwartz, F. W., and H. Zhang. 2004. Fundamentals of ground water. *Environmental Geology* 45:1037âĂŞ1038.

[75] Soelberg, N., S. Priebe, D. Gombert, and T. Bauer. 2009. Heat management strategy trade study. *Advanced Fuel Cycle Initiative, AFCI-SYSA-PMO-MI-DV-2009-000169, INL/EXT-09-16708*.

[76] Surma, Fabrice, and Yves Geraud. 2003. Porosity and thermal conductivity of the soultz-sous-forets granite. In *Thermo-hydro-mechanical coupling in fractured rock*, ed. Hans-Joachim KÃijmpel, 1125—1136. Pageoph Topical Volumes, Birkhauser Basel.

[77] Swift, Peter, and Mark Nutt. 2010. Applying insights from repository safety assessments. In *Proceedings of 11th information exchange meeting on partitioning and transmutation*. San Francisco, CA: OECD-NEA.

[78] Tikhonravova, P. I. 2007. Effect of the water content on the thermal diffusivity of clay loams with different degrees of salinization in the transvolga region. *Eurasian Soil Science* 40(1):47—50.

[79] Uleberg, K., and J. Kleppe. 1996. Dual porosity, dual permeability formulation for fractured reservoir simulation. In *Norwegian university of science and technology, trondheim RUTH seminar, stavanger*.

[80] Van Den Durpel, L., D. C Wade, and A. Yacout. 2006. DANESS: a system dynamics code for the holistic assessment of nuclear energy system strategies. *Proceedings of the 2006 System Dynamics Conference*.

[81] Williams, N. H. 2001. Total system performance AssessmentâĂŞAnalyses for disposal of commercial and DOE waste inventories at yucca MountainâĂŞInput to final environmental impact statement and site suitability evaluation REV 00 ICN 02. Tech. Rep.

[82] Wilson, P. P.H. 2011. Comparing nuclear fuel cycle options. *A report for the Reactor & Fuel Cycle Technology Subcommittee of the Blue Ribbon Commission on America's Nuclear Future*.

[83] Wilson, Paul. 2009. The adoption of advanced fuel cycle technology under a single repository policy. Tech. Rep.

[84] Wilson, Paul P. H., Kathryn Huff, Matthew Gidden, and Robert Carlsen. 2012. Cyclus: A nuclear fuel cycle code from the university of wisconsin madison. cyclus.github.com.

[85] Yacout, A. 2011. DANESS. http://www.anl.gov/techtransfer/Software_Shop/Daness/DANESS.ht

[86] Yacout, A. M., J. J. Jacobson, G. E. Matthern, S. J. Piet, D. E. Shropshire, and C. Laws. 2006. VISION – verifiable fuel cycle simulation of nuclear fuel cycle dynamics. In *Waste management symposium*.